STATE DIAGRAM FOR CONTACT-INHIBITION OF PROLIFERATION: A QUANTITATIVE FRAMEWORK FOR MODULATING GROWTH PATTERNS IN EPITHELIAL CELL CLUSTERS

Thesis by

Jin-Hong Kim

In Partial Fulfillment of the Requirements

For the Degree of

Doctor of Philosophy

California Institute of Technology

Pasadena, California

2010

(Defended May 7, 2010)

Acknowledgements

First, and most importantly, I would like to thank my advisor, Prof. Anand Asthagiri, for his guidance, inspiration, and encouragement throughout my graduate study. His breadth of knowledge and dedicated enthusiasm to science have guided me to conduct this project with interest and motivation. All that he taught me during these years will be invaluable assets throughout my career as a scientist.

I am grateful to Prof. David Tirrell, Prof. Elliot Meyerowitz, and Prof. Chin-Lin Guo for allowing their valuable time to serve on the committee. Their critical comments and insights were tremendous help to the improvements and completion of this study.

Thank you to the past and current members of the Asthagiri group, Claudiu Giurumescu, Nicholas Graham, Niki Galownia, Stephen Chapman, Ehsan Jabbarzadeh, Melissa Pope, Keiichiro Kushiro, Paul Minor, and Larry Dooling. I am thankful to their technical assistances for helping me with many aspects of my research, and more importantly to their friendships that made my time in Pasadena very memorable one.

I also want to acknowledge my collaborator, Jacob Notbohm, for working with me on the mechanics-related work. It was a great working and learning experience for me to venture a new field. I want to thank to Prof. Guruswami Ravichandran and Prof. Anand Asthagiri for setting up such opportunity.

All my love and thanks to my parents, my two sisters, Hye-Yeon and Hye-Jeen, and my grandmother. It was their unfailing love and trust that enabled me to accomplish this journey at ten-thousand miles away from home. To my father, you always have been my best mentor and my life-long role model. To my mother, none of this would have been possible without your unconditional love and sacrifice for me.

Abstract

Cell-cell contacts play a key role in the assembly and integrity of epithelial tissues. Cell-cell contact is not only a mere physical link between neighboring cells, but also a critical regulator of many cell behaviors including proliferation. Contact-inhibition of proliferation is a hallmark of normal epithelial tissues. Cancer development involves the loss of this key constraint. Both biochemical and physical mechanisms mediating contact-inhibition are emerging. A current, principal challenge is elucidating how the integrated performance of these mechanisms enforce or modulate contact-inhibition in a rich microenvironment that includes multiple, potentially conflicting cues such as soluble growth factors (GFs) and extracellular matrix (ECM).

Here, we propose a quantitative paradigm for contact-inhibition of proliferation. Our quantitative analysis of single cells within multicellular aggregates reveals that epithelial cells transition from a contact-inhibited to contact-independent mode of proliferation at a critical threshold EGF level. This transition point is a tunable property and can be modulated by varying the level of cell-cell contact. Furthermore, the proximity to this transition point is a quantitative gauge of “degree” of contact-inhibition. Using this metric, we demonstrate that stiffening the adhesive matrix, a widely observed phenomenon during cancer development, leads to the quantitative, progressive reduction in the EGF threshold needed to induce contact-independent proliferation. Thus, stiffening the ECM moves an epithelial cell system closer to the transition to contact-independence, thereby quantitatively reducing the amount of EGF amplification needed

to induce population-wide proliferation. Our results reveal that the potent effect of substratum compliance on contact-inhibition involves changes in contact-maturation and multicellular mechanics. The proposed quantitative model of contact-inhibition provides fundamental insights into our understanding of tissue morphogenesis and cancer progression in multicellular organisms. Furthermore, our findings provide design principles for engineering multicellular growth in applications such as tissue engineering.

Table of Contents

Acknowledgements…….iii

Abstract……..……..v

Table of Contents……..……...vii

List of Figures…….…….ix

Chapter I. Introduction…….……...I-1

References…….....I-5

Chapter II. Tunable interplay between epidermal growth factor and cell-cell contact governs the spatial dynamics of epithelial growth…….II-1

Abstract…….II-1

Introduction.……..II-3

Results and Discussion…….……II-5

Materials and Methods…….……II-20

Acknowledgements…….…….....II-22

References…….……..II-23

Supporting Information…….……..II-26

Chapter III. Substratum stiffening promotes the quantitative, progressive loss of contact-inhibition of proliferation…….…….III-1

Abstract……..……...III-1

Introduction…….…….III-3

Results……III-6

Discussion……..III-20

Materials and Methods…….…….…….III-24

Acknowledgements……..……..III-26

References……..……III-27

Supporting Information…….…….……III-30

Chapter IV. Substratum compliance and EGF co-regulate spatial patterns in traction forces, cell shape, and proliferation within epithelial multicellular clusters……..…IV-1

Abstract……...IV-1

Introduction…….IV-3

Results…….IV-5

Discussion……..IV-15

Conclusions…….……...IV-17

Materials and Methods……...IV-18

References……..IV-21

Appendix I. Intercellular mechanotransduction during multicellular morphodynamics…….....AI-1

Appendix II. Quantitative immunofluorescence for measuring spatial compartmentation of covalently-modified signaling proteins……..…...AII-1

List of Figures

Chapter II

Fig. 1. E-cadherin-mediated contact-inhibition triggers spatial patterns in cell cycle activity only when EGF depletes to a threshold concentration…….II-7

Fig. 2. Selective attenuation of Erk, but not Akt, among interior cells correlates with contact-inhibition……..II-11

Fig. 3. A quantitative balance between GFs and cell-cell contacts dictates the spatial pattern in cell cycle activity in epithelial cell clusters……..……II-15

Fig. 4. Spatial dynamics of epithelial growth can be modulated by tuning the critical thresholds at which contact-inhibition is triggered……..II-17

Chapter III

Fig. 1. State diagram for contact-inhibition of proliferation and the hypothesis of quantitative, progressive loss of contact-inhibition…….…….III-5

Fig. 2. Substratum compliance affects spatial patterns in cell cycle activity and contact-inhibition of proliferation…….……III-8

Fig. 3. Substratum stiffening reduces the EGF threshold needed to transition from contact-inhibited to contact-independent proliferation……...III-13

Fig. 4. Substratum compliance affects the molecular organization of adhesion structures at cell-cell contacts…….….III-16

Fig. 5. Substratum compliance affects subcellular localization of EGFR and selectively regulates EGFR and ERK, but not Akt, signaling…….....III-19

Chapter IV

Fig. 1. The effect of substratum compliance on contact-maturation and spatial pattern in cell-matrix interactions…….……IV-6

Fig. 2. The spatial patterns in cell adhesions correspond to spatial gradient in mechanical stresses within multicellular aggregates……...IV-10

Fig. 3. Treatment with supra-threshold levels of EGF induces rapid, short-lived traction forces and transient decondensation of clusters…….....IV-14

Chapter I. Introduction

Cellular organization into specialized, functional multicellular structures is achieved through dynamic interactions between cells and their surrounding microenvironment (1). The microenvironment presents instructions for orchestrating many cellular processes, including proliferation, migration, and differentiation in a spatio-temporally coordinated manner (2). Tight regulation of these cell behaviors in a multicellular context is essential for organ development, function, and homeostasis. Meanwhile, perturbations among environmental cues and/or in the cellular apparatus that senses and responds to these cues leads to significant pathological consequences, such as cancer development (3).

Epithelial tissues exhibit highly-ordered cell-cell junctions and polarized structures, mainly serving a barrier function for protection, partitioning, and sensation (4). In addition to its structural role, cell-cell contact is a key factor regulating epithelial tissue growth. Contact-inhibition of proliferation is a hallmark of normal epithelial cells, and the loss of contact-inhibition results in chaotic proliferation, leading to tumor formation (5). Given its role in cancer, “contact-inhibition” has been the subject of extensive research ever since it was first described in the early 1960s at a phenomenological level in a culture that had reached saturation density (6). Contact-inhibition is now better understood with greater resolution at the molecular and cellular levels.

While progress continues in uncovering the physicochemical mechanisms mediating contact-inhibition (7-12), the quantitative aspects of this key constraint are unclear. In particular, contact-inhibition and the loss of this constraint occur in a complex microenvironment replete with conflicting cues such as soluble growth factors (GF) and extracellular matrix (ECM). GFs bind receptors on the cell surface and activate a set of downstream intracellular signaling pathways that can stimulate proliferation (13). Cells are also anchored to the surrounding ECM whose physical and chemical properties regulate cellular mechanics (14-15) and adhesion-dependent growth signaling (16-17).

It remains unclear how contact-inhibition is enforced in such a complex microenvironment that includes multiple, potentially conflicting, cues. What perturbations in these environments potentially lead to the loss of contact-inhibition, transitioning the system to a contact-independent state? Ultimately, how do cells quantitatively integrate and converge these differential inputs into a net decision on cell cycle? Addressing these questions will provide insight into a pivotal step in the self-organization of multicellular systems during development and the disruption of multicellular morphology during cancer progression.

Deciphering quantitative principles of contact-inhibition can also offer design strategies for biomedical applications, such as tissue engineering and regenerative medicine. A quantitative understanding of contact-inhibition of proliferation is needed

to manipulate multicellular growth patterns and rates in synthetic microenvironments. Recent advances in material design (18-19) and microfabrication (20-21) techniques have enabled *in situ* fine-tuning of the degree of and context in which cells form contacts with their neighbors and the matrix. Furthermore, spatio-temporally controlled release of soluble growth factors is feasible with the use of advanced polymeric materials (22), microfluidics (23-24), and MEMS devices (25). How these powerful technologies to manipulate environmental cues may be applied to tune rationally the growth and organization of multicellular structures is a key engineering challenge.

Using a quantitative approach at a single cell level within two-dimensional multicellular aggregates, we elucidate a quantitative framework for contact-inhibition of proliferation when cells are presented with conflicting cues – cell-cell contact (growth-inhibitory) and EGF (growth-promoting) (Chapter 2). Our results demonstrate that epithelial cells transition between contact-inhibited and contact-independent modes of proliferation when the amount of EGF crosses a critical threshold level. Only when the level of EGF recedes to this threshold level, do contacts effectively suppress cell cycle activity among interior cells, driving a spatially patterned, contact-inhibited growth state. Furthermore, this transition point is tunable. We show that augmenting cell-cell contacts using micropatterned surfaces and molecular approaches enables contact-inhibition at a higher EGF threshold.

This state diagram perspective of contact-inhibition suggests that the attenuation

of contact-inhibition may occur progressively over the course of oncogenesis as cancer-promoting perturbations gradually accumulate in the epithelial system and surrounding environments. We directly tested this hypothesis by measuring the quantitative effects of stiffening the adhesive matrix, a broadly observed phenomenon during *in vivo* tumorigenesis (Chapter 3). We show that even when substratum stiffening has no apparent effect on contact-inhibition at a phenotypic level, it markedly reduces the threshold amount of EGF, quantitatively shifting normal cells closer to the transition line to contact-independence. By using the proximity to this transition point as a metric, we demonstrate that quantitative changes in matrix compliance modulate the "degree" of contact-inhibition. These potent effects of matrix stiffening involve the erosion of contact-maturation, which alters the subcellular localization of EGF receptor as well as cell-cell adhesion molecules. Moreover, we demonstrate that substratum compliance and EGF synergistically modulate multicellular mechanics in three-dimensions, which correspond to multicellular growth patterns (Chapter 4).

In summary, we elucidate quantitative principles for contact-inhibition co-regulated by cell-cell contact, EGF, and substratum compliance with implications in modulating the degree of contact-inhibition and multicellular growth patterns. The proposed quantitative model of contact-inhibition enhances our understanding of cancer progression and offers design principles for engineering spatial patterns and rates of growth of multicellular structures.

References

1. Engler AJ, Humbert PO, Wehrle-Haller B, & Weaver VM (2009) Multiscale modeling of form and function. *Science* 324(5924):208-212
2. Kirschner M & Gerhart J (1998) Evolvability. *Proc Natl Acad Sci USA* 95(15):8420-8427
3. Tlsty TD & Coussens LM (2006) Tumor stroma and regulation of cancer development. *Annu Rev Pathol* 1:119-150
4. Debnath J & Brugge JS (2005) Modelling glandular epithelial cancers in three-dimensional cultures. *Nat Rev Cancer* 5(9):675-688
5. Hanahan D & Weinberg RA (2000) The hallmarks of cancer. *Cell* 100(1):57-70
6. Martz E & Steinberg MS (1972) The role of cell-cell contact in "contact" inhibition of cell division: a review and new evidence. *J Cell Physiol* 79(2):189-210
7. Curto M, Cole BK, Lallemand D, Liu C-H, & McClatchey AI (2007) Contact-dependent inhibition of EGFR signaling by Nf2/Merlin. *J Cell Biol* 177(5):893-903
8. Hamaratoglu F, *et al.* (2006) The tumour-suppressor genes NF2/Merlin and Expanded act through hippo signalling to regulate cell proliferation and apoptosis. *Nat Cell Biol* 8(1):27-36
9. Lampugnani MG, Orsenigo F, Gagliani MC, Tacchetti C, & Dejana E (2006) Vascular endothelial cadherin controls VEGFR-2 internalization and signaling

from intracellular compartments. *J Cell Biol* 174(4):593-604

10. Nelson CM, *et al.* (2005) Emergent patterns of growth controlled by multicellular form and mechanics. *Proc Natl Acad Sci USA* 102(33):11594-11599
11. St Croix B, *et al.* (1998) E-cadherin-dependent growth suppression is mediated by the cyclin-dependent kinase inhibitor p27(KIP1). *J Cell Biol* 142(2):557-571
12. Yin F & Pan D (2007) Fat flies expanded the hippo pathway: a matter of size control. *Sci STKE* 2007(380):pe12
13. Jones SM & Kazlauskas A (2001) Growth-factor-dependent mitogenesis requires two distinct phases of signalling. *Nat Cell Biol* 3(2):165-172
14. Wozniak MA & Chen CS (2009) Mechanotransduction in development: a growing role for contractility. *Nat Rev Mol Cell Biol* 10(1):34-43
15. de Rooij J, Kerstens A, Danuser G, Schwartz MA, & Waterman-Storer CM (2005) Integrin-dependent actomyosin contraction regulates epithelial cell scattering. *J Cell Biol* 171(1):153-164
16. Danen EH & Yamada KM (2001) Fibronectin, integrins, and growth control. *J Cell Physiol* 189(1):1-13
17. Guo W & Giancotti FG (2004) Integrin signalling during tumour progression. *Nat Rev Mol Cell Biol* 5(10):816-826
18. Kloxin AM, Kasko AM, Salinas CN, & Anseth KS (2009) Photodegradable hydrogels for dynamic tuning of physical and chemical properties. *Science* 324(5923):59-63
19. Lutolf MP & Hubbell JA (2005) Synthetic biomaterials as instructive extracellular

microenvironments for morphogenesis in tissue engineering. *Nat Biotech* 23(1):47-55

20. Hui EE & Bhatia SN (2007) Micromechanical control of cell-cell interactions. *Proc Natl Acad Sci USA* 104(14):5722-5726

21. Sniadecki NJ, Desai RA, Ruiz SA, & Chen CS (2006) Nanotechnology for cell-substrate interactions. *Ann Biomed Eng* 34(1):59-74

22. Lee KY, Peters MC, Anderson KW, & Mooney DJ (2000) Controlled growth factor release from synthetic extracellular matrices. *Nature* 408(6815):998-1000

23. Li Jeon N, *et al.* (2002) Neutrophil chemotaxis in linear and complex gradients of interleukin-8 formed in a microfabricated device. *Nat Biotech* 20(8):826-830

24. Mao H, Cremer PS, & Manson MD (2003) A sensitive, versatile microfluidic assay for bacterial chemotaxis. *Proc Natl Acad Sci U S A* 100(9):5449-5454

25. Peterman MC, Noolandi J, Blumenkranz MS, & Fishman HA (2004) Localized chemical release from an artificial synapse chip. *Proc Natl Acad Sci USA* 101(27):9951-9954

Chapter II. Tunable interplay between epidermal growth factor and cell-cell contact governs the spatial dynamics of epithelial growth

Abstract

Contact-inhibition of proliferation constrains epithelial tissue growth, and the loss of contact-inhibition is a hallmark of cancer cells. In most physiological scenarios, cell-cell contact inhibits proliferation in the presence of other growth-promoting cues, such as soluble growth factors (GFs). How cells quantitatively reconcile the opposing effects of cell-cell contact and GFs, such as epidermal growth factor (EGF), remains unclear. Here, using quantitative analysis of single cells within multicellular clusters, we show that contact is not a "master switch" that overrides EGF. Only when EGF recedes below a threshold level, contact inhibits proliferation, causing spatial patterns in cell cycle activity within epithelial cell clusters. Furthermore, we demonstrate that the onset of contact-inhibition and the timing of spatial patterns in proliferation may be re-engineered. Using micropatterned surfaces to amplify cell-cell interactions, we induce contact-inhibition at a higher threshold level of EGF. Using a complementary molecular genetics approach to enhance cell-cell interactions by overexpressing E-cadherin also increases the threshold level of EGF at which contact-inhibition is triggered. These results lead us to propose a phase diagram in which epithelial cells transition from a contact-uninhibited state to a contact-inhibited state at a critical threshold level of GF, a property that may be tuned by modulating the extent of cell-cell contacts. This new quantitative model of contact-inhibition has direct implications for how tissue size may be determined and deregulated

during development and tumor formation, respectively, and provides design principles for engineering epithelial tissue growth in applications such as tissue engineering.

Reprinted from Kim, J.-H., K. Kushiro., N.A. Graham, and A.R. Asthagiri from *Proceedings of the National Academy of Sciences USA* (2009)

Introduction

Contact-inhibition of proliferation is a key constraint on the growth of epithelial tissues. The loss of contact-inhibition is a hallmark of cancer cells, leading to hyperproliferation of epithelial cells and tumor formation (1). In physiological scenarios, cell-cell contact inhibits proliferation in the presence of other growth-promoting environmental cues, such as soluble growth factors (GFs). However, how cells quantitatively reconcile these conflicting cues to make a "net decision" on cell cycle commitment remains unclear. Does cell-cell contact act as a potent switch that supercedes the stimulatory effect of GFs? Or, is there a quantitative titration between the extent of cell-cell contact and the amount of GFs that ultimately determines cell cycle activity?

Whether cells evaluate contact and GFs in a binary or graded manner has important implications for our understanding of cancer progression. Cancers develop through multiple molecular "hits." Each hit may modify how cells weigh the opposing effects of contact and GFs. Thus, the loss of contact-inhibition may occur progressively with gradations of deregulation building up over the course of oncogenesis. Whether the loss of contact-inhibition should be viewed from this quantitative perspective or from the more classical binary viewpoint remains unclear because the quantitative interplay between contact and GFs in regulating cell cycle activity remains to be elucidated.

A principal challenge to gauging the quantitative crosstalk between contact and GFs is that the underlying mechanisms are arranged into a complex physiochemical network. The cadherin family of transmembrane cell surface proteins plays a critical role (2). Both ectopic expression of cadherins and exposure to beads coated with cadherins arrest cell cycle activity (3-8). Cadherins in association with other membrane proteins, such as Merlin, bind and regulate the trafficking of growth factor receptors (9-12). In addition, cadherins regulate contact-inhibition through mechanotransduction pathways. Cadherin-mediated contacts are coupled to the actin cytoskeleton (2, 13) and alter the distribution of traction forces between the cell and the substratum. Thus, in the interior of multicellular clusters where cell-cell contacts are abundant, the traction forces are minimal, and cell cycle activity is inhibited (14). Assessing the integrated performance of these chemical and physical mechanisms is non-trivial and leaves open a systems-level question: How do cells quantitatively evaluate cell-cell contact and GFs to regulate cell cycle commitment?

To address this question, we undertook a quantitative experimental analysis of cell cycle activity of individual epithelial cells within multicellular clusters. We show that a quantitative titration of the amount of epidermal growth factor (EGF) and the level of cell-cell contact regulates cell cycle activity. Only below a critical threshold level of EGF, cadherin-mediated contacts suppress cell proliferation. Moreover, we demonstrate that this threshold amount of EGF is a tunable property. By manipulating cell-cell interactions using either micropatterned surfaces or molecular genetics, we induce contact-inhibition at a higher level of EGF. These findings suggest a new quantitative

model of contact-inhibition of proliferation: We propose a phase diagram in which epithelial cells transition from a contact-uninhibited state to a contact-inhibited state at a critical threshold level of GF, a property that may be tuned by modulating the extent of cell-cell contacts. This quantitative model of contact-inhibition has direct implications for how tissue size may be determined and deregulated during development and tumor formation, respectively, and provides design principles for engineering epithelial tissue growth in applications such as tissue engineering.

Results and Discussion

To examine the quantitative interplay between GFs and cell-cell contact in regulating cell proliferation, we quantified cell cycle activity in clusters of non-transformed mammary epithelial cells (MCF-10A) stimulated with different doses of EGF (Fig. 1A). In early time, BrdU uptake (a measure of DNA synthesis) was observed among cells both in the periphery and the center of clusters. Thus, cell-cell contact is not sufficient to halt cell cycle activity among interior cells at 24 h. Only later in time, BrdU uptake was localized to the periphery of cell clusters, while the growth of interior cells was impeded. This spatial pattern was especially evident at 48 and 72 h post-stimulation in cultures initially treated with 0.1 and 1 ng/ml EGF, respectively (Fig. 1A, panels d, h). Treatment with an E-cadherin function-blocking antibody eliminated the spatial pattern in cell cycle activity, while a non-specific mouse IgG had no effect (Fig. 1B). These results confirm that E-cadherin-mediated contact-inhibition triggers the spatial pattern in

proliferation and rules out alternative mechanisms, such as a diffusion-limited spatial gradient in EGF.

These results demonstrate that E-cadherin-mediated contact-inhibition induces spatial patterns in proliferation only at specific times in culture. Furthermore, cells stimulated with a higher dose of EGF take a longer time to exhibit spatial patterns in cell cycle activity (Fig. 1A, panels d and h). We reasoned that this apparent dependence of contact-inhibition on EGF dosage may be linked to receptor-mediated degradation of EGF. Upon binding its receptor, the EGF/EGF receptor complex is internalized and a fraction of the ligand is degraded in the lysosome (15). We hypothesized that the EGF concentration may have to dip to a critical threshold level in order for cell-cell contact to effectively suppress cell cycle activity of interior cells. Consistent with this hypothesis, in cultures treated with a high dose of EGF (10 ng/ml EGF), both interior and peripheral cells maintain equal levels of cell cycle activity at all three time points (24, 48, and 72 h) (Fig. S1). Furthermore, direct measurement of EGF concentration in the medium showed that the amount of EGF decreases by two to three orders-of-magnitude over time (Fig. 1C), revealing a significant rate of cell-mediated ligand depletion.

If contact-inhibition is in fact sensitized to a threshold EGF concentration, then this threshold ought to be independent of the initial dose of EGF. A closer examination of the EGF depletion data confirms this hypothesis. Regardless of the initial amount of EGF, approximately 3×10^3 EGF molecules/cell are present when spatial patterns in proliferation are observed (Fig. 1C). We note that the BrdU assay identifies cells that

have already committed to the cell cycle and are actively undertaking DNA synthesis. Based on the general timing of the cell cycle, the evaluation of environmental cues and the decision to enter the cell cycle likely occurred ~20 h earlier (16). Thus, we conclude that at the time when contacts inhibit cell cycle entry among interior cells, the critical threshold of EGF is approximately 3 x 10^4 molecules/cell.

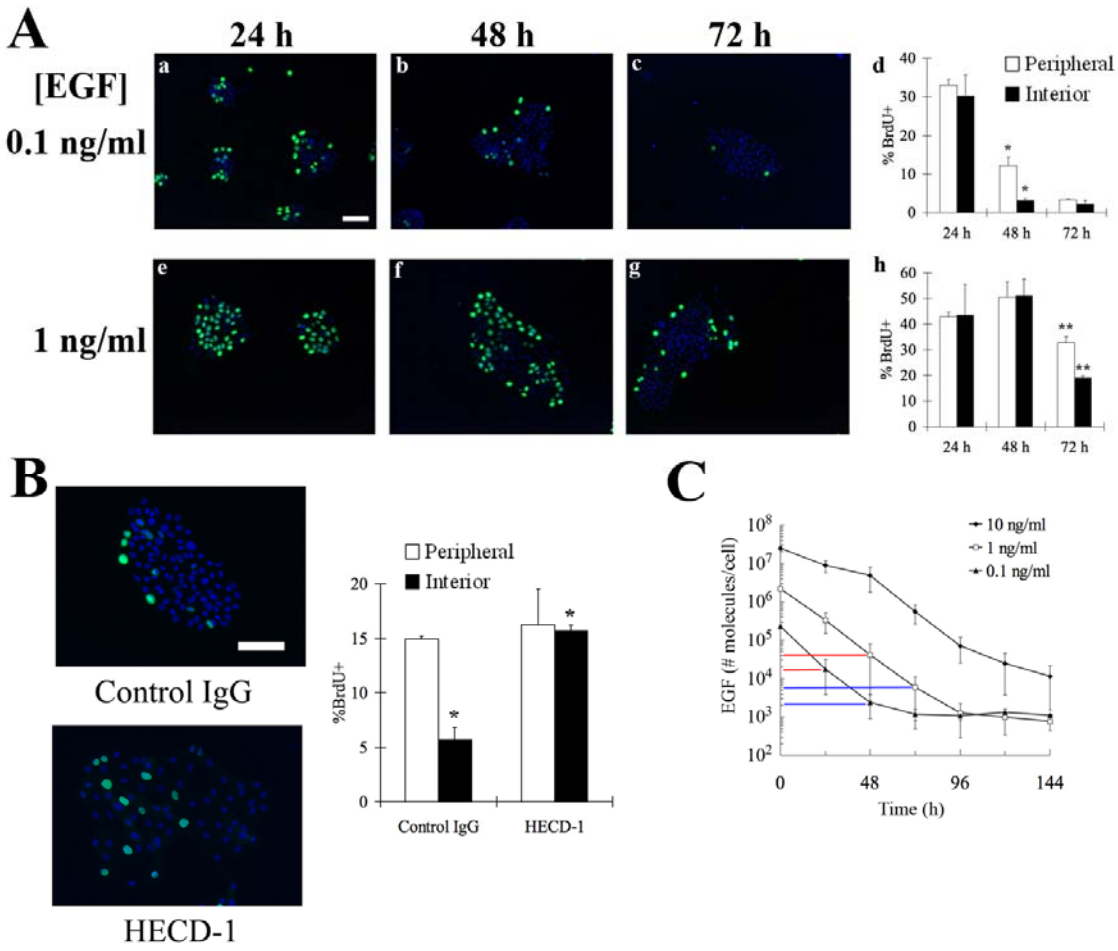

Figure 1. E-cadherin-mediated contact-inhibition triggers spatial patterns in cell cycle activity only when EGF depletes to a threshold concentration. (A) BrdU incorporation (green) and DAPI staining (blue) in MCF-10A cells initially seeded at 5x10^3 cell/cm^2 and treated with indicated doses of EGF for 24, 48 and 72 h. Panels d and

h show quantitation of the percentage of peripheral and interior cells incorporating BrdU. Error bars represent s.e.m. (n = 2-5). The *asterisk* and *double-asterisk* denote $p < 0.01$ and $p < 0.05$, respectively. (B) The effect of control IgG and anti-E-cadherin function blocking antibody on spatial pattern in cell cycle activity. Cells were treated with antibodies 24 h after stimulation with 0.1 ng/ml EGF. Twenty-four hours later, BrdU uptake (green) and DAPI (blue) was assessed. Percentage of peripheral and interior cells incorporating BrdU was quantified. Error bars indicate s.e.m. (n = 2). The *asterisk* indicates $p < 0.05$. (C) Amount of EGF in the medium for cultures treated initially with indicated doses of EGF. The vertical lines indicate the amount of EGF when a spatial pattern in proliferation is observed (blue) and 24 h prior (red). The error bars indicate s.e.m. (n = 2). The scale bar represents 100 μm.

To test further whether contact-inhibition occurs only at this critical EGF concentration, we designed an alternate approach to measure the threshold. Instead of waiting for ligand to deplete, we exposed cells to a broader range of EGF concentrations, including low levels that would emulate the late-depletion scenarios. Furthermore, we quantified cell cycle activity at a common time point, eliminating any changes in cells that could accumulate over time. In this assay at relatively high EGF concentrations (0.1, 1, and 10 ng/ml), both peripheral and central cells proliferate with nearly equal propensity (Fig. 2A and Fig. S3A). However, at lower EGF concentrations (0.001 and 0.01 ng/ml) BrdU uptake ceases selectively among interior cells, while peripheral cells maintain higher cell cycle activity. Thus, as in the previous assay format, contact-inhibition is triggered only when EGF dips below a critical threshold concentration (0.01

ng/ml). This threshold translates to ~10^4 EGF molecules/cell, demonstrating a common quantitative "setting" for contact-inhibition that is remarkably similar between the two assay formats.

We hypothesized that at this critical threshold level of EGF, cell-cell contact may be obstructing specific signaling pathways that are needed to stimulate cell cycle activity in interior cells. To examine this hypothesis, we focused on two major intracellular signals, Erk and Akt, that regulate cell cycle progression in many other cell systems (17) and are necessary for EGF-mediated proliferation in MCF-10A cells (Fig. S2). We quantified the activation of these signals in single cells at the periphery and interior of clusters. At relatively high EGF concentrations, Erk activation is uniform across the cluster (Fig. 2B and Fig. S3B). However, at 0.001 and 0.01 ng/ml EGF, the level of ppErk is distinctly higher in the peripheral cells (Fig. 2B and Fig. S3B). In contrast, Akt phosphorylation does not exhibit spatial heterogeneity at any of the EGF concentrations (Fig. 2C and Fig. S3C). Similar to Akt signaling, EGFR phosphorylation on Y1068 and Y1173 residues seemed to be uniform across the cell cluster for all EGF concentrations (Fig. S4). Thus, a spatial pattern in Erk signaling, but not Akt or EGFR phosphorylation, occurs at precisely the same threshold EGF dose at which contact inhibits cell cycle activity.

The emerging model from our data is that when the amount of EGF dips below a threshold value, cell-cell contact effectively inhibits EGF-mediated Erk signaling and thereby arrests cell cycle progression. If this model is accurate, supplying fresh ligand to

raise its concentration above the threshold should reverse spatial disparities in Erk signaling and cell cycle activity. To test this possibility, we treated serum-starved MCF-10A cells with 0.1 ng/ml EGF, and 24 h later, replenished the medium with fresh 0.1 ng/ml EGF. Following refreshment, the level of phosphorylated Erk in interior and peripheral cells was equivalent (Fig. S4A) in sharp contrast to the spatial pattern observed in non-replenished cultures (Fig. 2B). Furthermore, replenishing EGF entirely eliminates the spatial pattern in cell cycle activity (Fig. S4B). These results support our model and demonstrate that as EGF concentration dips below a threshold level, cadherin-mediated contacts selectively inhibit EGF-mediated Erk signaling and cell cycle activity among interior cells.

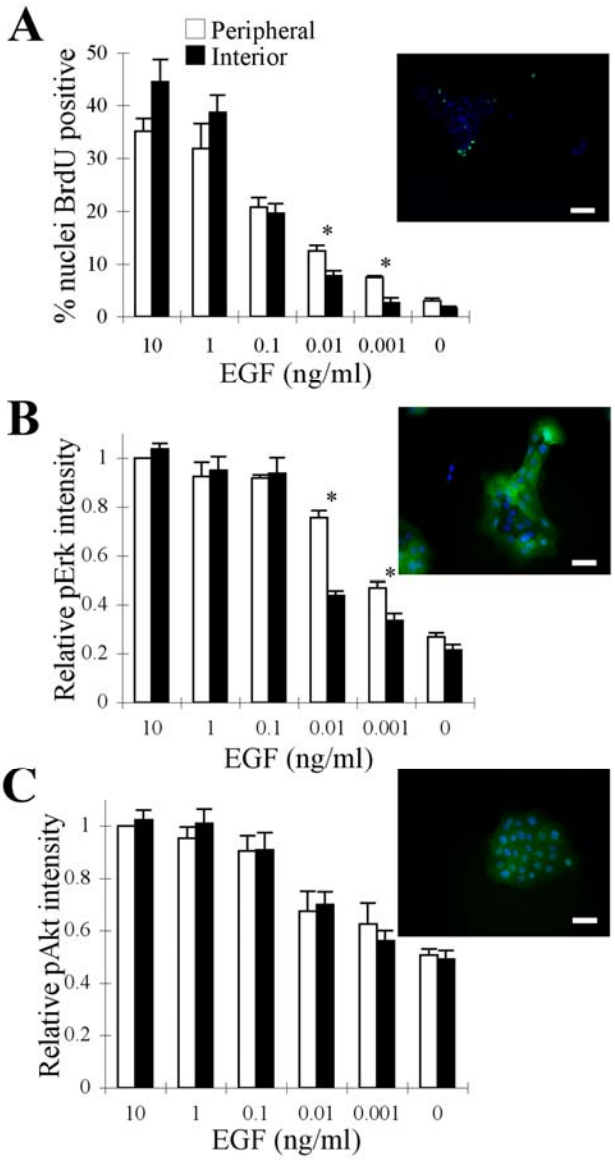

Figure 2: Selective attenuation of Erk, but not Akt, among interior cells correlates with contact-inhibition. MCF-10A cells seeded at a density of 10^4 cells/cm^2 were serum starved for 24 h and stimulated with the indicated doses of EGF or left untreated. BrdU uptake (A, green) and Erk/Akt (B/C, green) signals were assessed by immunostaining 24 h and 15 min, respectively, following EGF treatment. Nuclei were co-stained with DAPI (blue). Insets show representative images for cells treated with 0.01 ng/ml EGF. The bar graphs show percentage of nuclei incorporating BrdU (A), the relative nuclear intensity

of ppErk (B) and the relative nuclear intensity of pAkt (C) in peripheral and interior cells. Nuclear ppErk and pAkt intensities are reported relative to the amount of signal in peripheral cells treated with 10 ng/ml EGF. The *error bars* indicate s.e.m. (A: n=3, B: n=3, C: n=2). The *asterisks* denote $p < 0.05$. The scale bars represent (A) 100 μm and (B, C) 50 μm.

Furthermore, this threshold model seems relevant in other cell types. In Eph4 mouse mammary epithelial cells, when EGF level is increased above a threshold level, all cells in the cluster undergo DNA synthesis; meanwhile, a contact-inhibited pattern of proliferation is observed at the threshold amount of EGF (Fig. S6). Interestingly, the threshold in Eph4 cells occurs at approximately 1.5×10^3 EGF molecules/cell and is different from the threshold quantified in MCF-10A cells. Thus, while the interplay between EGF and contact seems to be a general feature, the quantitative set points for this threshold may vary across epithelial cell types.

In this manner, our analysis reveals a threshold amount of EGF at which contact-inhibition effectively induces a spatial pattern in cell cycle activity. An intriguing question is whether this competition operates bidirectionally. That is, instead of lowering EGF concentration to enable contact-inhibition, can cell-cell interactions be enhanced so that it competes more effectively with higher doses of EGF? Or, is the threshold EGF concentration a “hard-wired” parameter of contact-inhibition?

To examine this question, we first modulated cell-cell interactions using micropatterned substrates. By varying the number of cells seeded onto circular adhesive micropatterns of the same size, we manipulated the surface area of contact between neighboring cells (Fig. 3A). The density of DAPI staining confirmed the relative differences in cell density. Following stimulation with medium containing 20 ng/ml EGF, a spatial pattern in cell proliferation was evident in the culture with more extensive cell-cell interactions. Meanwhile, DNA synthesis in the low-density population was homogeneous. This result reveals that contact-inhibition of proliferation may be achieved at significantly higher doses of EGF if cell-cell interactions are augmented.

An important caveat, however, is that the growth arrest of interior cells in the high-density culture may be due to non-specific mechanical stresses at high cell density, space limitations due to overcrowding and/or reduced access to the underlying adhesive substrate. To determine whether cell-cell contacts are responsible for the observed spatial pattern in the high-density population, we examined the effect of downregulating E-cadherin expression using siRNA. Transfection with siRNA, but not a control construct, significantly reduced E-cadherin expression in MCF-10A cells (Fig. S6). Cells treated with the control siRNA and seeded at high density exhibited a spatial pattern in proliferation (Fig. 3B), revealing that the control siRNA treatment had no effect on contact-inhibition. In contrast, the spatial pattern was eliminated in cells plated at the same high density and treated with E-cadherin siRNA. These results demonstrate that E-cadherin plays a critical role in mediating the observed contact-inhibition on micropatterned substrates at higher doses of EGF. It remains unclear, however, whether

E-cdherin itself directly delivers the contact inhibition signal or whether E-cadherin interactions are needed to establish sufficient cell-cell contact for other proteins to mediate the contact inhibition signal. Indeed, the region of cell-cell contact is a rich environment of intercellular signaling involving proteins, such as Notch and ephrins, that may play a critical role in cell cycle regulation.

Our results suggest a quantitative phase diagram in which epithelial cells reside in two possible states: contact-uninhibited and contact-inhibited states (Fig. 3C). The transition into the contact-inhibited state occurs when the amount of EGF recedes below a critical threshold level. Furthermore, we showed that amplifying the level of cell-cell interactions using a micropatterned surface enables contact-inhibition at a higher level of EGF, suggesting that the tipping point at which contact-inhibition is triggered is tunable.

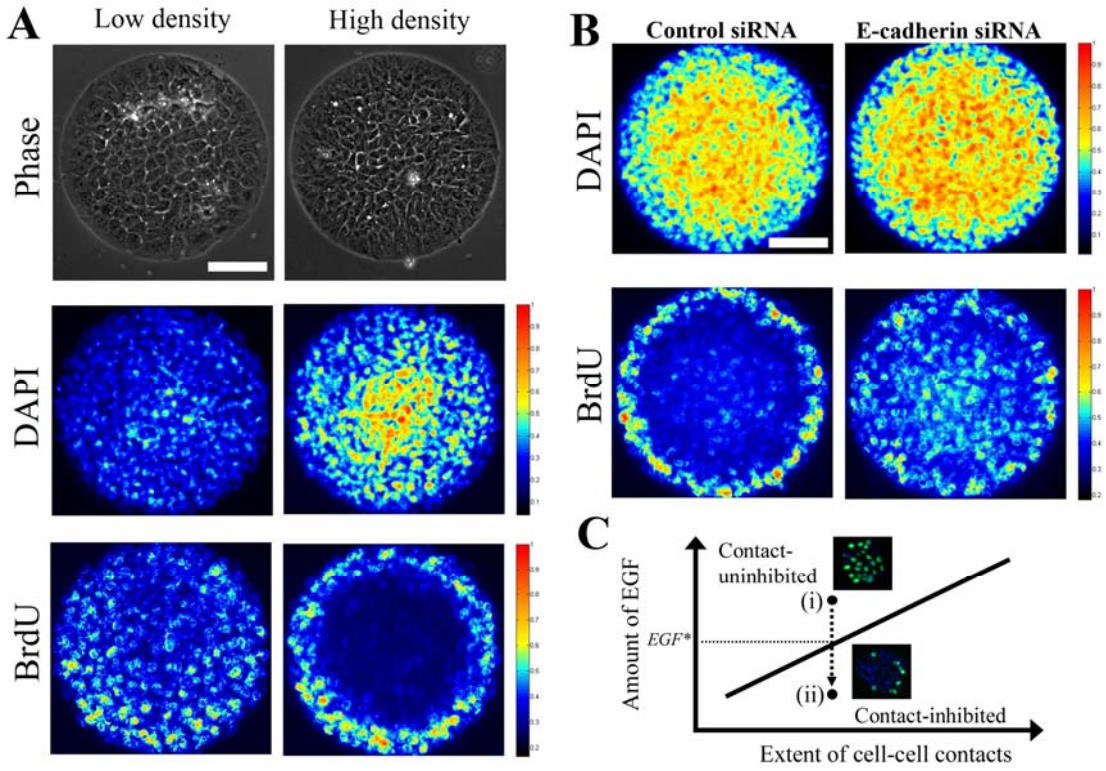

Figure 3: A quantitative balance between GFs and cell-cell contacts dictates the spatial pattern in cell cycle activity in epithelial cell clusters. (A) Low (*left*) and high (*right*) numbers of MCF-10A cells ($5x10^4$ and $1.2x10^5$ cells/cm^2, respectively) were plated on circular microdomains of the same size, serum starved for 24 h and stimulated with medium containing 20 ng/ml EGF for 24 h. By increasing the number of cells seeded, we force cells to acquire a more columnar morphology with an elevated amount of cell-cell contact area. Nuclear density (DAPI) and DNA synthesis (BrdU) was assessed by immunofluorescence. Images from 20 islands (n = 2) were stacked, and a heat map of their stacked intensities is shown. The top panel shows phase contrast images. (B) Cells treated with control or E-cadherin siRNA (50 nM) were plated at the same high density and stimulated with medium containing 20 ng/ml EGF for 24 h. Images of nuclear density (DAPI) and DNA synthesis (BrdU) were acquired from 30

islands (n = 2), and heat maps of their stacked intensities are shown. The scale bar represents 100 μm. (C) A phase diagram of epithelial cell growth as a function of growth factor and cell-cell interaction levels. Epithelial cells transition from (i) a contact-uninhibited state to (ii) a contact-inhibited state at a critical threshold level of growth factor (*EGF**). Insets show representative fluorescence images probed for BrdU uptake (green) and DAPI (blue) for clusters in contact-uninhibited and contact-inhibited phases.

To test further this phase diagram model and the tunability of the interplay between contact and GF, we revisited the relatively more straightforward scenario in which epithelial cells are growing on a non-patterned surface without any spatial constraints. According to our phase diagram model, increasing the level of cell-cell interactions in this context should enable the transition to a contact-inhibited state at higher EGF concentrations, driving the onset of the spatial pattern in cell cycle activity at an earlier time (Fig. 4A). To test this hypothesis, we retrovirally infected MCF-10A cells with either a vector encoding epitope-tagged human E-cadherin (pBabe-E-cad-HA) or an empty vector (pBabe). Cells transduced with virus encoding the exogeneous E-cadherin exhibited elevated E-cadherin expression compared to the cells infected with the virus prepared with an empty vector (Fig. 4B). Cells overexpressing E-cadherin exhibited a spatial disparity in cell cycle activity as early as 24 h at which time, non-infected MCF-10A cells (Fig. 1A, a, d) and those infected with a retrovirus encoding the empty vector exhibited a uniform growth pattern (Fig. 4C). These results reveal that the overexpression of E-cadherin induces contact-inhibition at an earlier time when EGF levels are higher, consistent with the phase diagram that we have proposed. Thus, by

tuning the level of cell-cell interactions, the spatial dynamics of epithelial proliferation may be re-engineered.

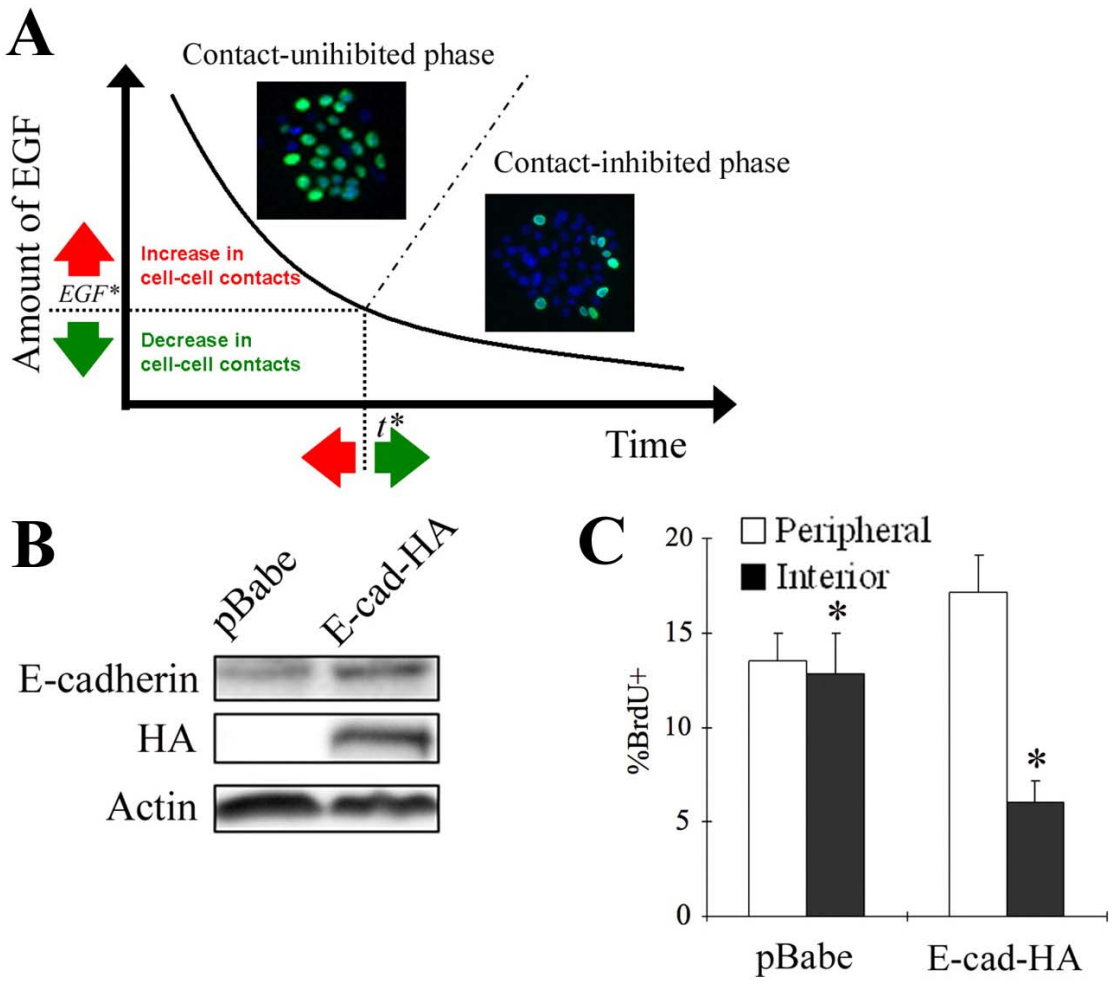

Figure 4: Spatial dynamics of epithelial growth can be modulated by tuning the critical thresholds at which contact-inhibition is triggered. (A) Model of tunable epithelial growth dynamics. Epithelial clusters grow in two modes: the first phase in which both interior and peripheral cells proliferate and a second phase in which only peripheral cells contribute to population growth. The transition from the first to second mode occurs at a threshold EGF concentration (*EGF**) at a critical time (*t**). According

to our phase diagram model, modulating the extent of cell-cell interactions should allow us to manipulate the threshold EGF concentration, and thereby affect the timing of spatial patterns in epithelial proliferation. Insets show representative fluorescence images probed for BrdU uptake (green) and DAPI (blue) for clusters in contact-uninhibited and contact-inhibited phases. (B) MCF-10A cells were retrovirally infected with the empty vector pBabe, or exogenous E-cadherin (E-cad-HA). Cells were seeded at a density of $5x10^3$ cell/cm^2, serum-starved, and treated with 0.1 ng/ml EGF. Ninety minutes later, whole cell lysates were collected, and the extent of overexpression in E-cadherin was determined by immunoblotting for E-cadherin and the epitope tag HA. Equal loading was confirmed by probing for actin. (C) MCF-10A cells infected with retrovirus encoding either the empty vector or E-cad-HA were starved and stimulated with 0.1 ng/ml EGF for 24 h. Percentage of peripheral and interior cells incorporating BrdU was quantified. Error bars indicate s.e.m. (n = 3). The *asterisk* indicates $p < 0.05$.

In summary, our quantitative measurements and analysis lead us to propose a tunable titration model for how contacts and growth factors compete to regulate cell cycle activity. This quantitative model modifies the classical notion that contact-inhibition acts as a switch that is either present or absent in normal versus tumor cells, respectively. Our findings support a more graded perspective of contact-inhibition: During cancer progression, contact inhibition may steadily erode as the threshold amount of EGF shifts lower with every genetic and epigenetic "hit." This tunability of the threshold amount of EGF would seem to be a fragility in cell cycle regulation that is exploited during cancer development. This raises the question of why this property would be preserved through

evolutionary selection. The answer may lie in its potential pivotal role in development. Theoretical models predict that an increase in cell density serves as a negative feedback that quantitatively desensitizes the mitogenic response to soluble factors, thereby self-regulating the size of developing tissues (18, 19). To our knowledge, our results provide the first experimental evidence for such a tunable, quantitative balance between contact and GFs in regulating cell cycle activity. Finally, our model indicates that epithelial clusters grow in two different modes: the first in which both interior and peripheral cells proliferate and a second mode in which only peripheral cells contribute to population growth. Manipulating cells between these modes of proliferation can provide control over population growth rate and tissue geometry, both key parameters in tissue engineering.

Materials and Methods

Cell culture and reagents

MCF-10A cells were cultured in growth medium as described previously (20). For experiments, cells were plated on either glass coverslips (VWR) or two-chambered coverslides (Lab-Tek) in growth medium for 24 h. For G_0 synchronization, cells were maintained in serum-free medium for 24 h (20). The following antibodies were used: anti-actin (Santa Cruz), anti-BrdU (Roche Applied Science), anti-E-cadherin (BD Transduction Laboratories), anti-HA (Covance), anti-phospho-Erk 1/2 (Cell Signaling Technology), anti-phospho-serine 473-Akt (Cell Signaling Technology), HECD-1 (Zymed Laboratories), mouse IgG (Sigma-Aldrich), and Alexa dye-labeled secondary antibodies (Invitrogen-Molecular Probe). The pharmacological inhibitors, PD98059 and LY294002, were obtained from Calbiochem.

Subcloning and retrovirus production and usage

The human cDNA of E-cadherin was kindly provided by P. Wheelock (University of Nebraska Medical Center), and was used to make pBabe-E-cadherin-HA construct. Briefly, the E-cadherin gene was amplified by PCR, with *Bgl*II and *Xho*I sites added to the 5' and 3' ends, respectively. In addition, to facilitate the detection of the exogenous proteins, HA epitope (YPYDVPDYA) was added to the C-terminus of the construct. The PCR product was digested with *Bgl*II and *Xho*I, and ligated into the pBabe vector. The coding sequence of pBabe-E-cadherin-HA was verified by DNA sequencing (Laragne).

Retrovirus was produced by triple transfection of HEK 293T cells and used to infect MCF-10A cells as described previously (20).

Knockdown using siRNA

siRNA targeting E-cadherin mRNAs (sense 5'-GAUUGCACCGGUCGACAAATT-3', antisense 5'-UUUGUCGACCGGUGCAAUCTT-3') was obtained from Integrated DNA Technology. Non-specific control siRNA was purchased from Ambion. siRNAs were transfected using Lipofectamine RNAiMAX (Invitrogen).

Quantification of ligand depletion

Cell number was determined by suspending cells with enzymatic treatment, and cell counting using a hemacytometer. To quantify the amount of EGF, samples from the medium were collected, pre-cleared by centrifugation and stored at -20^{o}C. EGF concentration was assayed simultaneously in all frozen samples using an enzyme-linked immunosorbent assay (ELISA) kit (R&D Systems).

Immunofluorescence and image acquisition

Fixed cells were permeabilized, blocked and sequentially incubated with primary and secondary antibodies. The cells were co-stained with DAPI (Sigma-Aldrich) or phalloidin (Molecular Probe) and mounted using ProLong Gold Antifade (Molecular Probe). Images were acquired using the Zeiss Axiovert 200M microscope. Reagents used for each type of stain are summarized in Supporting Text.

Cell lysis and Western blot

Cell lysis and Western blot were performed as described previously (20).

Fabrication of micro-patterned substrates

Fibronectin was micro-patterned on gold-coated, chambered coverslides by micro-contact printing using a PDMS stamp. Briefly, UV light was passed through a chrome mask containing the pattern (NRF at UCLA) onto a layer of SU-8 photoresist to make a mold. PDMS was cast into this mold to make the stamp. The stamp was "inked" with 16-Mercaptohexadecanoic acid (Sigma Aldrich) dissolved in 99% ethanol and was used to print gold-coated chambered coverslides. The unprinted area was passivated using PEG(6)-Thiol (Prochimia) dissolved in 99% ethanol. After washing, the coverslide was treated with EDC and Sulfo-NHS (Pierce) to activate the acid, priming it to cross-link with amine groups in fibronectin (Sigma-Aldrich).

Acknowledgements

We thank members of the Asthagiri group for helpful discussions, An-Tu Xie for his involvement in the early stages of image analysis, and Celeste Nelson and Casim Sarkar for comments on the manuscript. This work was supported by the Concern Foundation for Cancer Research and the Jacobs Institute for Molecular Engineering for Medicine.

References

1. Hanahan D & Weinberg RA (2000) The hallmarks of cancer *Cell* **100,** 57-70.
2. Steinberg MS & McNutt PM (1999) Cadherins and their connections: adhesion junctions have broader functions *Curr Opin Cell Biol* **11,** 554-560.
3. Caveda L, Martin-Padura I, Navarro P, Breviario F, Corada M, Gulino D, Lampugnani MG, & Dejana E (1996) Inhibition of cultured cell growth by vascular endothelial cadherin (cadherin-5/VE-cadherin) *J Clin Invest* **98,** 886-893.
4. Goichberg P & Geiger B (1998) Direct involvement of N-cadherin-mediated signaling in muscle differentiation *Mol Biol Cell* **9,** 3119-3131.
5. Gray DS, Liu WF, Shen CJ, Bhadriraju K, Nelson CM, & Chen CS (2008) Engineering amount of cell-cell contact demonstrates biphasic proliferative regulation through RhoA and the actin cytoskeleton *Exp Cell Res*. **314**: 2846-2854.
6. Levenberg S, Yarden A, Kam Z, & Geiger B (1999) p27 is involved in N-cadherin-mediated contact inhibition of cell growth and S-phase entry *Oncogene* **18,** 869-876.
7. Perrais M, Chen X, Perez-Moreno M, & Gumbiner BM (2007) E-cadherin homophilic ligation inhibits cell growth and epidermal growth factor receptor signaling independent of other cell interactions *Mol. Biol. Cell* E06-04-0348.
8. St Croix B, Sheehan C, Rak JW, Florenes VA, Slingerland JM, & Kerbel RS (1998) E-Cadherin-dependent growth suppression is mediated by the cyclin-dependent kinase inhibitor p27(KIP1) *J Cell Biol* **142,** 557-571.

9. Cole BK, Curto M, Chan AW, & McClatchey AI (2008) Localization to the cortical cytoskeleton is necessary for Nf2/merlin-dependent epidermal growth factor receptor silencing *Mol Cell Biol* **28,** 1274-1284.

10. Curto M, Cole BK, Lallemand D, Liu C-H, & McClatchey AI (2007) Contact-dependent inhibition of EGFR signaling by Nf2/Merlin *J Cell Biol* **177,** 893-903.

11. Lampugnani MG, Orsenigo F, Gagliani MC, Tacchetti C, & Dejana E (2006) Vascular endothelial cadherin controls VEGFR-2 internalization and signaling from intracellular compartments *J Cell Biol* **174,** 593-604.

12. Lampugnani MG, Zanetti A, Corada M, Takahashi T, Balconi G, Breviario F, Orsenigo F, Cattelino A, Kemler R, Daniel TO, *et al.* (2003) Contact inhibition of VEGF-induced proliferation requires vascular endothelial cadherin, beta-catenin, and the phosphatase DEP-1/CD148 *J Cell Biol* **161,** 793-804.

13. Weis WI & Nelson WJ (2006) Re-solving the cadherin-catenin-actin conundrum *J Biol Chem* **281,** 35593-35597.

14. Nelson CM, Jean RP, Tan JL, Liu WF, Sniadecki NJ, Spector AA, & Chen CS (2005) Emergent patterns of growth controlled by multicellular form and mechanics *Proc Natl Acad Sci USA* **102,** 11594-11599.

15. Carpenter G (2000) The EGF receptor: a nexus for trafficking and signaling *Bioessays* **22,** 697-707.

16. Liu WF, Nelson CM, Pirone DM, & Chen CS (2006) E-cadherin engagement stimulates proliferation via Rac1 *J Cell Biol* **173,** 431-441.

17. Jones SM & Kazlauskas A (2001) Growth-factor-dependent mitogenesis requires two distinct phases of signalling *Nat Cell Biol* **3,** 165-172.

18. Hufnagel L, Teleman AA, Rouault H, Cohen SM, & Shraiman BI (2007) On the mechanism of wing size determination in fly development *Proc Natl Acad Sci USA* **104,** 3835-3840.

19. Shraiman BI (2005) Mechanical feedback as a possible regulator of tissue growth *Proc Natl Acad Sci U S A* **102,** 3318-3323.

20. Graham NA & Asthagiri AR (2004) Epidermal growth factor-mediated T-cell factor/lymphoid enhancer factor transcriptional activity is essential but not sufficient for cell cycle progression in nontransformed mammary epithelial cells *J Biol Chem* **279,** 23517-23524.

Supporting Information

Quantification of immunofluorescne signals of phospho-proteins

For imaging ppErk or ppAkt, we started with a sample that is expected to give the highest FITC signal (e.g. 10 ng/ml EGF). Using this positive control, an exposure time was empirically chosen so that the highest pixel intensity in a given field is close to the saturation level (i.e. 255). The chosen exposure time was confirmed not to saturate the FITC signal in other fields of the positive control sample. These steps identify an exposure time that maximizes the dynamic range of quantification of ppErk and ppAkt. This exposure time was then used to capture images from all other samples in a given trial.

Nuclear phospho-protein signal intensity was quantified by first tracing the perimeter of each nucleus. The area and the total FITC intensity of each nucleus were determined using MATLAB. The mean background intensity per pixel was also calculated for each image from the region containing no cells. This background level was multiplied by the area of the nucleus and was subtracted from the total nuclear FITC intensity to determine the final phosphor-protein signal intensity for each nucleus.

Table 1: Details of reagents used in immunofluorescence for each stain

Application	Fixation reagents	Permeabilization	Dehydration	Blocking Solution
BrdU	70% EtOH (pH2) w/ 15 mM glycine (-20°C)	N/A	N/A	10% goat serum + 0.1% BSA in PBS
Vinculin	4% Formalin	0.2% TritonX-100	N/A	10% goat serum + 0.1% BSA in PBS
ppErk/pAkt	Freshly prepared 2% paraformaldehyde (pH 7.4) + Inhibitors[a]	0.5% NP-40 + Inhibitors	Pure MeOH (-20°C)	Blocking buffer[b]

Phosphatase inhibitors[a]: 1mM sodium orthovanadate (Sigma-Aldrich), 10mM sodium fluoride (Sigma Aldrich), and 10mM β-glycerophosphate (Sigma-Aldrich)

Blocking buffer[b]: 130 mM NaCl, 7 mM Na_2HPO_4, 3.5 mM NaH_2PO_4, 7.7 mM NaN_3, 0.1% bovine serum albumin, 0.2% Triton X-100, 0.05% Tween-20 (all from Sigma-Aldrich), and 10% goat serum (Debnath et al 2003)

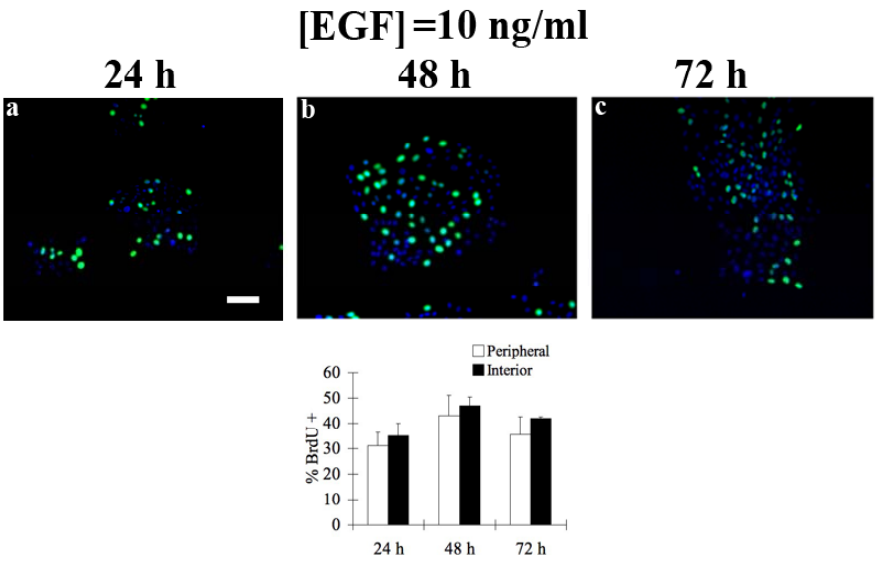

Figure S1: DNA synthesis following initial treatment with 10 ng/ml EGF. Percentage of peripheral and interior cells incorporating BrdU at 24, 48, 72 h after starved MCF-10A cells were stimulated with 10 ng/ml EGF. The *error bars* represent s.e.m. (n = 2). The scale bar represents 100 μm.

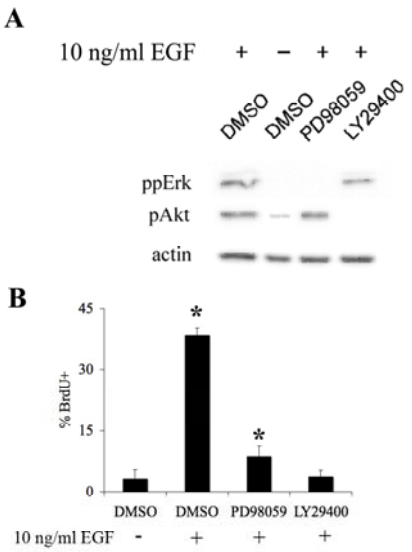

Figure S2: Erk and Akt signaling is essential for EGF-mediated proliferation of MCF-10A cells. (A) Serum-starved MCF-10A cells were pre-treated for 2 hours with PD98059 (50μM), LY29400 (50 μM), or the solvent DMSO and then stimulated with 10 ng/ml EGF or left untreated. The effect of the drugs on (A) Erk and Akt signaling pathways (15 min after stimulation) and (B) BrdU uptake (24 h after stimulation) was determined by Western blot and immunofluorescence staining, respectively. Western blotting was conducted with antibodies against ppErk (T202/Y204) and pAkt (S473), respectively. Equal loading was confirmed by probing with an anti-actin antibody. The *error bars* indicate s.e.m. (n=2). The *asterisk* indicates $p < 0.01$.

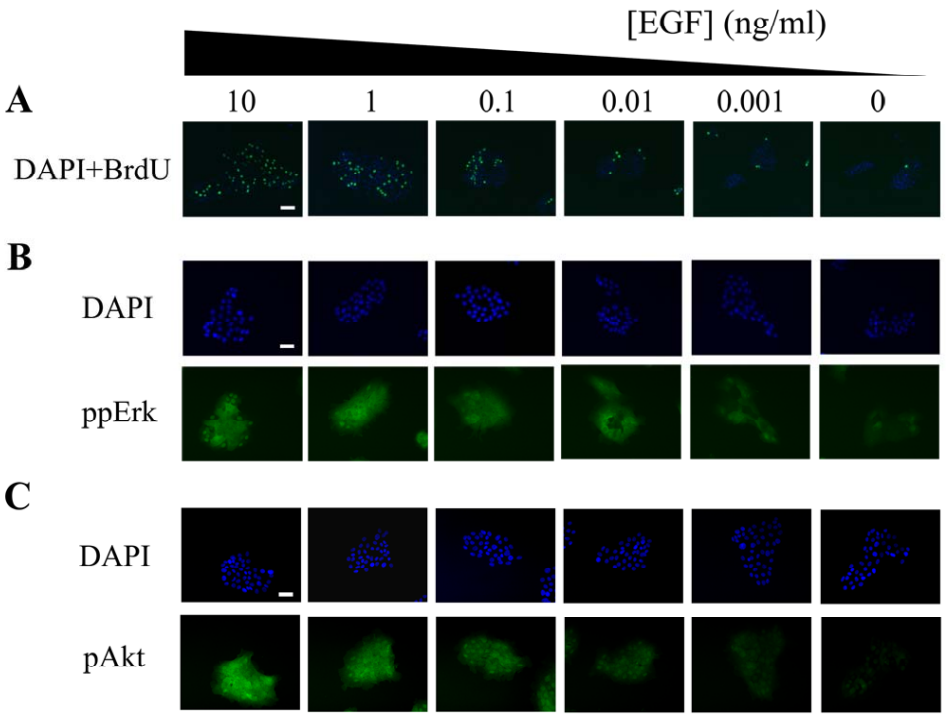

Figure S3: The effect of EGF treatment on DNA synthesis, ppErk and pAkt signals in MCF-10A cell clusters. See legend of Fig. 2 for experimental details. The scale bars represent (A) 100 and (B, C) 50 μm.

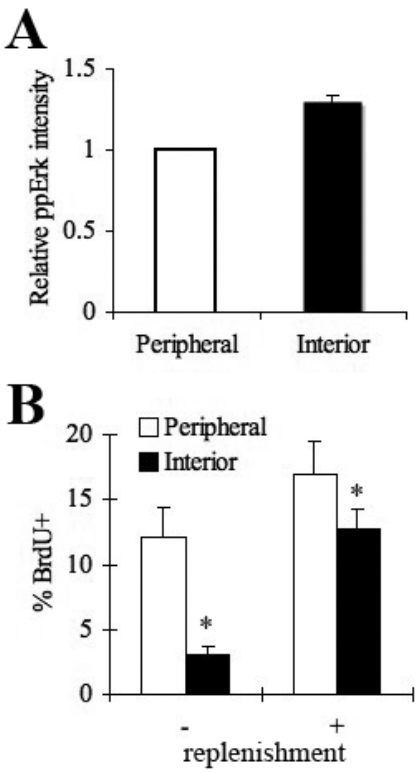

Figure S4: EGF replenishment rescues Erk signaling and cell cycle activity. (A) The level of ppErk in peripheral and interior cells following 15 min of EGF replenishment. (B) The percentage of peripheral and interior cells incorporating BrdU was quantified 24 h after medium was (+) or was not (-) replenished. The *error bars* indicate s.e.m. (n=2-5). The *asterisk* indicates $p < 0.01$.

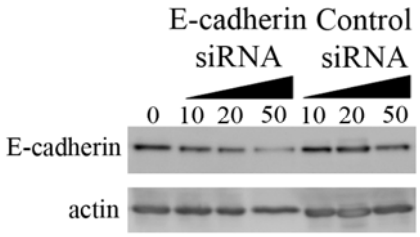

Figure S5. Effect of siRNA treatment on E-cadherin expression. Cells were transfected with control or E-cadherin siRNA in serum-free medium. The extent of knockdown in E-cadherin was determined by Western blot. Equal loading was confirmed by probing for actin.

Chapter III. Substratum stiffening promotes the quantitative, progressive loss of contact-inhibition of proliferation

Abstract

Cancer progression occurs through multiple genetic and epigenetic perturbations. Elucidating how these perturbations collectively confer selective advantages, such as unconstrained proliferation, is central to our understanding of disease progression and for developing treatment strategies. Here, we show that (1) there are measurable, quantitative degrees of contact-inhibition of proliferation, and that (2) the stiffening of the microenvironment, a widely observed perturbation during cancer development, promotes a quantitative, progressive loss of contact-inhibition. Even when substratum stiffening has no discernible effect on the phenotype of contact-inhibition, it significantly reduces the threshold amount of EGF needed to transition cells from contact-inhibited to contact-independent proliferation. Thus, the threshold amount of EGF provides a metric of the extent of contact-inhibition. Quantifying the threshold EGF level reveals the potent synergism between matrix stiffening and EGF signaling. Matrix stiffening reduces the EGF threshold by over two orders-of-magnitude, thereby markedly reducing the extent of EGF amplification needed to switch into contact-independent proliferation. These potent effects of substratum stiffening involve the erosion of cell-cell contacts, changes in nuclear compartmentation of ZO-1, and the disruption of subcellular localization of EGFR, leading to a selective effect on ERK, but not Akt, signaling. Our findings have direct implications for our understanding of multi-hit cancer progression and offer design

principles for engineering spatial patterns of growth of multicellular structures using synthetic mechanically-tunable biomaterials.

Manuscript prepared for submission by Kim. J.-H. and A. R. Asthagiri

Introduction

A hallmark of normal epithelial cells is contact-inhibition of proliferation (1). In contrast, cancer cells proliferate chaotically in a contact-independent manner, leading to tumor formation. Elucidating how epithelial cells transition from a contact-inhibited state to a contact-independent mode of proliferation will provide insight into a pivotal step in cancer progression.

Epithelial cells reside in a microenvironment replete with stimuli, and cell-cell contact is just one among many signals that regulate cell proliferation. Parsing how contact-inhibition is enforced in a rich microenvironment that also presents conflicting growth-promoting stimuli remains a challenge. Both biochemical and physical mechanisms seem to be involved. Cell-cell contacts affect GF-mediated intracellular signaling pathways, such as ERK and Akt, to suppress cell cycle progression (2-3). Further upstream, GF receptors themselves interact with receptors that mediate cell-cell adhesion, such as E/VE-cadherin (4-6). In addition, cadherins mediate contact-inhibition by mechanically coupling neighboring cells and affecting the distribution of traction forces in multicellular clusters (7). Atypical cadherin, Fat, and ERM family proteins, Merlin, and Expanded, are also implicated in the Hippo pathway which has emerged as one of the key regulators of contact-inhibition and organ size determination in both *Drosophila* and mammalian systems (8-9).

While progress continues in uncovering the physiochemical mechanisms mediating contact-inhibition, it remains unclear how these mechanisms collectively reconcile the competing influences of GFs and cell-cell contact on cell cycle activity. We recently proposed a quantitative framework for contact-inhibition in which the levels of cell-cell contact and epidermal growth factor (EGF) determine whether cell proliferation is contact-inhibited or contact-independent (Fig. 1) (10). A significant implication of the proposed state diagram is that contact-inhibition and its loss during cancer development must be viewed from a quantitative perspective. It suggests that cancer-promoting perturbations may quantitatively shift normal cells closer to the transition line to contact-independence. While the effect of such perturbations on the gross phenotype would remain latent (i.e., proliferation would still be contact-inhibited), the perturbations would have a quantitative, measureable effect on the threshold amount of EGF needed to transform cells into a contact-independent mode of proliferation. Thus, the proposition is that the "degree of contact-inhibition" may be quantified by how close a cell system is to the transition line and that the effect of multiple seemingly latent hits can be tracked by measuring changes in the EGF threshold.

Here, we set out to explore whether physiologically-relevant cancer-promoting events actually cause such measurable quantitative shifts in the degree of contact-inhibition of epithelial cells. To test this hypothesis, we focused on a key event during cancer progression: the increase in the rigidity of tumor environments (11-12). Our results demonstrate that stiffening the adhesive substratum quantitatively shifts non-transformed, contact-inhibited epithelial cells closer to the transition into a contact-

independent state. Increasing the stiffness of a collagen- or fibronectin-coated elastic substrate reduces the threshold amount of EGF needed to induce tumor-like, contact-independent proliferation. By reducing the EGF threshold, matrix stiffening reduces the extent to which EGF signaling must be amplified to enable contact-independent growth, thereby quantitatively facilitating transformation. Our findings provide quantitative insights into how matrix compliance and EGF signaling synergistically affect contact-inhibition. These insights have implications for our understanding of cancer progression and offer design principles for engineering spatial patterns and rates of growth of multicellular structures using synthetic mechanically-tunable biomaterials.

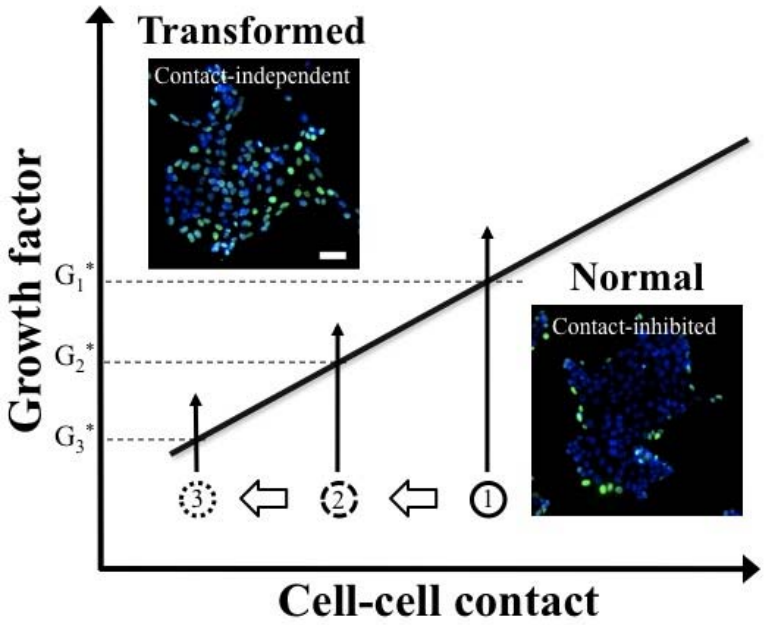

Fig. 1. State diagram for contact-inhibition of proliferation and the hypothesis of quantitative, progressive loss of contact-inhibition. Contact-inhibited cells (1)

transition to a contact-independent mode of proliferation upon crossing a critical threshold level of growth factor (G_1^*). We hypothesize that cancer-promoting perturbations may quantitatively shift normal cells closer to the transition line to contact-independence (1 → 2 → 3). Although such perturbations may not have a phenotypic effect (i.e., cells remain contact-inhibited), we hypothesize that these perturbations may have a quantitative, measurable effect on the threshold amount of EGF (G_1^* → G_2^* → G_3^*) needed to transform normal cells to achieve contact-independent growth. Insets show representative fluorescence images probed for BrdU incorporation (green) and DAPI (blue) for epithelial clusters in contact-inhibited and contact-independent states of proliferation. (Scale bar, 50 μm.)

Results

Substratum compliance affects spatial patterns in proliferation and contact-inhibition of proliferation

To explore the effect of substratum compliance on contact-inhibition of proliferation, we cultured Madin-Darby canine kidney (MDCK) epithelial cells on collagen (ColI)-coated polyacrylamide gels of varying stiffness and identical adhesion ligand composition (Fig. S1). Over a range of substratum compliance (7-31 kPa), cells formed two-dimensional multicellular clusters. On the most compliant substratum (7 kPa), treatment with a supra-saturating dose of EGF (100 ng/ml) induced BrdU uptake only at the periphery of clusters (Fig. 2Ai and B). Interior cells did not exhibit cell cycle activity on soft substrates. Increasing the stiffness of the substratum eliminated

this spatial pattern in proliferation (Fig. 2Aiii and B). Quantitative analysis showed that BrdU uptake of interior cells was equivalent to that of peripheral cells on the stiffer substrates (17-31 kPa) (Fig. 2B).

To confirm that the observed spatial pattern in proliferation on soft substrates was in fact due to contact-inhibition, we tested the effect of diminishing cell-cell interactions by down-regulating E-cadherin expression using siRNA. Compared to a control construct, transfection with siRNA reduced E-cadherin expression by ~50% in MDCK cells grown on the compliant substratum (Fig. S2). Transfection with a control siRNA had no effect on the spatial pattern in proliferation on soft substrates (Fig. 2C). In contrast, the spatial pattern was eliminated in cells treated with E-cadherin siRNA. These results demonstrate that E-cadherin-mediated cell-cell contact is involved in establishing the spatial pattern in proliferation on soft substrates.

Taken together, these observations reveal that cell-cell contact effectively inhibits cell cycle activity among interior cells on soft substrates, leading to spatial patterns in proliferation. In contrast, on stiffer substrates, cell-cell contact is not sufficient to halt cell proliferation, leading to uniform cell cycle activity throughout the multicellular cluster.

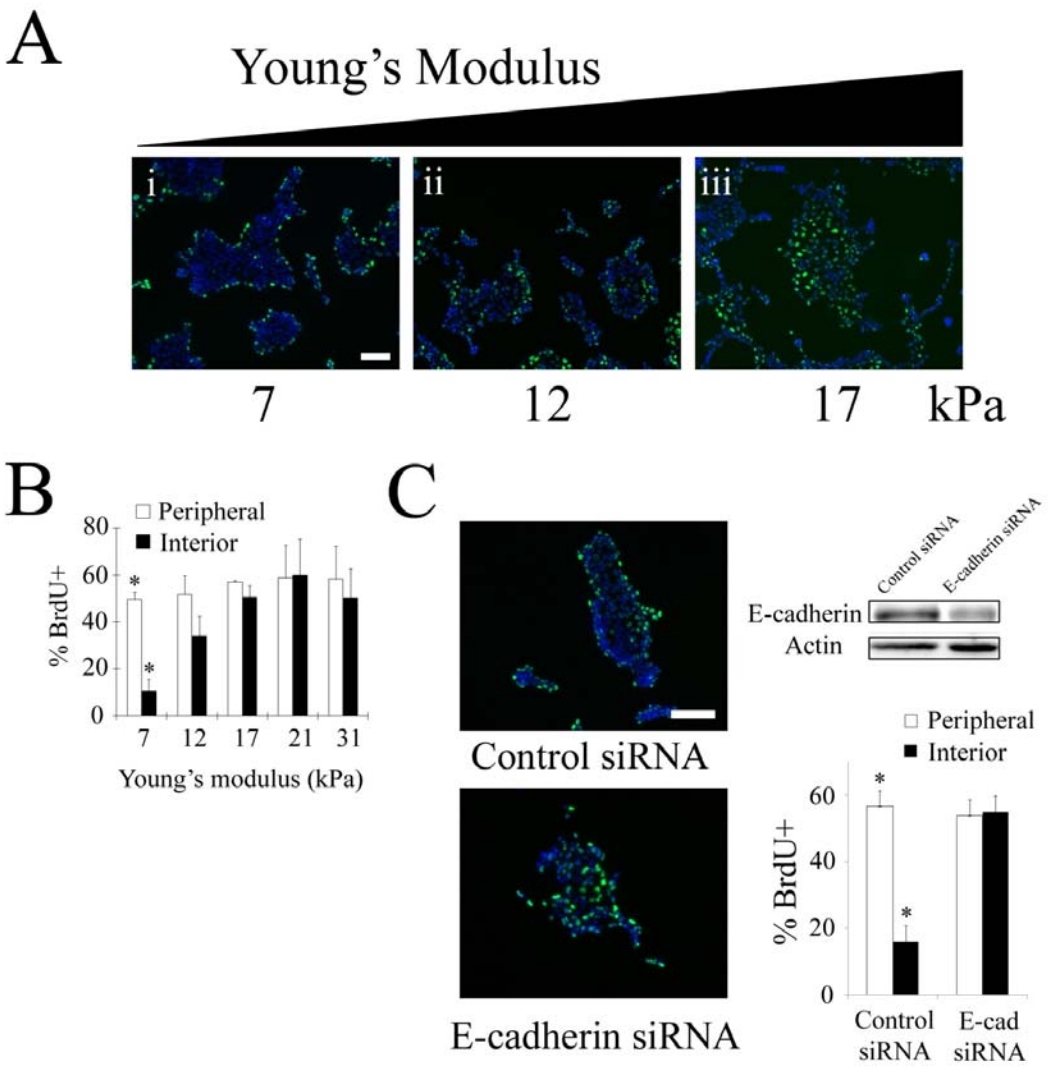

Fig. 2. Substratum compliance affects spatial patterns in cell-cycle activity and contact-inhibition of proliferation. (A) MDCK cells cultured on ColI-coated polyacrylamide gels of varying stiffness were treated with 100 ng/ml EGF following serum starvation. BrdU incorporation (green) and DAPI staining (blue) were assessed 16 h after EGF treatment. (B) The graph shows the quantitation of the percentage of peripheral and interior cells undergoing DNA synthesis. Error bars, s.d. (n = 2-5), *, $P < 0.01$. (C) The effect of down-regulating E-cadherin on spatial patterns in proliferation

induced by compliant substrata. MDCK cells grown on soft substrates were transfected with control or E-cadherin siRNA in serum-free medium for 24 h. Cells were then stimulated with 100 ng/ml EGF. BrdU uptake (green) and DAPI (blue) were assessed 16 h later. Percentage of peripheral and interior cells incorporating BrdU was quantified. The extent of knockdown in E-cadherin was determined by Western blot. Equal loading was confirmed by probing for actin. Error bars, s.d. (n = 2), *, $P < 0.01$. (Scale bars, 100 μm.)

Substratum compliance quantitatively modulates the transition between contact-inhibited and contact-independent proliferation

Our initial experiments showing the effect of substratum compliance on contact-inhibition were conducted at a single supra-saturating dose of EGF. We have previously shown that epithelial cells transition between contact-inhibited and contact-independent modes of proliferation when the amount of EGF crosses a critical threshold level (Fig. 1). Thus, we reasoned that it may be important to evaluate the effect of substratum compliance on contact-inhibition in the context of a third critical aspect of the microenvironment, soluble GFs.

To begin to examine this interplay between EGF, substratum compliance and cell-cell contact, we examined cell cycle activity in clusters of non-transformed human mammary epithelial cells (MCF-10A) cultured on substrates of different mechanical compliance and exposed to a broad range of EGF concentrations. On soft substrates (7 kPa), at the low and intermediate EGF concentrations (0.01 and 1 ng/ml EGF,

respectively), peripheral cells proliferated with a higher propensity than interior cells, exhibiting the spatially-patterned, contact-inhibited mode of proliferation (Fig. 3Ai and Aii). The fraction of interior cells undertaking DNA synthesis was approximately 2-fold lower than the fraction of cells uptaking BrdU in the periphery of the clusters (Fig. 3B). However, as the EGF concentration was increased above 1 ng/ml, the spatial disparity in proliferation diminished such that an equal fraction of interior and peripheral cells incorporated BrdU when stimulated with 100 ng/ml EGF (Fig. 3Aiii and B). These findings reveal that even on soft surfaces, both contact-inhibited and contact-independent modes of proliferation can occur and that the state of the system depends not only on substratum stiffness, but also on whether the level of EGF is above or below the threshold (in this case, ~1 ng/ml EGF).

A key question is whether this EGF threshold is sensitive to substratum compliance. That is, does changing substratum compliance quantitatively modulate the transition point between contact-inhibition and contact-independent proliferation? To address this question, we repeated the EGF dose study, now using stiffer substrates (31 kPa). As with the soft surface, we found that MCF-10A cells exhibited both contact-inhibited and contact-independent modes of proliferation. At relatively low EGF concentrations (0.001 and 0.01 ng/ml), BrdU uptake was concentrated at the periphery of clusters, exhibiting a spatial pattern in proliferation (Fig. 3Aiv and B). Upon increasing the EGF concentration above 0.01 ng/ml, the spatial pattern in cell cycle activity was eliminated (Fig. 3Av, Avi, and B). In particular, at an EGF concentration of 1 ng/ml when cells on the soft surface were contact-inhibited (Fig. 3Aii), cells on the stiff

substrate exhibited contact-independent growth with both peripheral and interior cells proliferating with equal propensity (Fig. 3Av).

These results demonstrate that substratum stiffening (from 7 to 31 kPa) quantitatively reduces the EGF threshold from 1 to 0.01 ng/ml in MCF-10A cells. Thus, growth is not simply contact-inhibited on soft substrates and contact-independent on stiff substrates. Rather, changes in substratum compliance have a quantitative effect on the degree of contact-inhibition. Matrix stiffening reduces the EGF threshold at which the system transitions from a contact-inhibited to contact-independent mode of proliferation, thereby quantitatively facilitating this transformation.

We corroborated this quantitative effect of substratum compliance in another epithelial cell system. Cell cycle activity was assessed in MDCK cell clusters, now in response to varying both substratum stiffness and EGF concentration. On soft substrates (7 kPa), MDCK cells exhibited contact-inhibition even at supra-saturating doses of EGF (100 ng/ml), suggesting that the threshold EGF is too high to attain contact-independent growth on these substrates (Fig. S3A and B). However, on substrates of intermediate stiffness (17 kPa), MDCK cells underwent a clear transition from contact-inhibited to contact-independent growth at a threshold of approximately 0.1 ng/ml EGF. Thus, stiffening the substrate reduces the EGF threshold to a physiologically-accessible level. Finally, upon further stiffening the substratum to a Young's modulus of 31 kPa, cells exhibited contact-independent proliferation for all EGF concentrations, suggesting that the threshold EGF has diminished below the range tested in our experiments.

Taken together, these results in MCF-10A and MDCK epithelial cells demonstrate that substratum stiffening quantitatively modulates contact-inhibition by reducing the EGF threshold needed to shift cells from contact-inhibited to contact-independent proliferation. In addition, the results show that epithelial cell systems can exhibit different sensitivities to substratum compliance (Fig S3C). Over the same range of substratum compliance (7-31 kPa), the EGF threshold shifted two orders-of-magnitude in MCF-10A cells. Meanwhile, in MDCK cells, the effect extended even beyond the range of EGF concentrations used in our experiments. This difference in sensitivity to substratum compliance may arise from the difference in adhesion structures between two cell types. For example, MCF-10A cells lack Crumbs3 required for the tight junction formation and full epithelial cell polarity (13).

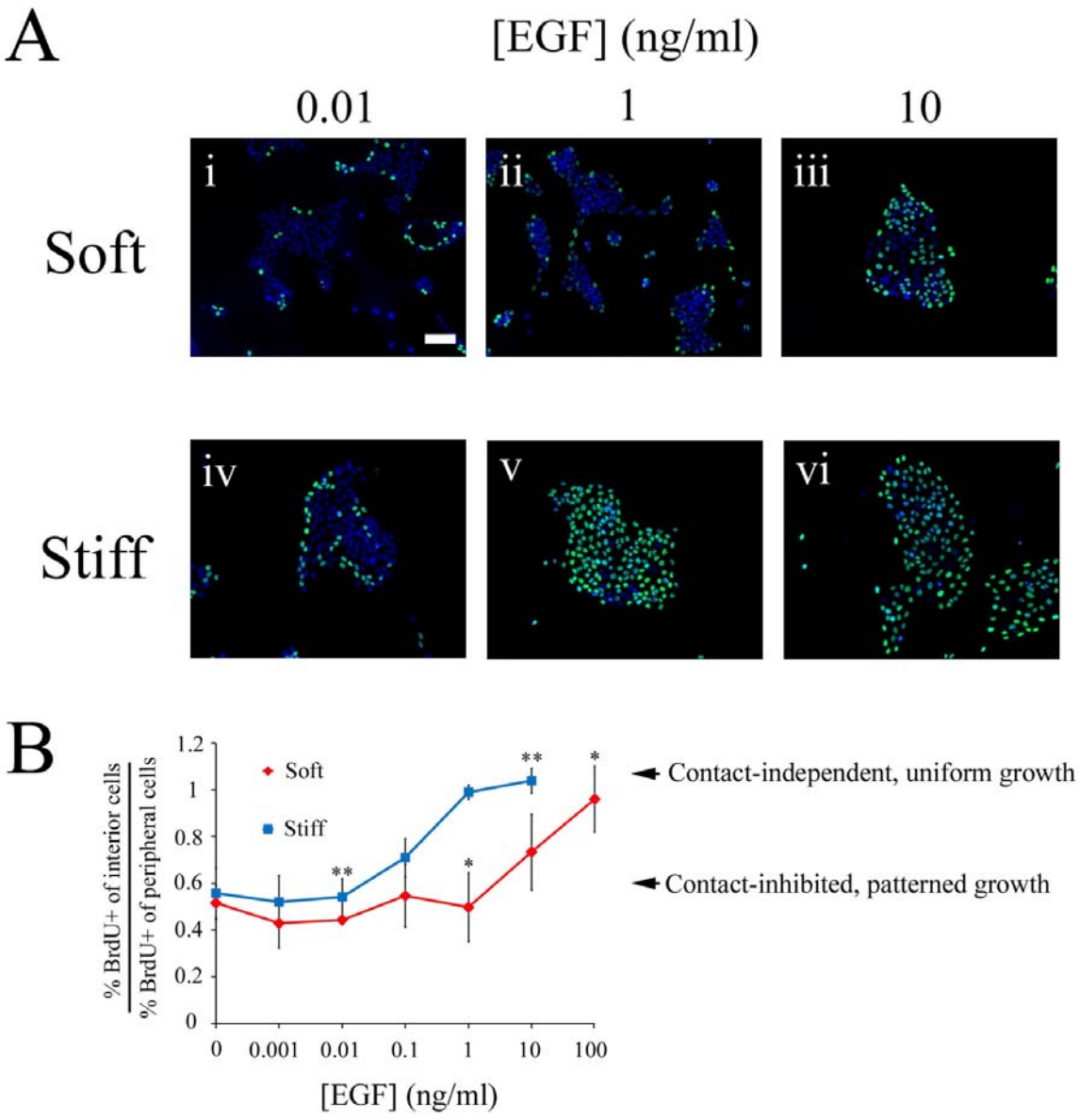

Fig. 3. Substratum stiffening reduces the EGF threshold needed to transition from contact-inhibited to contact-independent proliferation. MCF-10A cells plated on soft and stiff substrates coated with fibronectin were serum-starved for 24 h and stimulated with the indicated doses of EGF or left untreated. (A) BrdU uptake (green) and DAPI staining (blue) were assessed 22 h after EGF treatment. (B) The fractions of interior and

peripheral cells incorporating BrdU were quantified and the ratio of these two fractions is plotted as a function of EGF concentration. Error bars, s.d. (n = 2-3), * and **, $P < 0.01$. (Scale bar, 100 μm.)

Substratum compliance affects the maturation of cell-cell contacts

Our results reveal that stiffening the adhesive matrix reduces the threshold EGF at which the system transitions from contact-inhibited to contact-independent growth. This suggests that matrix stiffening may slide the cell system to the left on the state diagram (Fig. 1). That is, increasing stiffness may attenuate cell-cell contacts. To test this possibility, we examined the subcellular localization of E-cadherin and ZO-1. In mature epithelial monolayers, E-cadherin localizes typically to basolateral regions while ZO-1 is found in an apical band of mature cell-cell contacts (14).

In MDCK cells, we observed strong basolateral localization of E-cadherin at cell-cell junctions (indicated by white arrows) in cells seeded on soft substrates (Fig. 4A and B, left). In contrast, on stiff substrates, E-cadherin exhibited partial basolateral localization in addition to significant residual localization in the cytosol (Fig. 4A and B, right). These observations suggest that more mature cell-cell contacts are established on more compliant substrates.

This effect of substratum compliance on contact maturation was even more evident in the subcellular localization of the tight junction-associated protein, ZO-1. Apical localization of ZO-1 at cell-cell contacts was sharply evident in cells on soft

substrates, while only modestly present on stiff substrates (Fig. 4B). More strikingly, we observed significant differences in ZO-1 nuclear localization on soft versus stiff substrates (Fig 4B and C). On the soft surface, ZO-1 was found in the cytoplasm and nucleus only among the cells at the periphery of the cluster. The growth-arrested cells in the interior of the cluster did not exhibit nuclear ZO-1 localization. In contrast, on the stiff surface, significant nuclear localization of ZO-1 was observed among all cells in the cluster. This nuclear localization of ZO-1 was highly correlated with the proliferation patterns on soft and stiff substrates (Fig. 2). Together, these results demonstrate that increasing substratum stiffness disrupts contact maturation as evidenced by the disorganization of cell-cell junctions at a molecular level.

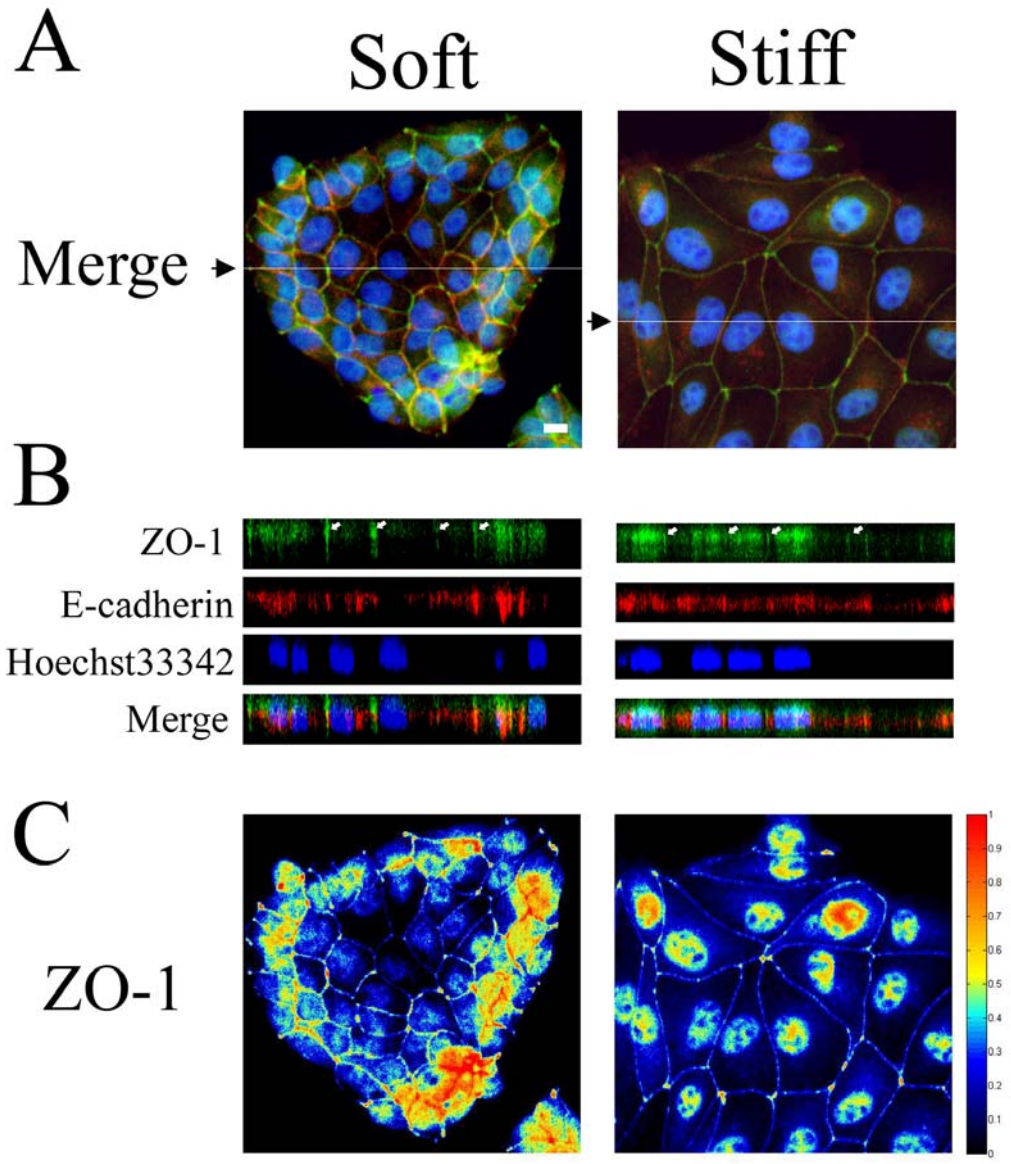

Fig. 4. Substratum compliance affects the molecular organization of adhesion structures at cell-cell contacts. MDCK cells cultured on soft and stiff substrata were serum starved for 24 h and immunostained for ZO-1 (green) and E-cadherin (red). Nuclei were co-stained with Hoechst33342 (blue). (A) Merged images were generated by projecting down in the *z*-direction so that each pixel represents the average intensity value over the *z*-stacks. White lines (pointed by black arrows) in the merged images

indicate the planes for which *x-z* section views were generated. (B) *x-z* view of the plane indicated by the white line in the merged image. White arrows indicate cell-cell contacts. (C) Heat maps of ZO-1 represent the relative abundance of the molecule within epithelial clusters across the *z*-stacks. (Scale bar, 10 μm.)

Enhanced contact-maturation on soft substrates selectively affects EGF receptor (EGFR) and ERK signaling, but not Akt signaling

The emerging model from our data is that stiff substrates disrupt cell-cell contacts and sensitize cellular response to EGF, thereby reducing the threshold EGF needed to transform the system into a contact-independent mode of proliferation. To elucidate how substratum stiffening-mediated disruption of cell-cell contacts affects EGF signaling, we examined the effect of modulating substratum compliance on the subcellular localization of EGFR. On a soft substratum, EGFR was highly localized to the basolateral membrane compartments at which stable E-cadherin-mediated adherens junctions formed (Fig. 5A, left, indicated by white arrows). In contrast, on a stiffer substratum, EGFR seemed to be evenly distributed among apical and basal membranes without co-localizing with E-cadherin (Fig. 5A, right). These results suggest that substratum stiffening may reduce the EGF threshold by disrupting cell-cell contacts and de-localizing EGFR from mature cell-cell contacts.

To determine whether this change in EGFR sequestration affects receptor signaling, we assayed the phosphorylation of EGFR on the Y1068 residue (Grb2 binding site) following 15 min of EGF stimulation at 100 ng/ml in MDCK clusters grown on soft

and stiff substrates. In contrast to the spatially uniform phosphorylation in cell clusters on the stiff substratum, both the level of EGFR phosphorylation and the formation of intracellular vesicles through EGFR internalization were diminished in the interior of cell clusters on the soft substratum (Fig. 5Bi). This spatial pattern in EGFR phosphorylation and internalization corresponds to the observed growth patterns (Fig. 2). We quantified the total cytoplasmic level of phospho-Y1068 EGFR in single cells at the periphery and interior of clusters. Consistent with our qualitative assessment, EGFR Y1068 phosphorylation was diminished in central cells by 20% relative to peripheral cells on the soft surface, but this spatial pattern was not found on the stiff substratum.

To determine whether these effects of substratum compliance on EGFR localization and phosphorylation transduce to downstream signaling pathways, we examined two EGF-mediated intercellular signals, ERK and Akt, that are involved in cell cycle regulation (15). Following 15 min of stimulation with 100 ng/ml EGF, cells were immunostained for phospho-ERK and phospho-Akt. On the soft substratum, ERK signaling was diminished by approximately 40% in the interior cells compared to their peripheral counterparts (Fig. 5Bii), correlating to the spatial pattern in EGFR phosphorylation and proliferation in this condition (Fig. 2 and 5Bi). Meanwhile, on stiffer substrates, ERK activation was homogeneous across the cell cluster, consistent with uniform patterns in both EGFR phosphorylation and proliferation. In contrast to ERK, Akt signaling was uniform within cell aggregates regardless of substratum compliance (Fig. 5Biii). Thus, substratum stiffening and the disruption of cell-cell contacts selectively enhance EGF-mediated ERK, but not Akt, signaling and thereby

eliminates the spatial disparity in proliferation, leading to contact-independent proliferation.

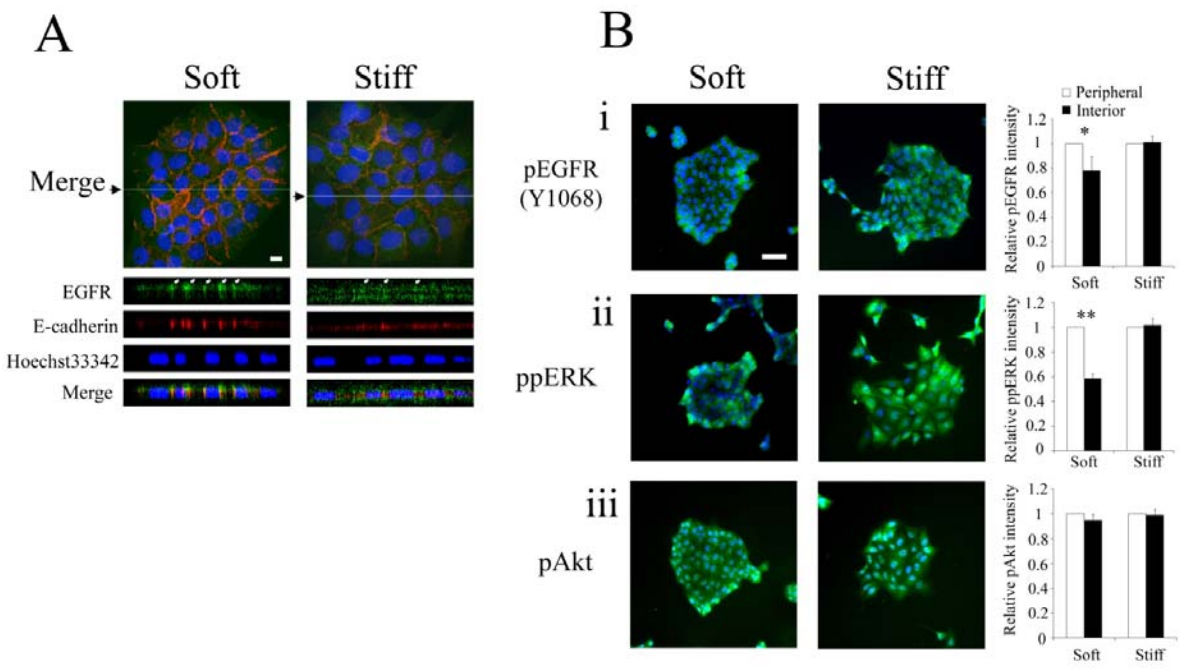

Fig. 5. Substratum compliance affects subcellular localization of EGFR and selectively regulates EGFR and ERK, but not Akt, signaling. (A) Effect of substratum compliance on subcellular localization of EGFR and E-cadherin. MCF-10A cells cultured on soft and stiff substrates were serum starved for 24 h and immunostained for EGFR (green) and E-cadherin (red). Nuclei were co-stained with Hoechst33342 (blue). Merged images represent the fluorescence signals averaged across the *z*-stacks acquired by confocal imaging. *x*-*z* views were generated at the planes indicated by white lines (pointed by black arrows) in the merged images. White arrows indicate cell-cell contacts. (Scale bar, 10 μm.) (B) Substratum compliance affects spatial patterns in EGFR and ERK, but not Akt, phosphorylation. MDCK cells plated on soft and stiff substrates were serum starved for 24 h and stimulated with 100 ng/ml EGF for 15 min.

Phosphorylation of (i) EGFR, (ii) ERK, and (iii) Akt (green) were assessed by immunofluorescence. Nuclei are labeled by staining with DAPI. The bar graphs show the relative intensities of pEGFR, ppERK, and pAkt in peripheral and central cells. Signaling intensities are reported relative to the amount of signals in peripheral cells. Error bars, s.d. ($n = 3$), *, $P < 0.05$, **, $P < 0.01$. (Scale bar, 50 μm.)

Discussion

The progressive loss of contact-inhibition: a quantitative and measurable effect of substratum stiffening

The stiffening of the tumor microenvironment is a hallmark of cancer progression (11). Here, we demonstrate that the microenvironment stiffness works synergistically with EGF signaling to regulate contact-inhibition of proliferation. We provide a framework for gauging how this interplay between mechanical and biomolecular cues in the microenvironment affects the *degree* of contact-inhibition (Fig. 1). Matrix stiffening reduces the EGF threshold that the epithelial system must cross to achieve tumor-like, contact-independent proliferation. Thus, the compliance of the microenvironment modulates how close the cellular system is to the transition line between contact-inhibited and contact-independent modes of proliferation.

The proximity of non-transformed epithelial cells to the transition line is a quantitative, measurable property of contact-inhibition. By measuring the threshold amount of EGF needed to enable contact-independent proliferation, we track

quantitatively the effect of substratum stiffening on contact-inhibition. The magnitude of the effect is significant. Increasing the elastic modulus by 4.5-fold shifts the threshold EGF nearly two orders-of-magnitude in MCF-10A cells (Fig. 3B).

This quantitative metric of contact-inhibition is an important complement to the classical qualitative perspective that normal cells are contact-inhibited while cancer cell proliferation is contact-independent. Cancer arises not from a single perturbation but from the accrual of multiple perturbations that collectively confer advantageous phenotypes, such as contact-independent proliferation. Thus, individual perturbations may have no discernible effect on gross phenotype but yet shift the system closer to a phenotypic transformation. Measuring such phenotypically latent changes in a multicellular system would give insights into how cancer-associated perturbations contribute to the complex process of transformation.

Our results reveal a metric that gauges the progressive loss of contact-inhibition. We demonstrate the utility of this metric in response to a physiologically relevant perturbation, the stiffening of substratum compliance. Unlike some genetic perturbations that produce discrete changes in the activity state of a signaling enzyme, the compliance of the microenvironment is an analog mechanical property whose magnitude may undergo graded changes during cancer progression. Our findings show that such quantitative changes in matrix compliance can modulate the degree of contact-inhibition.

The quantitative effect of substratum compliance on the EGF threshold involves the regulation of cell-cell contacts

Substratum compliance affects traction forces that isolated cells generate on the underlying substratum and the size and content of integrin-mediated focal adhesions (16). Elevated traction forces and integrin-mediated signaling in rigid environments promote proliferation (17). Furthermore, in multicellular aggregates grown on micropatterned surfaces, spatial gradients in traction forces develop across the cell cluster, corresponding to spatial patterns in proliferation (7). In this work, we focused on the effect of substratum compliance on cell-cell contacts. We observed that the quantitative effect of substratum stiffening on contact-inhibition involves the disruption of cell-cell contacts. Stiffer substrates disrupt the localization of E-cadherin and ZO-1 from cell-cell contacts. These observations on two-dimensional compliant substrates are consistent with the effects observed upon stiffening three-dimensional collagen gels and Matrigel (17), suggesting that the mechanical compliance, not the topography, of the cellular microenvironment is the principal effector of contact maturation.

Furthermore, we observed that cells on stiff substrates exhibit distinct nuclear localization of ZO-1 that correlates with the uniform, contact-independent mode of proliferation. In contrast, on soft substrates, nuclear localization of ZO-1 was observed only in the peripheral cells of a cluster, correlating with the spatial pattern in proliferation. This modulation of nuclear localization of ZO-1 by substratum compliance may be mechanistically involved in cell cycle regulation. Nuclear ZO-1 has been observed to shift to cell-cell junctions during the maturation of confluent MDCK monolayers (18),

and this event sequesters a transcription factor, ZONAB, out of the nucleus, preventing it from transcribing genes required for cell cycle activity (19).

In addition to modulating direct communication between cell-cell contacts and the nucleus, substratum compliance affected EGFR localization and downstream signaling pathways. EGFR was sequestered to the mature cell-cell contacts in cell clusters grown on soft substrates. This sequestration corresponded to reduced EGFR internalization and phosphorylation and the attenuation of ERK, but not Akt, signaling among central cells in the cluster. Similar attenuation of EGFR and ERK signaling has been observed in confluent epithelial monolayers that undergo contact-inhibition on tissue culture plastic (4). Our results demonstrate that modulating the mechanical properties of the adhesive substratum also affects contact maturation and the EGFR/ERK signaling pathways even without the spatial constraints associated with confluent epithelial sheets.

Implications for cancer treatment and tissue engineering

In conclusion, our findings demonstrate that changes in substratum compliance quantitatively modulate the degree of contact-inhibition. Stiffening the extracellular matrix moves an epithelial cell system closer to the transition to contact-independent proliferation, thereby quantitatively reducing the amount of EGF amplification needed to transform the system. Our results suggest that detecting early stages of matrix stiffening may be a particularly important diagnostic tool. During these initial stages, matrix stiffening may not render a phenotypic change but could be quantitatively pushing the

system to more easily transform. Intervening during these early stages by reducing matrix stiffness would quantitatively push the system further away from the transition point and diminish its sensitivity to molecular oncogenic signals, such as EGF. Finally, our findings provide a quantitative framework for how modulating mechanical compliance would affect spatial patterns and rates of growth of multicellular structures. This framework may facilitate the use of synthetic biomaterials whose mechanical properties may be fine-tuned, in some cases *in situ* (20), for tissue engineering applications.

Materials and Methods

Preparation and Characterization of Adhesion Ligand-coated Polyacrylamide Substrates

Polyacrylamide substrates were prepared using techniques described by Wang and colleagues (21). Substrate stiffness was manipulated by varying bis-acrylamide concentrations while keeping the acrylamide (National Diagnostic) concentration constant (10%). Type I collagen (Sigma-Aldrich) and fibronectin (Sigma-Aldrich) were covalently bound to the substrates by using a heterobifunctional cross-linker, sulfo-SANPAH (Pierce). The surface density of adhesion ligands on the substrates were examined as described in Fig. S1. Finally, Young's modulus of polyacrylamide substrates were measured by performing compression testing (22).

Cell Culture and Reagents

MCF-10A cells were cultured in growth medium as described previously (23). MDCK cells were cultured in Dulbecco's modified Eagle's medium containing HEPES and L-glutamine (Invitrogen) supplemented with 10% (v/v) fetal bovine serum (Invitrogen). For experiments, adhesion ligand-coated polyacrylamide gels bound to 25 mm circular glass coverslips (VWR) were placed in 35 mm petri-dishes (Corning), and equilibrated in growth medium for 30 min at 37°C. Then, cells were plated in growth medium for 24 h and serum starved for additional 24 h for G_0 synchronization. The following antibodies were used: anti-actin (Santa Cruz), anti-BrdU (Roche Applied Science), anti-E-cadherin (BD Transduction Laboratory), anti-EGFR, anti-phospho-Tyr1068-EGFR, anti-phospho-Thr202/Tyr204-ERK 1/2, anti-phospho-serine 473-Akt (Cell Signaling Technologies), anti-ZO1 (Zymed), DECMA-1 (Sigma-Aldrich), and Alexa dye-labeled secondary antibodies (Invitrogen). Fluorescent nuclear stains, DAPI and Hoechst33342 were obtained from Sigma-Aldrich and Invitrogen, respectively.

Knockdown Using siRNA

siRNA targeting E-cadherin and control siRNA were purchased from Ambion, and used at 50 nM. siRNA were transfected using Lipofectamine RNAiMax (Invitrogen).

Immunofluorescence and Image Acquisition

Fixed cells were permeablized, blocked, and sequentially incubated with primary and secondary antibodies. The cells were co-stained with either DAPI or Hoechst 33342, and mounted using ProLong Gold Antifade (Invitrogen). Fluorescence and confocal images were acquired using the Zeiss Axiovert 200M microscope and the Zeiss LSM 510

upright confocal microscope, respectively. The procedures followed for the quantitation of fluorescence images and reagents used for each type of stains are summarized in SI text.

Cell Lysis and Western Blot Analysis

Cell lysis and Western blot analysis were performed as described previously (23).

Acknowledgments

We thank members of the Asthagiri group for helpful discussions, Dongying Shen for her involvement in image analysis, and the Caltech Biological Imaging Center for access to the Zeiss LSM 510 upright confocal microscope. We thank J. Notbohm and G. Ravichandran for help characterizing the mechanical properties of polyacrylmaide gels. This work was supported by the Jacobs Foundation for Molecular Engineering for Medicine and the NCI Physical Sciences of Oncology Center at USC (U54CA143907).

References

1. Hanahan D & Weinberg RA (2000) The hallmarks of cancer. *Cell* 100(1):57-70.
2. Li S, Gerrard ER, Jr., & Balkovetz DF (2004) Evidence for ERK1/2 phosphorylation controlling contact inhibition of proliferation in Madin-Darby canine kidney epithelial cells. *Am J Physiol Cell Physiol* 287(2):C432-439.
3. LeVea CM, Reeder JE, & Mooney RA (2004) EGF-dependent cell cycle progression is controlled by density-dependent regulation of Akt activation. *Exp Cell Res* 297(1):272-284.
4. Curto M, Cole BK, Lallemand D, Liu C-H, & McClatchey AI (2007) Contact-dependent inhibition of EGFR signaling by Nf2/Merlin. *J Cell Biol* 177(5):893-903.
5. Lampugnani MG, Orsenigo F, Gagliani MC, Tacchetti C, & Dejana E (2006) Vascular endothelial cadherin controls VEGFR-2 internalization and signaling from intracellular compartments. *J Cell Biol* 174(4):593-604.
6. Lampugnani M, *et al.* (2003) Contact inhibition of VEGF-induced proliferation requires vascular endothelial cadherin, beta-catenin, and the phosphatase DEP-1/CD148. *J Cell Biol* 161(4):793-804.
7. Nelson CM, *et al.* (2005) Emergent patterns of growth controlled by multicellular form and mechanics. *Proc Natl Acad Sci USA* 102(33):11594-11599.
8. Hamaratoglu F, *et al.* (2006) The tumour-suppressor genes NF2/Merlin and Expanded act through Hippo signalling to regulate cell proliferation and apoptosis. *Nat Cell Biol* 8(1):27-36.

9. Yin F & Pan D (2007) Fat flies expanded the hippo pathway: a matter of size control. *Sci STKE* 2007(380):pe12.

10. Kim JH, Kushiro K, Graham NA, & Asthagiri AR (2009) Tunable interplay between epidermal growth factor and cell-cell contact governs the spatial dynamics of epithelial growth. *Proc Natl Acad Sci USA* 106(27):11149-11153.

11. Butcher DT, Alliston T, & Weaver VM (2009) A tense situation: forcing tumour progression. *Nat Rev Cancer* 9(2):108-122.

12. Levental KR, *et al.* (2009) Matrix crosslinking forces tumor progression by enhancing integrin signaling. *Cell* 139(5):891-906.

13. Fogg VC, Liu CJ, & Margolis B (2005) Multiple regions of Crumbs3 are required for tight junction formation in MCF10A cells. *J Cell Sci* 118(Pt 13):2859-2869.

14. Balkovetz DF, Pollack AL, & Mostov KE (1997) Hepatocyte growth factor alters the polarity of Madin-Darby canine kidney cell monolayers. *J Biol Chem* 272(6):3471-3477.

15. Jones SM & Kazlauskas A (2001) Growth-factor-dependent mitogenesis requires two distinct phases of signalling. *Nat Cell Biol* 3(2):165-172.

16. Discher DE, Janmey P, & Wang YL (2005) Tissue cells feel and respond to the stiffness of their substrate. *Science* 310(5751):1139-1143.

17. Paszek MJ, *et al.* (2005) Tensional homeostasis and the malignant phenotype. *Cancer Cell* 8(3):241-254.

18. Gottardi CJ, Arpin M, Fanning AS, & Louvard D (1996) The junction-associated protein, zonula occludens-1, localizes to the nucleus before the maturation and

during the remodeling of cell-cell contacts. *Proc Natl Acad Sci USA* 93(20):10779-10784.

19. Balda MS, Garrett MD, & Matter K (2003) The ZO-1-associated Y-box factor ZONAB regulates epithelial cell proliferation and cell density. *J Cell Biol* 160(3):423-432.

20. Kloxin AM, Kasko AM, Salinas CN, & Anseth KS (2009) Photodegradable hydrogels for dynamic tuning of physical and chemical properties. *Science* 324(5923):59-63.

21. Pelham RJ, Jr. & Wang Y (1997) Cell locomotion and focal adhesions are regulated by substrate flexibility. *Proc Natl Acad Sci USA* 94(25):13661-13665.

22. Franck C, Hong S, Maskarinec SA, Tirrell DA, & Ravichandran G (2007) Three-dimensional full-field measurements of large deformations in soft materials using confocal microscopy and digital volume correlation. *Exp Mech* 47(3):427-438.

23. Graham NA & Asthagiri AR (2004) Epidermal growth factor-mediated T-cell factor/lymphoid enhancer factor transcriptional activity is essential but not sufficient for cell cycle progression in nontransformed mammary epithelial cells. *J Biol Chem* 279(22):23517-23524.

Supporting Information

Quantification of immunofluorescne signals of phospho-proteins

For the quantitation of cytoplasmic pEGFR signal, cells were co-stained for E-cadherin using DECMA-1 antibody to provide a clear visualization of cell-cell contacts from the cell body. The perimeter of cell body was traced along cell-cell contacts. The area and total FITC intensity of single cell body were determined using MATLAB. The mean background intensity per pixel was also calculated for each image from the region containing no cells. This background level was multiplied by the area of the cell body and was subtracted from the total cytoplasmic FITC intensity to determine the final cytoplasmic pEGFR signal intensity for each cell.

Nuclear ppERK and pAkt signal intensities were quantified by first tracing the perimeter of each nucleus using DAPI co-staining. The area and the total FITC intensity of each nucleus were determined using MATLAB. The average background level was multiplied by the area of the nucleus and was subtracted from the total nuclear FITC intensity to determine the final ppERK or pAkt for each nucleus.

Table S1. Details of reagents used in immunofluorescence for each stain

Application	Fixation Reagents	Permeabilization	Dehydration	Blocking solution
BrdU	70% EtOH (pH 2) w/ 15 mM glycine (-20 °C)	N/A	N/A	10% goat serum + 0.1% BSA in PBS
EGFR/ZO-1/E-cadherin	Freshly prepared 4% paraformaldehyde (pH 7.4)	0.2 % Triton in PBS	N/A	Image-iT FX Signal Enhancer (Invitrogen) & 10% goat serum + 0.1% BSA in PBS
pEGFR/DECMA-1	Freshly prepared 4% paraformaldehyde (pH 7.4) + Inhibitors*	0.2 % Triton in PBS + Inhibitors*	N/A	Image-iT FX Signal Enhancer (Invitrogen) & 10% goat serum + 0.1% BSA in PBS
ppERK/pAkt	Freshly prepared 2% paraformaldehyde (pH 7.4) + Inhibitors*	0.5% NP-40 in PBS + Inhibitors*	Pure MeOH (-20 °C)	Image-iT FX Signal Enhancer (Invitrogen) & Blocking buffer**

*Phosphatase inhibitors: 1mM sodium orthovanadate, 10mM sodium fluoride, and 10mM β-glycerophosphate (all from Sigma-Aldrich)

**Blocking buffer: 130 mM NaCl, 7 mM Na_2HPO_4, 3.5 mM NaH_2PO_4, 7.7 mM NaN_3, 0.1% bovine serum albumin, 0.2% Triton X-100, 0.05% Tween-20 (all from Sigma-Aldrich), and 10% goat serum

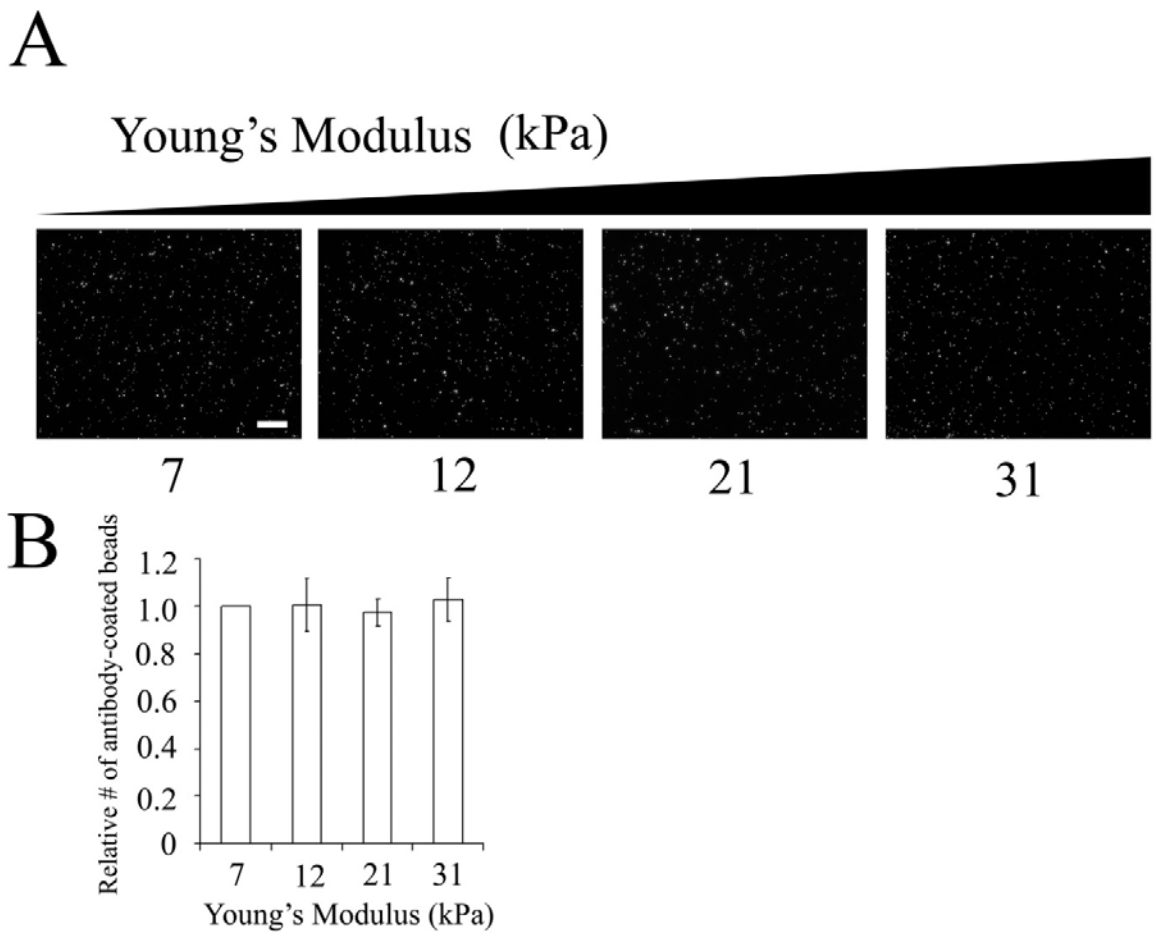

Fig. S1. Identical surface density of adhesion-ligand bound to polyacrylamide gels of varying stiffness. (A) Surface density of ColI bound to polyacrylamide gels was probed by immunofluorescence. ColI-coated substrates were sequentially incubated with anti-ColI mouse antibody (Sigma-Aldrich), and 1μm FluoSpheres® carboxylate-modified microspheres (Invitrogen) coated with anti-mouse IgG (Sigma-Aldrich). After each incubation step, the substrates were rigorously washed with PBS on the shaker multiple times. Fluorescence images of the microbeads bound to the substrate surface were acquired using the Zeiss Axiovert 200M microscope. (Scale bar, 100 μm.) (B) The

relative number of bound antibody-coated microbeads was counted at multiple image fields by using MATLAB. As a negative control, non-ColI-coated polyacrylamide gels were used and only a negligible number of microbeads was detected (data now shown). Error bars, s.d. (n = 3-4).

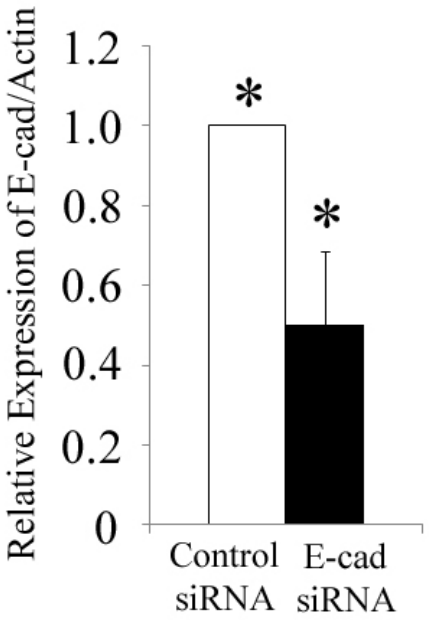

Fig. S2. Effect of siRNA treatment on E-cadherin expression. The extent of knockdown in E-cadherin was determined by quantitative Western blot analysis of relative expression of E-cadherin to actin. Error bars, s.d. (n = 3), *, $P < 0.05$.

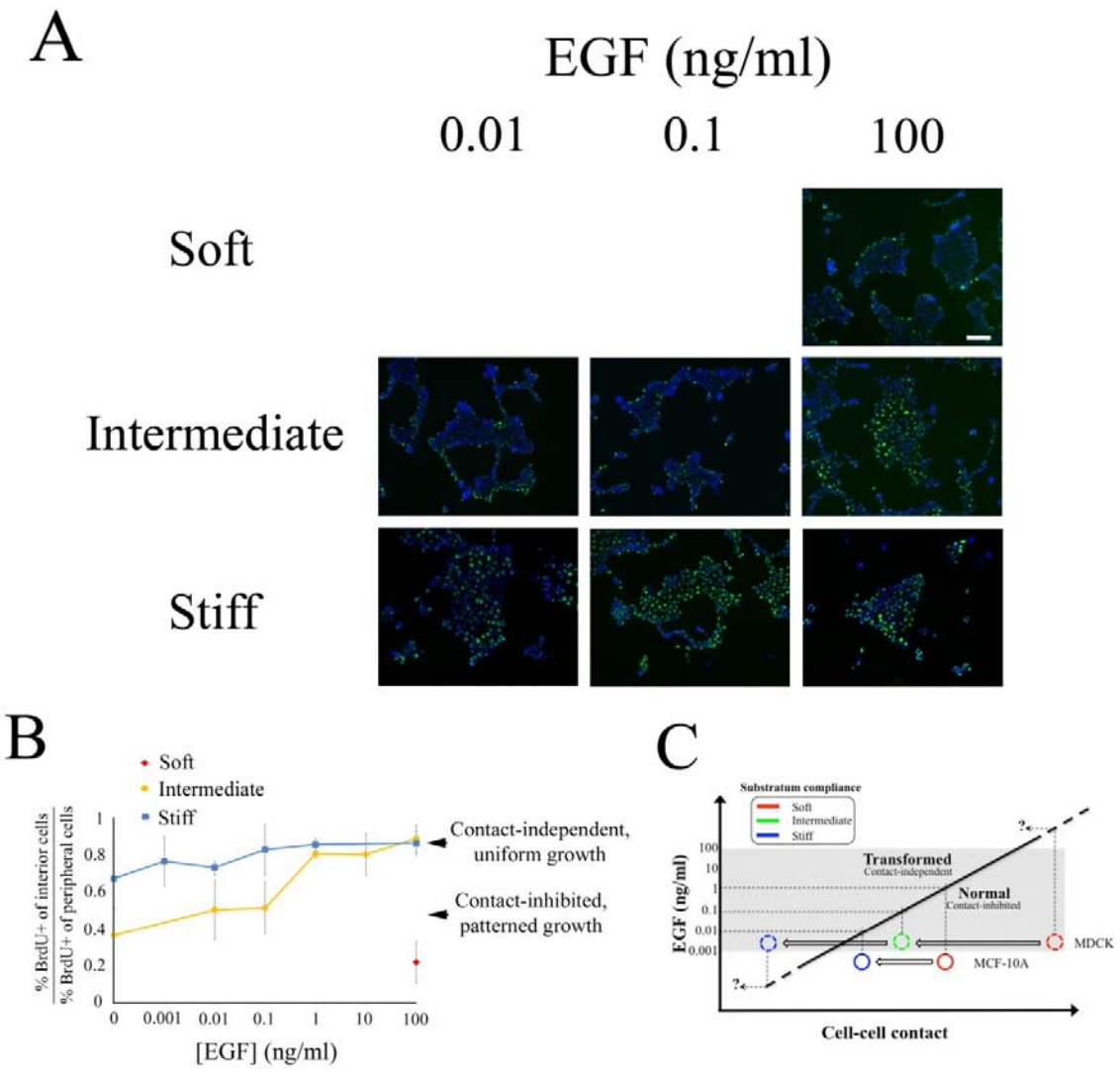

Fig. S3. The effect of substratum compliance on the threshold EGF levels for contact-inhibition. MDCK cells grown on soft, intermediate, and stiff surfaces were serum starved and stimulated with different doses of EGF. (A) BrdU uptake (green) and DAPI staining (blue) were assessed 16 h after EGF treatment. The 0.01 and 0.1 ng/ml EGF cases were not conducted for soft gels because spatial patterns in proliferation were evident even on 100 ng/ml EGF. (B) The fraction of interior cells synthesizing DNA is reported relative to the fraction of cells synthesizing DNA in the periphery of clusters. (C) Substratum stiffening quantitatively shifts the system closer to the transformed state in

both MCF-10A and MDCK cells. The two non-transormed cell lines exhibit different sensitivity to this perturbation. The shaded area in the graph refers to the range of EGF concentrations explored experimentally. MDCK on soft and stiff surfaces intersect with the transition line at a point outside of the experimentally accessible level of threshold EGF. Error bars, s.d. (n = 2), *, $P < 0.05$.

Chapter IV. Substratum compliance and EGF co-regulate spatial patterns in traction forces, cell shape, and proliferation within epithelial multicellular clusters

Abstract

Cell-generated mechanical forces that act upon cell adhesions play a major role in multicellular morphogenesis. These adhesions undergo dynamic modulations through continuous cellular interactions with the surrounding microenvironment. Elucidating how these microenvironmental cues regulate the biophysical aspects of multicellular structures is pivotal to understanding the emergence of multicellular growth patterns. Here, we demonstrate that substratum compliance and epidermal growth factor (EGF) co-regulate spatial patterns in cell adhesions, traction forces, and cell shape within multicellular clusters. These patterns in adhesions and cell morphology correspond to patterns in proliferation. In the absence of EGF, soft matrices selectively promote the maturation of intercellular contacts and block focal adhesion formation among central cells. In contrast, substratum compliance does not have any apparent effect on focal adhesion formation among peripheral cells. The spatial patterns in cell adhesions correspond to patterns in traction force. Our measurements of traction forces in three-dimensions (3-D) reveal significant spatial gradients in mechanical stresses normal to the substratum as well as in the plane of the substratum. Cells at the interior of a cluster push down upon the matrix, while those in the periphery pull up on the substratum. These pre-established patterns in cell adhesions and traction forces are modified upon

EGF treatment in an EGF dose-dependent manner. Our preliminary results indicate that supra-threshold levels of EGF induce rapid, short-lived traction forces and transient de-compaction of clusters. In contrast, sub-threshold EGF levels do not induce any apparent mechanical or morphological changes. These dose-dependent effects correspond to uniform proliferation versus spatially patterned proliferation in response to supra- and sub-threshold EGF treatment, respectively. These results suggest a model wherein EGF stimulation at supra-threshold levels may eliminate pre-established patterns in adhesions and traction forces en route to driving uniform proliferation. Future studies will test this model by investigating whether the traction forces generated by treatment with supra-threshold EGF act to reduce the pre-established spatial gradient in mechanical stresses and whether this reversal is necessary for the elimination of a spatial pattern in proliferation.

Introduction

Epithelial cells organize into multicellular structures by establishing highly structured adhesions with their neighbors and the surrounding extracellular matrix (ECM) (1). During morphogenesis, cells continuously sense cues in their microenvironment, such as ECM ligands and soluble growth factors, and respond by modulating their adhesions, cytoskeletal mechanics, and cell shape (2). These biophysical changes in turn affect intracellular signal transduction and control many cellular behaviors including proliferation. Thus, deciphering how these environmental cues control multicellular mechanics and spatial patterns in cell shape and proliferation is central to our understanding of multicellular morphodynamics.

The ECM is dynamic and undergoes continuous remodeling during development (3), aging (4), and disease progression (5). In particular, a physical property of the ECM, compliance, plays a central role in maintaining epithelial organization through tensional homeostasis (6). The stiffening of the matrix is frequently associated with tumor formation (5). Stiffer matrices enable isolated cells to generate larger traction forces on the underlying substratum, leading to bigger and more mature focal adhesions (7). In a multicellular context, these cell-generated forces are also transmitted through cell-cell adhesions, leading to spatial patterns in mechanical stresses and proliferation within multicellular aggregates (8). It is unknown how these spatial patterns in traction forces affect the spatial distribution of focal adhesions in multicellular clusters.

In addition to the mechanical property of matrix, soluble growth factor (GF) may also regulate cellular mechanics and shape by affecting protrusions and actomyosin contractility. EGF stimulates the membrane translocation of Rac1 and its localized activation (9), facilitating lamellipodial extensions. Meanwhile, EGF activates the Rho GTPase effector, ROCK, leading to the phosphorylation of myosin-II regulatory light chains and inactivation of myosin-II phosphatases, which together gives rise to the increased non-muscle myosin-II-mediated contractility (10). In isolated cells, these mechanisms are associated with the formation of new adhesions at the leading edge and the destabilization of focal adhesions in trailing edges, together driving cell migration. Precisely how EGF affects cell mechanics and shape within multicellular clusters remains to be elucidated.

Here, we set out to quantitatively interrogate how substratum compliance and EGF affect cell mechanics and shape within multicellular clusters and how these effects correspond to spatial patterns in proliferation. We find that softening collagen- or fibronectin-coated elastic substrates promotes spatial patterns in focal adhesions. These spatial patterns in cell-matrix adhesions corresponds to patterns in mechanical stresses in three-dimensions, which include both in-plane and significant out-of-plane traction forces. These pre-established patterns in cell adhesion and mechanics are modified upon EGF treatment in an EGF dose-dependent manner. Treatment with a supra-threshold level of EGF leads to the generation of actomyosin contractility and de-compaction of cell clusters. Our quantitative findings illustrate the integrated role of substratum

compliance and EGF in regulating spatial patterns in traction forces, cell shape, and proliferation within multicellular clusters.

Results

Substratum compliance affects spatial patterns in cell-cell and cell-matrix adhesions.

To explore the effect of substratum compliance on cell adhesion with its neighbors and with the underlying substratum, we monitored molecular markers associated with the maturation of cell-cell contacts and focal adhesions (FA) – E-cadherin and paxillin, respectively – in normal rat kidney epithelial cells (NRK-52E) cells grown on ColI-coated polyacrylamide (pAc) gels of varying stiffness. On soft substrata, continuous, linear E-cadherin staining was observed (Fig. 1A). In contrast, punctate E-cadherin structures, indicative of immature cell-cell adhesions (11), were found at cell boundaries of NRK-52E cell clusters seeded on stiff substrata. This qualitative observation was corroborated by quantifying the number of discontinuities in cadherin-mediated contacts around the cell perimeter for a range of substratum compliance. These results in NRK-52E cells are consistent with our previous observation in MDCK cells that softer substrata promote the maturation of cell-cell contacts by enhancing the subcellular localization of contact molecules, such as E-cadherin and ZO-1 (Chapter 3).

In addition to its effects on cell-cell adhesions, modulating substratum compliance affected the formation and maturation of FAs in the interior of clusters (Fig.

1B). On soft surfaces, only nascent adhesions remained in the interior of clusters while mature adhesions were concentrated among peripheral cells, establishing a spatial gradient in the extent of cell-matrix interactions. An increase in substratum stiffness diminished this spatial disparity in FA distribution by allowing the formation of mature adhesions in the interior of clusters. In contrast, substratum compliance did not significantly affect the formation of mature FAs at the free edges of the peripheral cells.

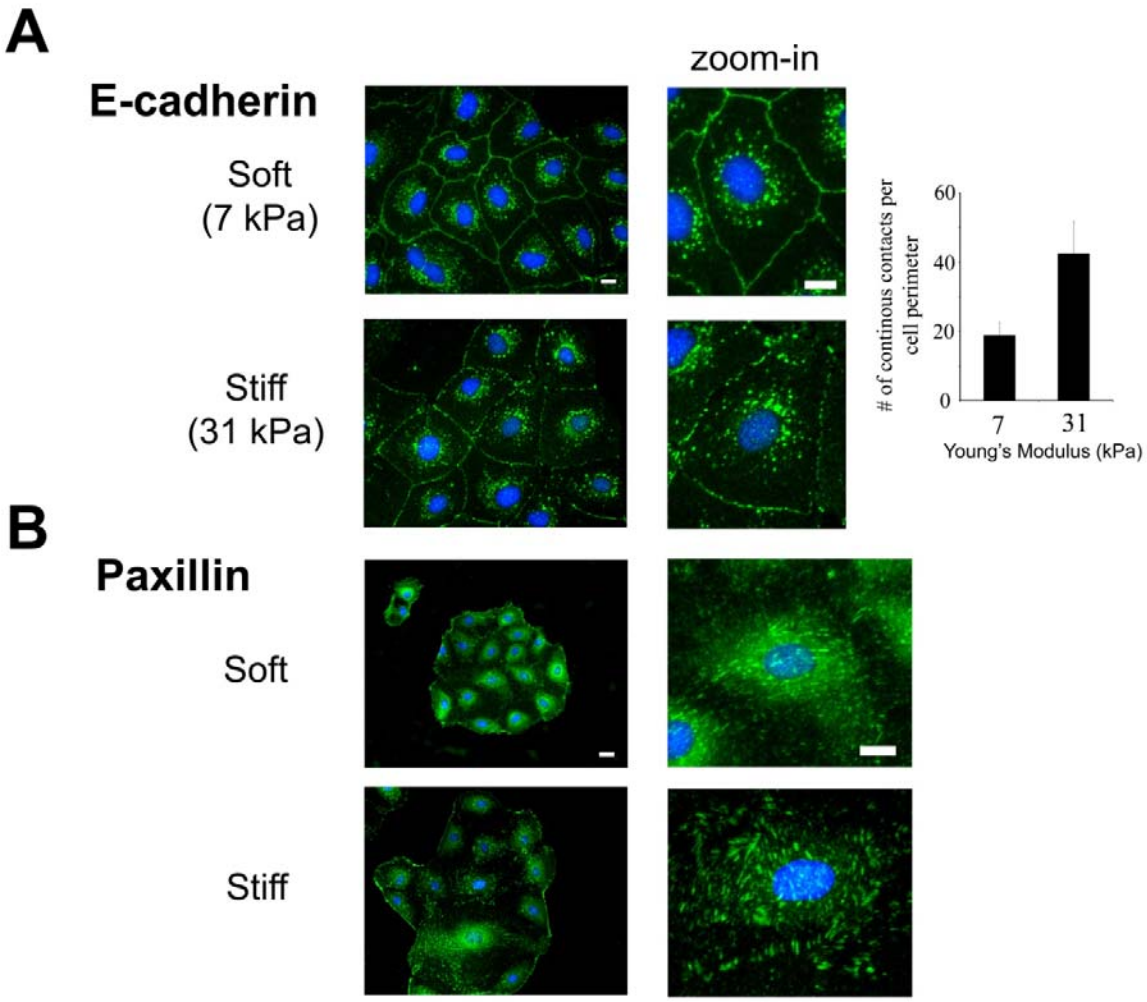

Fig. 1. The effect of substratum compliance on contact-maturation and spatial pattern in cell-matrix interactions NRK-52E cells cultured on ColI-coated

polyacrylamide gels of two different stiffnesses (Soft: 7 kPa and Stiff: 31 kPa) were starved and immunostained for (A) E-cadherin and (B) paxillin. Nuclei were co-stained with DAPI. The right panel images represent the magnified views of stained cells located in the interior of clusters. The bar graph shows the immaturity of cell-cell contacts on each substrate. To quantify the immaturity of cell-cell contacts, the number of discontinuities in E-cadherin-mediated contacts was counted and normalized to the cell perimeter. At minimum,10 cells were analyzed per condition. The *error bars* indicate s.d. (n = 3) with duplicates performed in each trial. (Scale bars, (A) 12.5 μm, (B) 25 μm).

The spatial pattern in cell adhesions corresponds to patterns in traction force in three-dimensions.

The generation of traction forces influences the formation and stabilization of focal adhesions in isolated cells (12). We asked whether the spatial patterns in cell-matrix adhesions observed in multicellular clusters correspond to spatial differences in traction forces generated by interior versus peripheral cells. Traction force measurements have been conventionally restricted to in-plane stresses (12-13) and have missed the possibility of normal (*z*-directional) forces that cells may exert. Recent data using the three-dimensional digital volume correlation (3D-DVC) method in isolated migrating cells suggests that the magnitude of normal forces may be on par with those of in-plane forces (14). Here, we used the 3D-DVC technique to assess both in-plane and normal traction forces within multicellular clusters.

In MDCK cells grown on soft surfaces, we observed that cells generated in-plane, pulling forces toward the center of clusters overall. The magnitude of these forces markedly decreased toward the center of clusters so that peripheral cells generated approximately 3- to 5-fold higher traction forces than interior cells (Fig. 2A). Intriguingly, the spatial differences in mechanical stresses also existed in normal stresses as peripheral cells pulled on the underlying substrate (out-of-plane) while cells collectively pressed the matrix in the interior of clusters (into-the-plane). These normal stresses were even greater in magnitude than the in-plane forces in some instances.

Thus, our measurements of traction forces in three-dimensions reveal significant gradients in normal forces in addition to the previously observed spatial patterns in in-plane forces within multicellular clusters (8). In particular, spatial patterns in normal forces involve the directional changes (i.e., out-of-plane at the periphery versus into-the-plane at the interior), revealing that most tugging forces against the underlying substratum are exerted at the periphery of clusters. This is consistent with our observations that matured focal adhesions are predominantly found along the free edges of peripheral cells. Thus, the spatial patterns in traction forces correspond to spatial patterns in the extent of focal adhesion maturation in multicellular clusters.

Finally, we examined the role of these 3-D mechanics developed within multicellular aggregates on spatial patterns in proliferation. We assessed cell cycle activity within clusters whose myosin-mediated contractility was abrogated by applying a myosin-II ATPase inhibitor, blebbistatin. In contrast to a vehicle control wherein cell

aggregates exhibited a spatially patterned growth at 100 ng/ml EGF stimulation, cells pretreated with blebbistatin displayed uniform growth (Fig. 2B). These effects of blebbistatin treatment confirm the previous observation that cell-generated traction forces play a key role in regulating growth patterns (8). Here, we show that these traction forces are patterned not only in the plane of the substratum but also normal to the substratum. Furthermore, we demonstrate that these spatial patterns in traction forces correspond to patterns in the maturity of cell-matrix and cell-cell adhesions (Fig. 1).

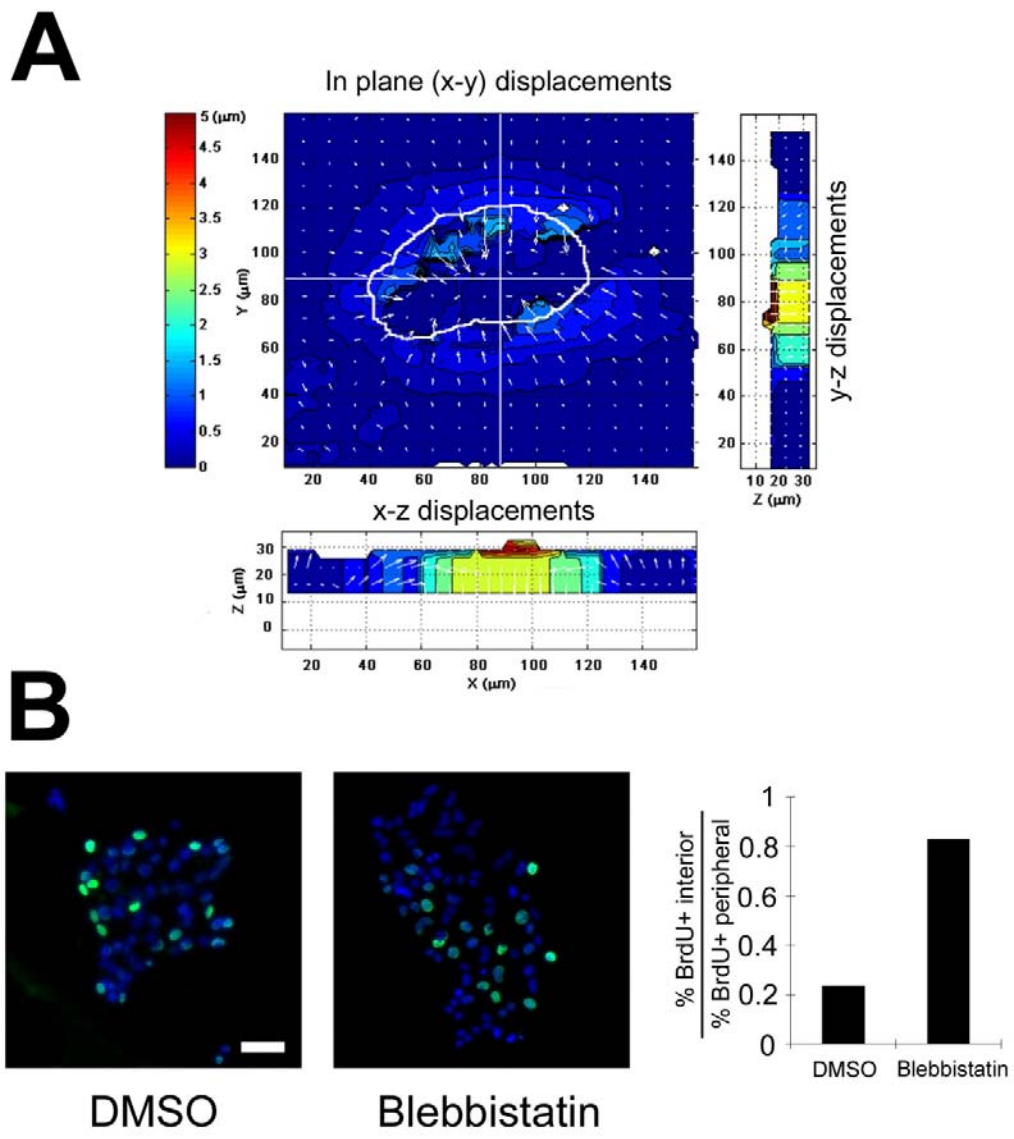

Fig. 2. The spatial patterns in cell adhesions correspond to spatial gradient in mechanical stresses within multicellular aggregates. (A) Traction forces within a multicellular cluster seeded on a soft gel. MDCK cells grown on bead-containing pAc gels (7 kPa) were serum starved and live-stained with mitotracker for fluorescence imaging of clusters. Bead displacements induced by cell-generated traction forces were

measured by comparing the bead distribution before and after lysing cells with 0.5 % Triton. White lines in parallel and vertical directions indicate the planes for which *x-z* and *x-y* directional displacements were measured, respectively. Total of two independent trials were performed. At least, three samples were examined per condition in each trial. (B) The effect of inhibiting traction forces on the spatial pattern in proliferation. Serum-starved MDCK cells on soft surfaces were pretreated for 2 h with blebbistatin or the solvent DMSO, and then stimulated with 100 ng/ml EGF. The effect of the pharmacological inhibition of non-muscle myosin-II activity on BrdU uptake (green) was determined by immunofluorescence. Nuclei were co-stained with DAPI (blue). The fractions of interior and peripheral cells incorporating BrdU were quantified. The graph shows the ratio of these two fractions for cells pretreated with DMSO or blebbistatin. (Scale bar, 50 μm)

Treatment with supra-threshold amount of EGF induces traction forces and transient de-compaction of cell clusters

Our results reveal that cells seeded on soft matrices establish spatial gradients in cell-cell and cell-matrix adhesions and in traction forces. These spatial patterns in adhesive events are established in the absence of serum or exogenous growth factors. Yet, these pre-established patterns clearly correspond to a pattern in proliferation following EGF stimulation. Furthermore, we have shown previously that if clusters are treated with a supra-threshold level of EGF, the cell clusters will exhibit uniform proliferation (Chapter 3). These observations raise the possibility that supra-threshold

levels of EGF may eliminate pre-established patterns in adhesions and traction forces en route to stimulating uniform cell proliferation (Fig. 3A). Alternatively, supra-threshold EGF may not affect spatial patterns related to adhesion but yet induce uniform proliferation by overriding downstream inhibitory pathways or providing compensatory activation pathways.

To resolve between these alternative scenarios, we sought to evaluate the effect of EGF stimulation on the spatial pattern in adhesive events. As an initial study, we focused on quantifying changes in cell shape as a gross phenotypic measure that would lump together any effect on cell-matrix and cell-cell adhesions and traction forces. We treated MCF-10A clusters grown on soft surfaces (7 kPa) with 0.1 and 100 ng/ml EGF, which are sub- and supra-threshold amounts of EGF in this system. Treatment with 100 ng/ml EGF induced a transient de-condensation of MCF-10A clusters so that the projected area of the clusters increased up to ~40% by 100 min after stimulation (Fig. 3B, left panel). In contrast, treatment with 0.1 ng/ml EGF did not induce any apparent changes in cluster size. Thus, supra-threshold EGF levels that eliminate the spatial pattern in proliferation also trigger a transient decompaction of the cell cluster. We hypothesize that such de-compaction involves an increase in cell-matrix adhesions and a diminishment of cell-cell adhesions. Future studies will examine this more closely using the aforementioned tools to probe cell-matrix and cell-adhesions.

In addition to measurements of morphology, we conducted preliminary experiments to measure the cell-generated forces transmitted to the underlying

substratum during the transient EGF-mediated de-compaction. We measured bead displacements in 20 min time windows following stimulation with 100 ng/ml EGF (Fig. 3B, right panel). Initial observations suggest measurable traction force responses to treatment with 100 ng/ml EGF. In contrast, treatment with 0.1 ng/ml EGF did not produce measureable bead displacements. Future studies will test the hypothesis that the traction forces generated by treatment with supra-threshold EGF act to diminish the spatial disparity in pre-established traction forces.

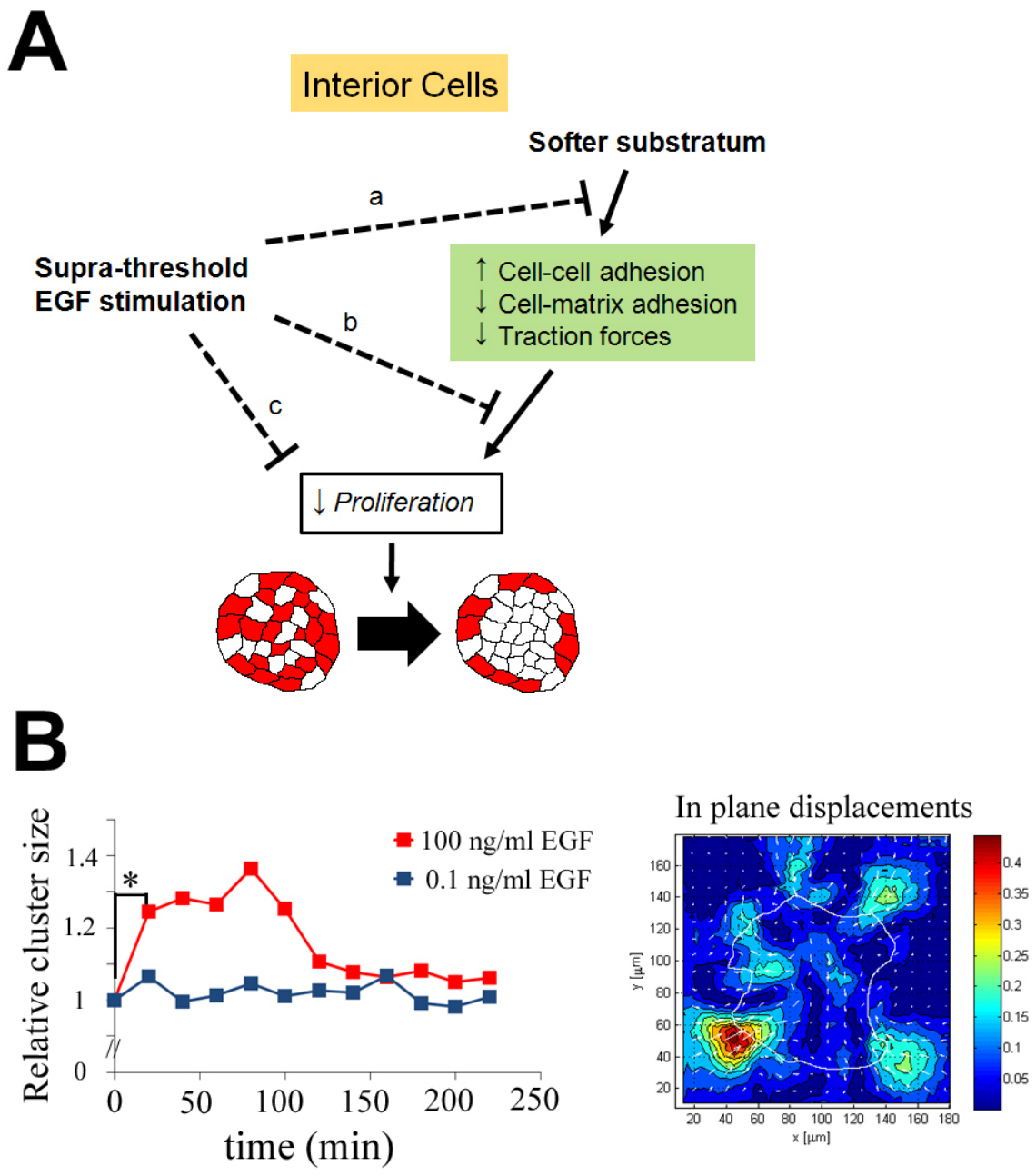

Fig. 3. Treatment with supra-threshold levels of EGF induces rapid, short-lived traction forces and transient de-condensation of clusters. (A) The emerging model from our results is that soft substratum promotes cell-cell adhesions and blocks the formation of focal adhesions and generation of traction forces among interior cells.

These events correspond to the cell cycle arrest of interior cells and the onset of spatial pattern in proliferation. We hypothesized three possible scenarios wherein treatment with supra-threshold levels of EGF acts to rescue interior cells from their cell cycle arrest en route to eliminating the spatial pattern in proliferation. Supra-threshold levels of EGF may (a) reverse the effect of soft matrices on cell-cell and cell-matrix adhesions and traction forces, (b) override downstream inhibitory pathways, or (c) activate compensatory activation pathways. (B) Serum-starved MCF-10A clusters on soft surface were stimulated with 0.1 and 100 ng/ml EGF. The relative changes in cluster area and bead displacements caused by cell-generated forces were quantified over time at 20 min intervals. The *inset* shows a representative displacement map between 0 and 20 min for clusters treated 100 ng/ml EGF (indicated by *asterisk*). Cluster sizes are reported relative to the cluster area at the time of EGF stimulation (i.e., 0 min).

Discussion

.

Here, we demonstrate that substratum compliance and EGF co-regulate spatial patterns in cell adhesions, traction forces, and cell shape within multicellular clusters. The patterns observed in these adhesive and morphological processes correspond to spatial patterns in proliferation within multicellular clusters.

In the absence of EGF, softening the adhesive matrix promotes the maturation of intercellular contacts and diminishes focal adhesions among central cells. Meanwhile, cells at the periphery remain strongly anchored to the underlying substratum exhibiting

mature focal adhesions along the free edge. This spatial pattern in cell-matrix adhesions corresponds to spatial disparities in traction forces. Our measurements of mechanical stresses in three-dimensions reveal that in addition to the previously reported spatial gradients in *in-plane* forces (8), there exists a significant spatial pattern in *normal* forces. These normal forces are predominantly pulling up on the matrix at the periphery of clusters and push into the matrix toward the center of clusters.

Treatment with EGF modulates the spatial patterns in cell shape and traction forces that were pre-established under serum- and growth factor-free conditions. Importantly, the effect depends on the dose of EGF used. When the level of EGF is below a threshold amount needed to maintain patterned proliferation, stimulation with EGF has no effect on the area of the cell cluster and traction forces. In contrast, treatment with a supra-threshold amount of EGF induces rapid, short-lived decompaction of clusters and traction forces. These results suggest a model wherein treatment with supra-threshold levels of EGF attenuates pre-established spatial disparities in cell adhesivity and shape en route to eliminating the spatial pattern in proliferation.

During single-cell migration, acute EGF stimulation rapidly promotes protrusion and forms new adhesions at a leading edge, which are followed by myosin-II-mediated retraction at a trailing edge, together pushing a cell body forward (10). In a mature multicellular cluster, however, interior cells that are surrounded by neighboring cells cannot form protrusions and may not readily form additional adhesions with the substratum, thus failing to generate traction forces on their own. Instead, cells at the

periphery of the cluster may extend protrusions toward their free edges, strengthen their adhesions, and generate traction forces. These contractile forces are further transmitted toward the interior of clusters through cell-cell adhesions. The transmitted forces may contribute to pulling interior cells toward the periphery and disrupting their cortical contractility, consequently leading to the re-arrangements of the actin cytoskeleton and spreading of interior cells. Finally, these series of events are likely to allow them to eliminate spatial patterns in cell shape during a critical window of time for cell cycle decision, thus initiating cell cycle activity among interior cells.

Conclusions

In conclusion, our findings demonstrate that substratum compliance and EGF jointly control spatial patterns in cell adhesions, traction force and cell shape, and proliferation within multicellular aggregates. *In vivo*, maintaining proper cellular mechanics and shapes is the central model of tissue homeostasis (4). Events that perturb tensional balances among multicellular structures lead to malignant transformation (6). Meanwhile, our results reveal that EGF signaling, a canonical mitogenic pathway, modulates the spatial dynamics of multicellular mechanics and organization. This property may play a pivotal role in several physiological processes such as branching and wound healing by spatially imparting advantageous phenotypes for tissue outgrowth. However, during cancer progression, it may provide a pathway for genetic mutations in oncogenes to affect morphological evolution. Finally, quantitative insights on controlling multicellular patterns in mechanics, shapes, and proliferation using a

combination of soluble growth factors and mechanically compliant materials may provide design strategies for constructing synthetic microenvironments for applications such as tissue engineering and regenerative medicine.

Materials and Methods

Preparation and Characterization of Adhesion Ligand-coated Polyacrylamide Substrates

Polyacrylamide substrates were prepared using techniques described by Wang and colleagues (15). Substrate stiffness was manipulated by varying bis-acrylamide concentrations while keeping the acrylamide concentration constant (10%). Type I collagen (Sigma-Aldrich) and fibronectin (Sigma-Aldrich) were covalently bound to the substrates by using a heterobifunctional cross-linker, sulfo-SANPAH (Pierce). The surface density of adhesion ligands on the substrates were examined as described in Fig. S1 of Chapter 3. Finally, Young's modulus of polyacrylamide substrates were measured by performing compression testing (16).

Cell Culture and Reagents

MCF-10A cells were cultured in growth medium as described previously (17). MDCK cells were cultured in Dulbecco's modified Eagle's medium containing HEPES and L-glutamine (Invitrogen) supplemented with 10% (v/v) fetal bovine serum (Invitrogen). NRK-52E were cultured in Dulbecco's modified Eagle's medium containing HEPES and L-glutamine (Invitrogen) supplemented with 5 % (v/v) calf serum (Invitrogen). Experiments were conducted following the procedures dscribed by Chapter 3.

The following antibodies were used: anti-BrdU (Roche Applied Science), anti-E-cadherin (BD Transduction laboratory), anti-paxillin, anti-vinculin (Sigma-Aldrich), anti-ZO1 (Zymed), DECMA-1 (Sigma-Aldrich), and Alexa dye-labeled secondary antibodies (Invitrogen). DAPI and phalloidin were obtained from Sigma-Aldrich and Invitrogen, respectively. The pharmacological inhibitor, blebbistatin, was purchased from Calbiochem.

Immunofluorescence and Image Acquisition

Fixed cells were permeablized, blocked, and sequentially incubated with primary and secondary antibodies. The cells were co-stained with DAP and mounted using ProLong Gold Antifade (Invitrogen). Fluorescence images were acquired using the Zeiss Axiovert 200M microscope.

Traction force microscopy

Displacements of fluorescence beads (Invitrogen) embedded in pAc gels were tracked using DVC algorithm described by Ravichandran and colleagues (14).

Subcloning membrane-mCherry construct into a retroviral vector

The membrane-mCherry construct was kindly provided by S. Fraser (California Institute of Technology). The construct was subcloned from its original parent vector (pCS) into the 5' *Hpa*I and 3' *Cla*I sites of the retroviral vector pLHCX (Clontech). Briefly, pCS-membrane-mCherry was used as the PCR template to amplify the complete membrane-

mCherry coding sequence, with *Hpa*I and *Cla*I sites added to the 5' and 3' ends, respectively. The PCR product was digested with *Hpa*I and *Cla*I, and subcloned into the multiple cloning site (MCS) of pLHCX vector through these two sites, generating pLHCX-membrane-mCherry. The coding sequence of pLHCX-membrane-mCherry was verified by DNA sequencing (Laragne) with 5' and 3' pLHCX primers and alignment with the original membrane-mCherry sequence provided by Scott Fraser.

Retrovirus production and usage

Retroviral infection was used for the stable expression of mCherry in MCF-10A cells. Retrovirus was produced by triple transfection of HEK 293T cells with 5 μg each of VSV-G, gag-pol, and pLHCX-membrane-mCherry using Lipofectamine (Invitrogen). Virus-containing supernatant was collected and used to infect MCF-10A cells in the presence of essential growth factors and 8 μg/ml polybrene.

References

1. Debnath J & Brugge JS (2005) Modelling glandular epithelial cancers in three-dimensional cultures. *Nat Rev Cancer* 5(9):675-688
2. Engler AJ, Humbert PO, Wehrle-Haller B, & Weaver VM (2009) Multiscale modeling of form and function. *Science* 324(5924):208-212
3. Wiseman BS & Werb Z (2002) Stromal effects on mammary gland development and breast cancer. *Science* 296(5570):1046-1049
4. Butcher DT, Alliston T, & Weaver VM (2009) A tense situation: forcing tumour progression. *Nat Rev Cancer* 9(2):108-122
5. Tlsty TD & Coussens LM (2006) Tumor stroma and regulation of cancer development. *Annu Rev Pathol* 1:119-150
6. Paszek MJ, *et al.* (2005) Tensional homeostasis and the malignant phenotype. *Cancer Cell* 8(3):241-254
7. Discher DE, Janmey P, & Wang YL (2005) Tissue cells feel and respond to the stiffness of their substrate. *Science* 310(5751):1139-1143
8. Nelson CM, *et al.* (2005) Emergent patterns of growth controlled by multicellular form and mechanics. *Proc Natl Acad Sci USA* 102(33):11594-11599
9. Dise RS, Frey MR, Whitehead RH, & Polk DB (2008) Epidermal growth factor stimulates Rac activation through Src and phosphatidylinositol 3-kinase to promote colonic epithelial cell migration. *Am J Physiol Gastrointest Liver Physiol* 294(1):G276-285

10. Schneider IC, Hays CK, & Waterman CM (2009) Epidermal growth factor-induced contraction regulates paxillin phosphorylation to temporally separate traction generation from de-adhesion. *Mol Biol Cell* 20(13):3155-3167
11. Adams CL, Chen Y-T, Smith SJ, & James Nelson W (1998) Mechanisms of epithelial cell-cell adhesion and cell compaction revealed by high-resolution tracking of E-cadherin-green fluorescent protein. *J Cell Biol* 142(4):1105-1119
12. Tan JL, *et al.* (2003) Cells lying on a bed of microneedles: an approach to isolate mechanical force. *Proc Natl Acad Sci USA* 100(4):1484-1489
13. Dembo M, Oliver T, Ishihara A, & Jacobson K (1996) Imaging the traction stresses exerted by locomoting cells with the elastic substratum method. *Biophy J* 70(4):2008-2022
14. Maskarinec SA, Franck C, Tirrell DA, & Ravichandran G (2009) Quantifying cellular traction forces in three dimensions. *Proc Natl Acad Sci USA* 106(52):22108-22113
15. Pelham RJ, Jr. & Wang Y (1997) Cell locomotion and focal adhesions are regulated by substrate flexibility. *Proc Natl Acad Sci USA* 94(25):13661-13665
16. Franck C, Hong S, Maskarinec SA, Tirrell DA, & Ravichandran G (2007) Three-dimensional full-field measurements of large deformations in soft materials using confocal microscopy and digital volume correlation. *Exp Mech* 47(3):427-438
17. Graham NA & Asthagiri AR (2004) Epidermal growth factor-mediated T-cell factor/lymphoid enhancer factor transcriptional activity is essential but not sufficient for cell cycle progression in nontransformed mammary epithelial cells. *J Biol Chem* 279(22):23517-23524

Appendix I. Intercellular mechanotransduction during multicellular morphodynamics

Abstract

Multicellular structures are held together by cell adhesions. Forces that act upon these adhesions play an integral role in dynamically re-shaping multicellular structures during development and disease. Here, we describe different modes by which mechanical forces are transduced in a multicellular context: (a) indirect mechanosensing through compliant substratum, (b) cytoskeletal "tug-of-war" between cell-matrix and cell-cell adhesions, (c) cortical contractility contributing to line tension, (d) stresses associated with cell proliferation, and (e) forces mediating collective migration. These modes of mechanotransduction are recurring motifs as they play a key role in shaping multicellular structures in a wide range of biological contexts. Tissue morphodynamics may ultimately be understood as different spatiotemporal combinations of a select few multicellular transformations, which in turn are driven by these mechanotransduction motifs that operate at the bicellular to multicellular length scale.

Reprinted from Kim, J.-H., L. J. Dooling, and A. R. Asthagiri from *Journal of Royal Society Interface* (2010)

Introduction

The remarkable dynamism of multicellular structures is in full display during development and continues in adult tissues, such as the intestinal epithelium (1) and the mammary gland (2). Meanwhile, disruptions in multicellular morphology, and consequently tissue function, play a major role in diseases such as cancer (3). Elucidating the forces that form and re-shape multicellular structures is integral to our understanding of development and disease and has clear implications for biomedical applications, such as tissue engineering.

Transformations in multicellular structure are achieved through mechanical forces that act upon cell adhesions. Cells adhere to their neighbors and to the surrounding extracellular matrix (ECM). Significant advances have been made in our understanding of the molecular composition of adhesions (4-5) and their mechanosensitivity (6). Acting as mechanosensors and as an interface for force transmission, cell adhesions play a pivotal role in regulating single-cell behaviors, such as rolling (7), spreading and migration (8), survival and proliferation (9), and differentiation (10-11).

Multicellular morphodynamics, however, is not the simple consequence of cell autonomous responses to local forces. Local forces are transmitted over longer length scales and propagate their effects at a mesoscopic level. In this review, we discuss different modes by which mechanical forces are transduced in a multicellular context, ranging from bicellular interactions to larger tissue-scale structures (figure 1). Here, we

use the term “mechnotransduction” broadly to include both this transmission and re-distribution of mechanical forces and the interconversion of mechanical forces and biochemical signals.

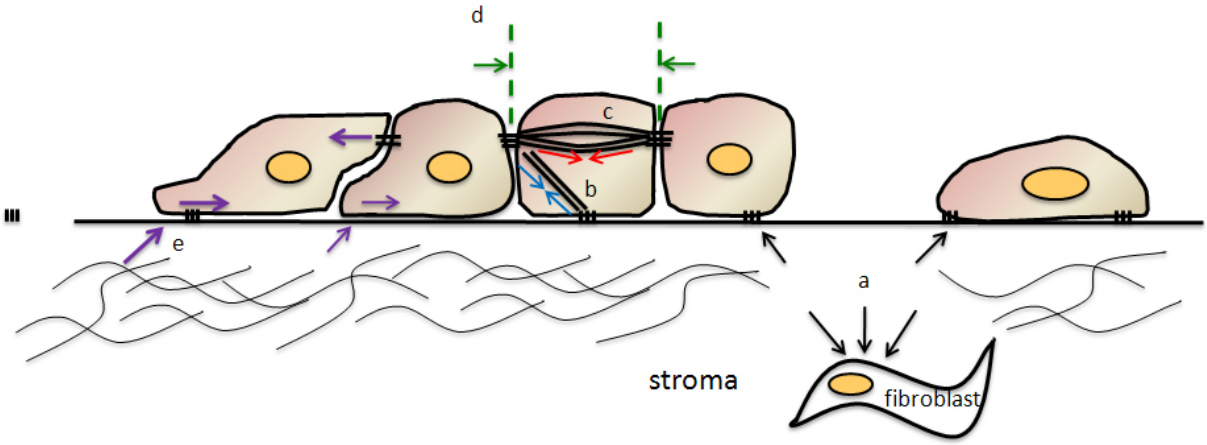

Figure 1: Modes of force transmission in multicellular systems. In a multicellular context, several intercellular mechanotransduction motifs can be identified: (a) indirect mechanosensing through compliant substratum (black arrows), (b) cytoskeletal “tug-of-war” between cell-matrix and cell-cell adhesions (blue arrows), (c) cortical contractility contributing to line tension (red arrows), (d) compressive stresses (green arrows) acting on the planes represented by the dashed lines and resulting from the proliferation of neighboring cells, and (e) forces mediating collective migration (purple arrows) including traction forces, such as those depicted at the leading edge, and tension that is propagated through cell-cell contacts.

1. Indirect cell-cell mechanosensing through a compliant extracellular matrix

An emerging mechanism for cell-cell communication involves exerting and sensing traction forces on the ECM. When a cell contracts, it pulls on its surroundings through integrin-mediated adhesions. This allows the cell to sense the mechanical response of its environment and react appropriately (12-13). As a result, the physical properties of the matrix, in particular its compliance, have a significant effect on cell behaviors such as spreading (14-15), migration (16-18), proliferation (19), and differentiation (10-11). In *in vitro* studies of contractility, substrates of varying compliance are commonly prepared using synthetic polymers, such as polyacrylamide, by varying the extent of crosslinking while keeping the adhesive ligand composition constant (17). Fluorescent beads can be embedded within these substrates, and their displacements are measured to produce a map of the traction forces (20).

It is becoming increasingly apparent that contractile forces generated against the ECM not only influence the behavior of individual cells but also play a role in governing how cells interact with each other. As a cell contracts on a compliant substrate, it produces stress and strain that can be sensed by its neighbors, thus providing a mechanical pathway for cell-cell communication even in the absence of direct contact. Reinhart-King *et al.* (21) have demonstrated this concept by investigating how substrate compliance influences the contact and migratory behaviors of pairs of bovine aortic endothelial cells. Using traction force microscopy, they show that the distance over which a cell significantly deforms its substrate decreases with increasing substrate stiffness, and they postulate that this distance represents the maximum range of ECM-mediated cell-cell mechanosensing. On soft surfaces, two cells that collide remain in

contact throughout the duration of the experiment, most likely because the soft substrate prevents them from generating enough traction force to break the cadherin bonds formed at the cell-cell junction. Conversely, cellular collisions on stiff surfaces are very elastic and cells remain in contact for short durations before migrating away from one another. On substrates of intermediate compliance, a pair of cells repeatedly forms a contact and breaks it. As a result, they exhibit a lower dispersion than isolated cells and fail to migrate beyond the measured distance of significant substrate deformation. This behavior suggests that even after contact is broken, the cells still communicate mechanically through the matrix and that the substrate compliance influences cell-cell interactions.

Cell-cell communication mediated by the ECM has also been observed between human mesenchymal stem cells (hMSC) on fibrin (22). In this case, the communication is believed to involve the strain-stiffening property of nonlinear elastic matrices. The strain produced by cell contraction stiffens the substrate by several orders of magnitude thereby changing the microenvironment of nearby cells. This results in an alignment and elongation of hMSCs cultured on such substrates.

The two previous examples demonstrate how contractile forces generated on the ECM may be responsible for influencing the interactions between cells cultured *in vitro* on compliant substrates. Similar behavior may be observed at the tissue level as well. Epithelial and endothelial cells are often separated from underlying stromal cells by a basement membrane consisting of proteins, such as laminin and collagen. The presence

of stromal cells significantly alters the mechanical properties of the ECM through contractility and matrix remodeling. Elson and colleagues have shown that fibroblasts compress and stiffen collagen gels *in vitro* (23), and that the mechanical properties of the tissue vary with fibroblast concentration (24). These effects can be sensed by the basal surface of the epithelium and endothelium, and may play an important role in tissue homeostasis, development, and tumor progression (25-26).

2. Direct cell-cell interactions and their mechanical interplay with cell-matrix adhesions

While cells are capable of communicating indirectly with each other through the ECM, as cells get close enough to interact directly using cell-cell adhesion receptors, such as cadherins, various short-range modes of crosstalk unfold between cell-cell and cell-matrix adhesions. The differential adhesion paradigm considers the antagonistic interplay between cell-cell and cell-matrix interactions at the level of the cell surface. Steinberg and colleagues observed this antagonism during the transition between aggregation and spread phenotypes of multicellular clusters (27). Cells with minimal cadherin expression level exhibited low cohesivity and a spread phenotype even on substrata that are only moderately adhesive. However, increasing cell-cell cohesivity by raising cadherin expression reverts this spread phenotype and promotes aggregation. Their results demonstrate that tissue spreading is the outcome of a competition between cell-cell cohesivity and cell-substratum adhesivity (figure 2a).

In addition to this antagonism at the level of the cell surface, cell-cell and cell-matrix adhesions are also coupled mechanically through their joint affiliation with the cytoskeleton. At the molecular level, actin cables associate with adherens junctions at cell-cell contacts and provide a physical mechanism for cell-generated contractile forces to act upon cell-cell adhesions. This non-muscle myosin-mediated tension at sites of cell-cell adhesion is necessary for the formation and maturation of cell-cell contacts, which are destabilized upon loss of myosin-generated contractility (28-29). However, excessive contractile forces can compromise cell-cell adhesions (29). Precisely how much contractile force is imposed upon cell-cell adhesions will depend on the level of cell-matrix adhesions, which are also linked to the actin cytoskeleton (figure 2b). In situations where cell-matrix adhesions are enhanced, as observed upon hepatocyte growth factor (HGF) treatment and on stiff substrates, they are better able to withstand contractile forces, while cell-cell adhesions are compromised, thereby promoting cell scatter (29). Consistent with these observations, cells are better able to form multicellular aggregates and undergo tissue-like compaction on a compliant substratum than on stiff substrates (30). Furthermore, using mammary epithelial cells cultured in 3D matrix, Weaver and colleagues showed that increasing matrix stiffness elevates ROCK-generated contractility and FA formations among mammary epithelial cells, in turn weakening adherens junctions and disrupting organized acinar structures (31). In this manner, cell-generated contractile forces mediate a “tug-of-war” between cell-cell adhesions and cell-matrix adhesions that has implications for multicellular organization in both two- and three-dimensional contexts. It is important to note, however, that these forces at cell adhesions may also induce changes in gene expression that contribute to cell scatter. For example,

enhanced adhesion-mediated signaling on stiff surfaces may lead to gene expression patterns facilitating the loss of cell-cell contacts and cell scatter as observed in epithelial-mesenchymal transition (EMT).

The crosstalk between cell-cell and cell-matrix interactions can also promote spatial gradients in mechanical stresses within multicellular structures. Cells at the periphery of a cluster extend their free edge into the surrounding ECM and exert greater traction forces through their adhesions to the matrix than cells in the interior of the cluster. In contrast, interior cells are surrounded by neighbors, and the contractile forces generated within these cells are imposed upon their neighbors through cell-cell contacts. By measuring the deflection of vertical elastomeric micropillars, Chen and colleagues directly quantified the gradient in traction forces in multicellular clusters and correlated this gradient to spatial patterns in proliferation (figure 2c) (32). The introduction of the cytoplasmic-deletion mutant of VE-cadherin, which is defective in linking cadherin to the actin cytoskeleton, ablated the spatial gradient in traction forces and the pattern in cell cycle activity across cell clusters.

In addition to the distribution of traction forces within multicellular aggregates, the level of soluble growth factors, such as epidermal growth factor (EGF), also play an important role in shaping spatial patterns in proliferation. We recently have demonstrated that in epithelial clusters, cadherin-dependent contact-inhibition is enforced only below a critical threshold level of EGF (33). Thus, only when the growth-promoting activity of EGF dips below a threshold, cell-cell contact is able to inhibit effectively the

proliferation of cells in the interior of a cluster, leading to a spatial pattern in proliferation. When EGF concentration is raised above this threshold, epithelial cells exhibit contact-independent, uniform proliferation. Intriguingly, this threshold amount of EGF is tunable: augmenting cell-cell interactions increases the EGF threshold at which the system transitions from contact-inhibited to contact-independent proliferation. Thus, it is evident that crosstalk between hormonal/growth factor pathways and the physical distribution of traction forces is involved in regulating patterns in cell proliferation in epithelial clusters.

The maturation of cell-cell contacts in epithelial sheets can be accompanied by the recruitment of the focal adhesion protein, vinculin, from sites of cell-matrix adhesions to cell-cell junctions. This change in vinculin localization leads to the reorganization of stress fibers associated with focal adhesions at cell-substratum interfaces into cortical bundles that run parallel with cell-cell contacts (34). During epidermal stratification, cortical actin bundles further polarize into the apical plane and form a continuous cytoskeletal network spanning the entire epithelial sheet. Coordinated tension developed through these apical actin cables enables cells to slide under neighboring cells by transiently disrupting their cell-substratum interactions (35).

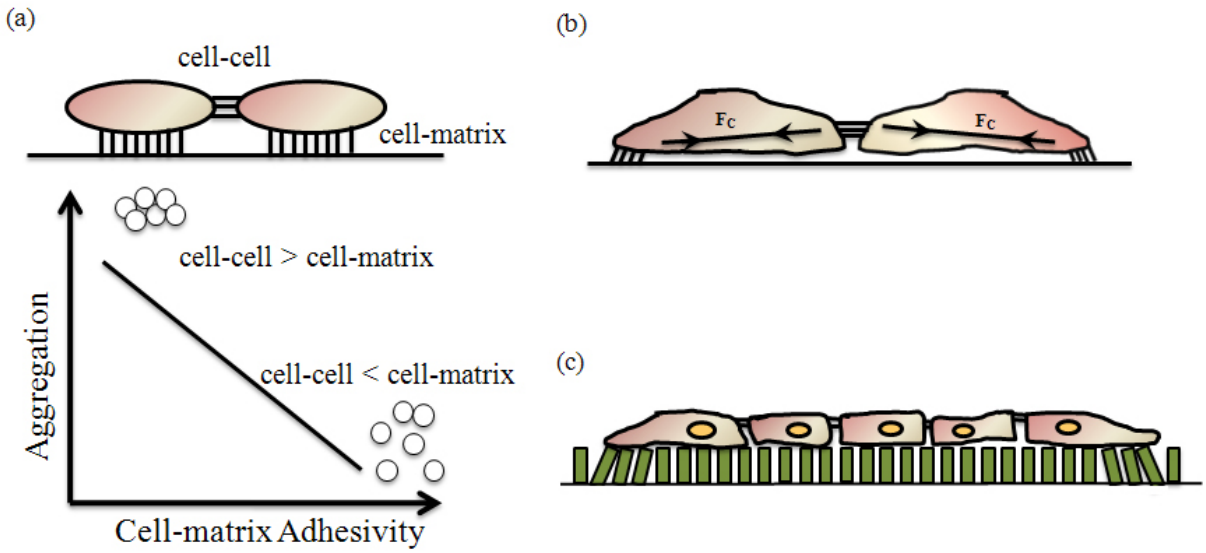

Figure 2: Crosstalk between cell-matrix and cell-cell adhesions. (a) The differential adhesion paradigm states that aggregation is preferred when cell-cell cohesivity outweighs cell-matrix adhesivity, while a spread phenotype is promoted when cell-matrix adhesivity dominates. (b) Cell-generated contractile forces mediate a "tug-of-war" between cell-cell and cell-matrix adhesions. (c) A multicellular implication of (b) is depicted in two-dimensional cell culture on elastomeric micropillars. Peripheral cells exhibit high traction forces on the substrate resulting in the bending of the pillars while cells in the interior of the cluster dissipate cell-generated contractile forces against their neighbors.

3. Cortical contractility and line tension along cell-cell contacts

Cell-generated contractile forces along cortical actin structures in the apical region of epithelial cells also contribute to line tension along cell-cell interfaces. This

line tension plays a significant role in cellular rearrangements during processes such as intercalation in response to external and internal forces, in shaping and sizing cells in growing epithelial sheets and in maintaining multicellular compartments (figure 3).

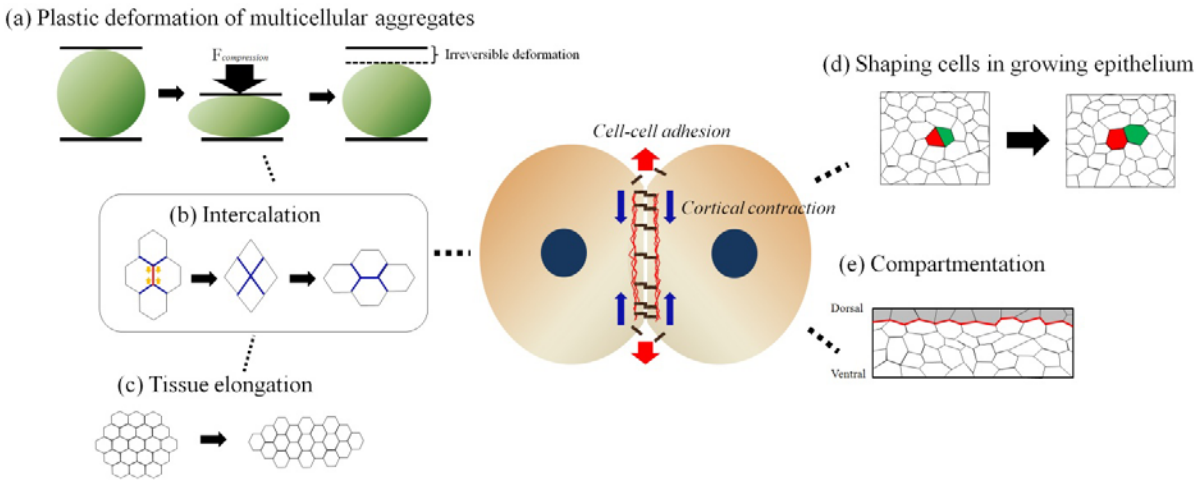

Figure 3: Cortical contractility and interfacial line tension as a recurring motif in multicellular morphodynamics. Cell-generated contractile forces acting along the cortical actin structures are counterbalanced by cell-cell adhesion, contributing to the development of line tension at the interface between cells. (a) This line tension presents an energy barrier to cellular rearrangements under externally applied forces, giving rise to irreversible deformation of multicellular aggregates. (b) Internal asymmetry in local cortical tension drives intercalation involving the collapse of dorsal/ventral junctions (indicted by the red line) followed by the addition of anterior-posterior contacts (indicated by blue lines). (c) Collective cell intercalation propels tissue-wide change in morphology such as tissue elongation. (d) In a growing epithelium, cell division predominantly results in daughter cells sharing an edge and cleaving at a side rather than

a vertex, posing “geometric rules” governing distribution of cell shapes. (e) Anisotropic line tension developed at the boundary of two cell populations (indicated by red line) is responsible for the maintenance multicellular compartmentation such as dorsal-ventral (DV) demarcation of wing imaginal discs.

3a. Line tension as an energy barrier for plastic deformation

At a macroscopic scale, line tension is involved in the plasticity of multicellular aggregates (i.e., irreversible shape change of the aggregates) exposed to external compressive load (36). Line tension provides an energy barrier for cellular rearrangements within the aggregates. Cell aggregates under high compressive stress overcome this barrier and undergo not only elastic cell shape change, but also cellular rearrangements involving shuffling of cells (intercalation). These cellular rearrangements persist even after the imposed external stress is removed, rendering a plastic deformation (figure 3a). In contrast, in a low stress regime where line tension is not overcome, aggregates exhibit only cell shape changes through spontaneous membrane fluctuations, and when the external force is removed, the original aggregate shape is recovered.

3b. Line tension in intercalation

Asymmetric line tension provides the driving force for intercalation during germband elongation in *Drosophila* embryos (37). In this process, the epithelial tissue elongates along the anterior/posterior axis through the intercalation of cells along the dorsal/ventral axis. This process involves the shrinkage of dorsal/ventral contacts (v-junctions) followed by the establishment of new cell-cell contacts parallel to the anterior-

posterior axis (t-junctions) (figure 3b). Myosin-II is preferentially localized at v-junctions (38), and this localization corresponds to greater tension at v-junctions than along t-junctions as quantified by local laser ablation and the consequent recoil speed of the cell-cell interface (37). This asymmetry in local cortical tension drives the tissue-wide change in morphology (figure 3c). Furthermore, this tension increases as the v-junction collapses, suggesting that cortical elasticity is also a critical factor.

3c. Line tension in shaping cells in growing epithelium

During the intercalation process described above, the number of epithelial cells remains fixed and the predominant activity involves the relative shuffling in position of cells within the epithelium. In other situations, the epithelium undergoes a significant change in cell number while the relative position of cells does not change markedly. An important feature of such growing epithelial sheets is the distribution of polygonal cell shapes. While most cells are hexagonal, there are also significant numbers of cells with a shape that ranges from quadrilateral to octagon. Gibson *et al.* (39) show that simple "geometric rules" of epithelial cell divisions are sufficient to predict the distribution of polygonal shapes in the developing epithelial wing primordium of *Drosophila melanogaster*. These rules were based on observations such as the following: The vast majority of epithelial divisions (94%) result in daughter cells that share an edge, and cell divisions tend to cleave a side rather than a vertex (figure 3d). A Markov model based on these and other geometric rules predicts that a growing epithelial sheet reaches a distribution of polygonal shapes consistent with that observed in developing wings. In fact, the predicted distribution of cell shapes matches that observed in epithelial tissues

from vertebrate, arthropod, and cnidarian organisms, suggesting that a common set of geometric division rules governs the shapes of epithelial cells in growing tissues throughout the metazoa.

It should be noted, however, that the distribution of polygonal shapes is not the only feature of interest in a growing epithelium. For example, the average size of a cell increases as cell number increases, and cells occasionally desorb or delaminate from the epithelium. Furthermore, the geometric constraints of cell divisions likely arise from mechanical forces and biophysical properties, such as membrane elasticity, contractility and cell-cell adhesion. This raises the question of how these forces and biophysical properties shape cells within a growing epithelium. Farhadifar *et al.* (40) examined this issue by developing a model in which the positions of vertices in a growing epithelium are determined by the minimization of energy associated with the contractility of the cortical actin-myosin network, line tension along apical junctions and cell surface elasticity. Their model predictions of frequency of cell delamination, cell area and polygonal shapes matched those in the developing *Drosophila* wing disc only for specific ranges of parameter values. These results suggest that the biophysical properties of epithelial cells are wired to give rise to the observed cell shapes in growing epithelial tissues. It would be interesting to determine whether these parameter values are also necessary to give rise to the geometric rules of cell divisions used in the Gibson model.

3d. Line tension in compartmentation

Anisotropic line tension is involved not only in local re-shuffling of neighboring cells during intercalation (figure 3b), but also in maintaining long range barriers between two cell populations (figure 3e). This role of partitioning cell populations was first suggested in the context of dorsal-ventral (DV) demarcation of wing imaginal discs (41-42). More recently, the magnitude of anisotropic line tensions has been directly measured and computationally modeled in anterior-posterior (AP) demarcation of wing imaginal discs (43-44), and eliminating this line tension has been shown to compromise the re-establishment of anterior-posterior compartmentation following cell divisions at this interface during *Drosophila* embryonic development (45). Consistent with the idea that anisotropic line tension may be a recurring motif for maintaining cell compartments, the above studies span AP and DV compartmentation in *Drosophila* wing discs and AP compartmentation in *Drosophila* embryonic development.

3e. Contractility and cell-cell adhesion: opposing contributions to line tension?

In the above models of line tension along cell-cell junctions, contractility opposes cell-cell adhesion (figure 3). However, there is some evidence that contractility can influence the endocytosis of cell adhesion receptors (46) while planar cell polarity (PCP) proteins regulate the exocytosis and recycling of cell adhesion proteins (47). Furthermore, in the case of cell adhesion to the extracellular matrix, contractility is essential to forming and maintaining focal adhesions; in a similar manner, contractile forces are involved in promoting the maturation of cell-cell adhesions (48). Thus, it remains an open question to what extent cortical contractility and cell-cell adhesion ought to be viewed as independent opposing contributions to line tension.

4. Forces associated with cell behaviors

The loss, accrual and movement of cells due to apoptosis, proliferation, and migration, respectively, can generate local forces on direct neighbors and even propagate to affect tissue morphology at a mesoscopic scale.

4a. Forces associated with apoptosis

The extrusion of apoptotic cells from an epithelial sheet has been observed in the context of various developmental processes and is essential to maintain the integrity of the epithelium and its barrier function. Rosenblatt *et al.* (49) showed that an apoptotic cell within an epithelial layer rapidly develops an actomyosin ring around its periphery and signals to its neighboring cells to induce actin cable formation at the interface between the apoptotic cell and neighboring live cells (figure 4a). Rho-mediated contraction of these actin cables pulls neighboring cells toward the apoptotic cell and extrudes the apoptotic cell out of its parental epithelia, rapidly sealing the opening that could have been left by the removal of the dead cell. In fact, selective blocking of Rho activity in neighboring cells aborted the extrusion of the apoptotic cells completely, disrupting the integrity of epithelia. Thus, apoptotic force involves not only an autonomous contractile force in a cell undergoing the death, but also collective force developed among live cells surrounding the apoptotic cell.

Such forces involved in the extrusion of apoptotic cells also propagate through cell-cell interactions to affect the long-range morphology of tissues. An example involves dorsal closure of the *Drosophila* embryo. During this process, an elliptical opening in the dorsal epidermis is occupied by the amnioserosa and is covered by two dorsally migrating epithelial leading edges with the two flanks advancing along the dorsal midline (figure 4b). A precise coordination of forces, including the contractility of the amnioserosa, contributes to sheet migration and dorsal closure (50) . The apoptosis of amnioserosa cells contributes significantly to the contractility of this tissue and thus the rate of dorsal closure (51). By quantitatively comparing the recoiling velocity of the leading edge of lateral epidermis upon laser ablation in wild type and apoptotic mutants, it was estimated that apoptosis of aminoserosa cells accounts for approximately one-third to one-half of the net force developed at the leading edge of lateral epidermis. The contractile forces involved in extruding apoptotic cells may be transmitted by cell-cell contacts to the lateral epidermis, contributing the force needed for dorsal migration of lateral epithelia and fusion.

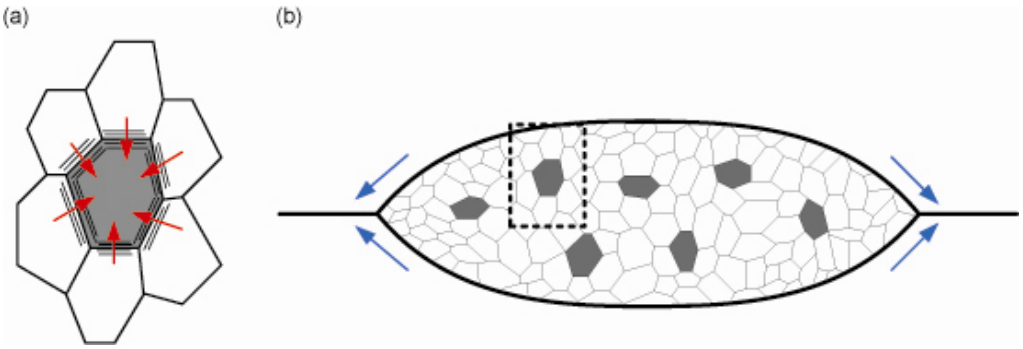

Figure 4: Forces associated with apoptosis and their implications for *Drosophila* dorsal closure. (a) An actomyosin ring forms in both the cell undergoing apoptosis (grey) and its live neighbors. Contractile forces along this actomysin ring generate a force (red arrows) that pulls neighboring cells into the space occupied by the extruded cell and prevents gaps in the epithelium. (b) This force associated with apoptosis contributes to dorsal closure in the *Drosophila* embryo. The contractile forces generated by apoptotic cells (grey) in the amnioserosa (AS) contribute to tension (blue arrows) along the leading edge of the lateral epithelia tissues (LET).

4b. Mechanical stresses imposed by proliferation

In a growing tissue in which cellular rearrangements are restricted in the time scale of cell division, mechanical stresses imposed by an increase in cell mass (i.e., proliferation) are not fully released and thus rapidly accumulate in a local environment. One of the phenotypic features of rapidly growing tissue is that cell spreading against underlying substrate decreases with increasing cell density. Restricted cell spreading further correlates with decrease in stress fiber formation, which in turn destabilizes focal adhesions. Consistent with these changes, when plated on varying sizes of adhesive patterns consisting of micropillars, cells grown on smaller islands exhibited significantly reduced cytoskeletal tension and contraction force (52). In addition, accumulation of mechanical stresses accompanying aforementioned events has been correlated with cell cycle arrests in high density culture (53).

Notably, coupled with other microenvironmental factors, force induced by proliferation plays a central role in patterning multicellular behaviors in the context of developmental processes (figure 5). Patterning and growth regulation of *Drosophila* wing imaginal discs involves the gradients of morphogens including Decapentaplegic (Dpp). However, while it is clear how reduced morphogen concentration far from the source would halt cell proliferation at the edge of a developing tissue, how cell proliferation and tissue growth stop near the morphogen source remained unclear. Shraiman (54) theoretically showed that at the region of high morphogen concentration, mechanical stresses rapidly accumulate as a result of a high rate of proliferation. This accumulated mechanical stress in turn inhibits morphogen-induced proliferation. Thus, once cell proliferation ceases at the edge of a developing tissue due to low morphogen concentration, continued proliferation near the morphogen source would escalate the local mechanical stress and stop the growth of tissue as a whole. Thus, mechanical stresses would serve as a local negative regulator of growth, thereby affecting growth patterns and organ size (55).

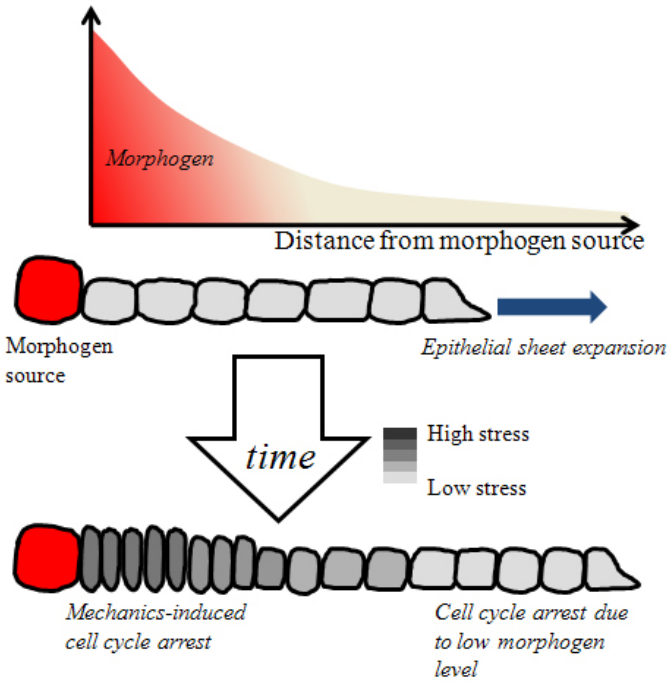

Figure 5. Role of proliferation-induced mechanical stresses in growth patterning and organ size determination. During development of *Drosophila* wing imaginal discs, spatial gradients in morphogens regulating cell growth are established by their localized secretion and transport from source cells (red cell). The graph depicts the steady-state gradient in morphogen concentration as a function of distance from the morphogen source. Below the graphs, grayscale color gradients in the cells indicate the level of mechanical stress due to crowding. At early stages of the development (top cell array), cells proliferate uniformly, expanding the epithelium without local accumulation of mechanical stresses. Later, cell growth ceases at the edge of the epithelium due to low morphogen level (bottom cell array), and mechanical stresses accumulate near the morphogen source as a result of imbalanced growth. It is postulated that this mechanical

stress may desensitize cells to the locally high levels of growth factor and lead to mechanics-induced cell cycle arrest (Shraiman 2005).

4c. Forces driving collective migration

The mechanics of migration in single cells have been widely studied, revealing the importance of protrusive forces that drive the extension of the leading edge of the cell and contractile forces that detach the trailing edge and pull the cell body forward (56). However, less is known about the mechanics of sheets and strands of cells moving together, a process known as collective migration. Given that these cells not only adhere to the surrounding matrix but also remain in contact with each other through cell-cell adhesion proteins, such as cadherins, one would expect the interplay between mechanical forces involved in cell-cell and cell-matrix adhesion to play a major role in the behavior of such systems. Understanding how collective migration forces are generated and transmitted between cells has important implications in disease and physiology.

Collective migration is a key phenomenon in tissue morphogenesis and is widely observed in developing organisms (57-58). Wound healing is a classic example of collective motility, and *in vitro* assays of this process have provided a powerful model system to study the movement of two-dimensional cell sheets. Other examples include border cell motility during *Drosophila* ovary development (59-60) and branching morphogenesis in mammary epithelia (61).

Two important questions arise concerning how the forces that lead to wound closure are generated. The first is whether wound healing is driven predominantly by proliferation within the monolayer that pushes it forward or whether cell migration propels the healing process by pulling the sheet into the wound. The emerging consensus appears to be that cell migration at the healing front is the key driver with proliferation helping to maintain the monolayer (62). Several studies have suggested a leader-follower model wherein the leading cells at the wounded edge migrate and pull along the trailing cells. For example, in both IAR-2 and MDCK epithelial sheets exposed to model wounds, leaders temporarily lose their epithelial character and develop lamellipodia and focal adhesions that protrude into the wound (63-64). Leader-follower behavior is also observed in a wounded endothelial monolayer in the presence of fibroblast growth factor (65).

Rho-dependent cytoskeleton reorganization appears to play a significant role in the leader-follower model of wound healing. Omelchenko *et al.* (2003) note that leader cells disassemble their cortical actin cables upon wounding and reorient filaments perpendicular to the advancing front. Follower cells maintain their cortical actin cables but exhibit radial, rather than tangential, cell-cell contacts with leaders, indicating that tension is generated by the leader cells. Pojade *et al.* (2007) observe similar behavior in leader cells and also note the development of a supracellular actin belt in follower cells that may transmit force as in the purse-string wound closure mechanism.

If we accept the notion that wound healing is driven primarily by cell migration rather than proliferation, a second question that arises is where the traction forces necessary for migration are generated. In the simplest leader-follower model, traction forces would be generated by the first row of cells (i.e., the leaders) so that followers need only to release their attachments and be pulled forward. Recent findings, however, suggest that this is not the case and that instead, the traction forces involved in propelling wound healing may be generated by cells much farther into the monolayer (66). Thus, in growing MDCK sheets, significant traction forces are observed far away from the leading edge. Furthermore, a force balance shows that the tensional stress is propagated into and accumulates within the sheet, suggesting long-range transmission of forces from the leading edge into the interior of a growing epithelial sheet (67). This view may be supported by the observation of cryptic lamellipodia protruding from submarginal cells in the direction of the wound as well as the ability for these cells to compensate for a loss of motility in the first row of the advancing edge (68-69).

The observations from these studies suggest that collective sheet migration and wound healing may occur by different modes depending on the tissue environment. In one extreme, cells within a monolayer may behave nearly autonomously and generate their own motile forces (70). While leader cells may be present in such cases, they act primarily to guide or polarize their followers to move in the direction of the wound. In the other extreme, leader cells may exert enough force to physically drag follower cells behind them (71). Most observations appear to suggest a mode in which both behaviors are important. As a result, the migration of each cell arises from its own traction forces

as well as the forces exerted by its neighbors. The relative strength of these forces could depend on a number of factors, including monolayer size and density, the strength of cell-cell adhesions, the matrix over which the sheet is migrating, and the presence of soluble factors. Such behavior would be consistent with the recent hypothesis that collective morphogenic movements are controlled *in vivo* by modular mechanical properties (72).

5. Concluding remarks

The modes of force propagation described in this review are recurring motifs as they contribute to morphodynamics across several distinct multicellular contexts. An intriguing possibility is that these and other force transmission modalities may enable a well-defined set of multicellular transformations. Indeed, seemingly diverse morphological patterns observed *in vivo* may be an outcome of different coupling and executions of these common motifs. For example, diverse epithelial morphogenetic phenotypes observed during dorsal closure and germband extension in the *Drosophila* embryo and during convergence of the zebrafish trunk neural ectoderm are simply quantitative combinations of cellular deformation and intercalation (Blanchard *et. al.* 2009). The rapidly growing interest in dynamical imaging of development in several model organisms should add to these findings and provide a more complete description of possible multicellular transformations. Tissue morphodynamics may ultimately be understood as different spatiotemporal combinations of a select few multicellular transformations, which in turn are driven by a small group of mechanotransduction motifs that operate at the bicellular to multicellular length scale.

References

1. van der Flier LG & Clevers H (2009) Stem Cells, Self-Renewal, and Differentiation in the Intestinal Epithelium. *Ann Rev Physiol* 71(1):241-260
2. Nelson CM & Bissell MJ (2006) Of extracellular matrix, scaffolds, and signaling: Tissue architecture regulates development, homeostasis, and cancer. *Ann Rev Cell Dev Bi* 22(1):287-309
3. Debnath J & Brugge JS (2005) Modelling glandular epithelial cancers in three-dimensional cultures. *Nat Rev Cancer* 5(9):675-688
4. Zaidel-Bar R, Itzkovitz S, Ma'ayan A, Iyengar R, & Geiger B (2007) Functional atlas of the integrin adhesome. *Nat Cell Biol* 9(8):858-867
5. Zamir E & Geiger B (2001) Molecular complexity and dynamics of cell-matrix adhesions. *J Cell Sci* 114(20):3583-3590
6. Geiger B, Spatz JP, & Bershadsky AD (2009) Environmental sensing through focal adhesions. *Nat Rev Mol Cell Biol* 10(1):21-33
7. Chang K-C, Tees DFJ, & Hammer DA (2000) The state diagram for cell adhesion under flow: Leukocyte rolling and firm adhesion. *Proc Natl Acad Sci USA* 97(21):11262-11267
8. Beningo KA, Dembo M, Kaverina I, Small JV, & Wang Y-L (2001) Nascent focal adhesions are responsible for the generation of strong propulsive forces in migrating fibroblasts. *J Cell Biol* 153(4):881-888
9. Chen CS, Mrksich M, Huang S, Whitesides GM, & Ingber DE (1997) Geometric control of cell life and death. *Science* 276(5317):1425-1428

10. Engler AJ, *et al.* (2004) Myotubes differentiate optimally on substrates with tissue-like stiffness: pathological implications for soft or stiff microenvironments. *J Cell Biol* 166(6):877-887

11. Engler AJ, Sen S, Sweeney HL, & Discher DE (2006) Matrix Elasticity Directs Stem Cell Lineage Specification. *Cell* 126(4):677-689

12. Discher DE, Janmey P, & Wang Y-l (2005) Tissue Cells Feel and Respond to the Stiffness of Their Substrate. *Science* 310(5751):1139-1143

13. Vogel V & Sheetz M (2006) Local force and geometry sensing regulate cell functions. *Nat Rev Mol Cell Biol* 7(4):265-275

14. Engler A, *et al.* (2004) Substrate compliance versus ligand density in cell on gel responses. *Biophys J* 86(1):617-628

15. Yeung T, *et al.* (2005) Effects of substrate stiffness on cell morphology, cytoskeletal structure, and adhesion. *Cell Motil Cytoskel* 60(1):24-34

16. Lo C-M, Wang H-B, Dembo M, & Wang Y-L (2000) Cell Movement Is Guided by the Rigidity of the Substrate. *Biophys J* 79(1):144-152

17. Pelham RJ & Wang Y-l (1997) Cell locomotion and focal adhesions are regulated by substrate flexibility. *Proc Natl Acad Sci USA* 94(25):13661-13665

18. Peyton SR & Putnam AJ (2005) Extracellular matrix rigidity governs smooth muscle cell motility in a biphasic fashion. *J Cell Physiol* 204(1):198-209

19. Wang H-B, Dembo M, & Wang Y-L (2000) Substrate flexibility regulates growth and apoptosis of normal but not transformed cells. *Am J Physiol Cell Physiol* 279(5):C1345-1350

20. Dembo M & Wang Y-L (1999) Stresses at the Cell-to-Substrate Interface during Locomotion of Fibroblasts. *Biophys J* 76(4):2307-2316

21. Reinhart-King CA, Dembo M, & Hammer DA (2008) Cell-Cell Mechanical Communication through Compliant Substrates. *Biophys J* 95(12):6044-6051

22. Winer JP, Oake S, & Janmey PA (2009) Non-Linear Elasticity of Extracellular Matrices Enables Contractile Cells to Communicate Local Position and Orientation. *PLoS ONE* 4(7):e6382

23. Wakatsuki T, Kolodney MS, Zahalak GI, & Elson EL (2000) Cell Mechanics Studied by a Reconstituted Model Tissue. *Biophys J* 79(5):2353-2368

24. Marquez J, Genin G, Pryse K, & Elson E (2006) Cellular and Matrix Contributions to Tissue Construct Stiffness Increase with Cellular Concentration. *Ann Biomed Eng* 34(9):1475-1482

25. Grinnell F (2003) Fibroblast biology in three-dimensional collagen matrices. *Trends in Cell Biology* 13(5):264-269

26. Lopez JI, Mouw JK, & Weaver VM (2008) Biomechanical regulation of cell orientation and fate. *Oncogene* 27(55):6981-6993

27. Ryan PL, Foty RA, Kohn J, & Steinberg MS (2001) Tissue spreading on implantable substrates is a competitive outcome of cell-cell vs. cell-substratum adhesivity. *Proc Natl Acad Sci USA* 98(8):4323-4327

28. Conti MA, Even-Ram S, Liu C, Yamada KM, & Adelstein RS (2004) Defects in cell adhesion and the visceral endoderm following ablation of nonmuscle myosin heavy chain II-A in mice. *J Biol Chem* 279(40):41263-41266

29. de Rooij J, Kerstens A, Danuser G, Schwartz MA, & Waterman-Storer CM (2005) Integrin-dependent actomyosin contraction regulates epithelial cell scattering. *J Cell Biol* 171(1):153-164

30. Guo WH, Frey MT, Burnham NA, & Wang YL (2006) Substrate rigidity regulates the formation and maintenance of tissues. *Biophys J* 90(6):2213-2220

31. Paszek MJ, *et al.* (2005) Tensional homeostasis and the malignant phenotype. *Cancer Cell* 8(3):241-254

32. Nelson CM, *et al.* (2005) Emergent patterns of growth controlled by multicellular form and mechanics. *Proc Natl Acad Sci USA* 102(33):11594-11599

33. Kim J-H, Kushiro K, Graham NA, & Asthagiri AR (2009) Tunable interplay between epidermal growth factor and cell-cell contact governs the spatial dynamics of epithelial growth. *Proc Natl Acad Sci USA* 106(27):11149-11153

34. Maddugoda MP, Crampton MS, Shewan AM, & Yap AS (2007) Myosin VI and vinculin cooperate during the morphogenesis of cadherin cell cell contacts in mammalian epithelial cells. *J Cell Biol* 178(3):529-540

35. Vaezi A, Bauer C, Vasioukhin V, & Fuchs E (2002) Actin cable dynamics and Rho/Rock orchestrate a polarized cytoskeletal architecture in the early steps of assembling a stratified epithelium. *Dev Cell* 3(3):367-381

36. Marmottant P, *et al.* (2009) The role of fluctuations and stress on the effective viscosity of cell aggregates. *Proc Natl Acad Sci USA* 106(41):17271-17275

37. Rauzi M, Verant P, Lecuit T, & Lenne PF (2008) Nature and anisotropy of cortical forces orienting Drosophila tissue morphogenesis. *Nat Cell Biol* 10(12):1401-1410

38. Lecuit T & Lenne PF (2007) Cell surface mechanics and the control of cell shape, tissue patterns and morphogenesis. *Nat Rev Mol Cell Biol* 8(8):633-644

39. Gibson MC, Patel AB, Nagpal R, & Perrimon N (2006) The emergence of geometric order in proliferating metazoan epithelia. *Nature* 442(7106):1038-1041

40. Farhadifar R, Roper JC, Aigouy B, Eaton S, & Julicher F (2007) The influence of cell mechanics, cell-cell interactions, and proliferation on epithelial packing. *Curr Biol* 17(24):2095-2104

41. Major RJ & Irvine KD (2005) Influence of Notch on dorsoventral compartmentalization and actin organization in the Drosophila wing. *Development* 132(17):3823-3833

42. Major RJ & Irvine KD (2006) Localization and requirement for Myosin II at the dorsal-ventral compartment boundary of the Drosophila wing. *Dev Dyn* 235(11):3051-3058

43. Landsberg KP, *et al.* (2009) Increased cell bond tension governs cell sorting at the Drosophila anteroposterior compartment boundary. *Curr Biol* 19(22):1950-1955

44. Vincent JP & Irons D (2009) Developmental biology: tension at the border. *Curr Biol* 19(22):R1028-1030

45. Monier B, Pelissier-Monier A, Brand AH, & Sanson B (2010) An actomyosin-based barrier inhibits cell mixing at compartmental boundaries in Drosophila embryos. *Nat Cell Biol* 12(1):60-65; sup pp 61-69

46. Sahai E & Marshall CJ (2002) ROCK and Dia have opposing effects on adherens junctions downstream of Rho. *Nat Cell Biol* 4(6):408-415

47. Classen AK, Anderson KI, Marois E, & Eaton S (2005) Hexagonal packing of Drosophila wing epithelial cells by the planar cell polarity pathway. *Dev Cell* 9(6):805-817

48. Yamada S & Nelson WJ (2007) Localized zones of Rho and Rac activities drive initiation and expansion of epithelial cell-cell adhesion. *J Cell Biol* 178(3):517-527

49. Rosenblatt J, Raff MC, & Cramer LP (2001) An epithelial cell destined for apoptosis signals its neighbors to extrude it by an actin- and myosin-dependent mechanism. *Curr Biol* 11(23):1847-1857

50. Kiehart DP, Galbraith CG, Edwards KA, Rickoll WL, & Montague RA (2000) Multiple forces contribute to cell sheet morphogenesis for dorsal closure in Drosophila. *J Cell Biol* 149(2):471-490

51. Toyama Y, Peralta XG, Wells AR, Kiehart DP, & Edwards GS (2008) Apoptotic force and tissue dynamics during Drosophila embryogenesis. *Science* 321(5896):1683-1686

52. Tan JL, *et al.* (2003) Cells lying on a bed of microneedles: an approach to isolate mechanical force. *Proc Natl Acad Sci USA* 100(4):1484-1489

53. Liu WF, Nelson CM, Pirone DM, & Chen CS (2006) E-cadherin engagement stimulates proliferation via Rac1. *J Cell Biol* 173(3):431-441

54. Shraiman BI (2005) Mechanical feedback as a possible regulator of tissue growth. *Proc Natl Acad Sci USA* 102(9):3318-3323

55. Hufnagel L, Teleman AA, Rouault H, Cohen SM, & Shraiman BI (2007) On the mechanism of wing size determination in fly development. *Proc Natl Acad Sci USA* 104(10):3835-3840

56. Lauffenburger DA & Horwitz AF (1996) Cell Migration: A Physically Integrated Molecular Process. *Cell* 84(3):359-369

57. Friedl P & Gilmour D (2009) Collective cell migration in morphogenesis, regeneration and cancer. *Nat Rev Mol Cell Biol* 10(7):445-457

58. Rørth P (2009) Collective Cell Migration. *Ann Rev Cell Dev Bi* 25(1):407-429

59. Montell DJ (2003) Border-cell migration: the race is on. *Nat Rev Mol Cell Biol* 4(1):13-24

60. Rørth P (2002) Initiating and guiding migration: lessons from border cells. *Trends Cell Biol* 12(7):325-331

61. Ewald AJ, Brenot A, Duong M, Chan BS, & Werb Z (2008) Collective Epithelial Migration and Cell Rearrangements Drive Mammary Branching Morphogenesis. *Dev Cell* 14(4):570-581

62. Gov NS (2007) Collective cell migration patterns: Follow the leader. *Proc Natl Acad Sci USA* 104(41):15970-15971

63. Omelchenko T, Vasiliev JM, Gelfand IM, Feder HH, & Bonder EM (2003) Rho-dependent formation of epithelial "leader" cells during wound healing. *Proc Natl Acad Sci USA* 100(19):10788-10793

64. Poujade M, *et al.* (2007) Collective migration of an epithelial monolayer in response to a model wound. *Proc Natl Acad Sci USA* 104(41):15988-15993

65. Vitorino P & Meyer T (2008) Modular control of endothelial sheet migration. *Gene Dev* 22(23):3268-3281

66. Trepat X, *et al.* (2009) Physical forces during collective cell migration. *Nat Phys* 5(6):426-430

67. Ladoux B (2009) Biophysics: Cells guided on their journey. *Nat Phys* 5(6):377-378

68. Farooqui R & Fenteany G (2005) Multiple rows of cells behind an epithelial wound edge extend cryptic lamellipodia to collectively drive cell-sheet movement. *J Cell Sci* 118(1):51-63

69. Fenteany G, Janmey PA, & Stossel TP (2000) Signaling pathways and cell mechanics involved in wound closure by epithelial cell sheets. *Curr Biol* 10(14):831-838

70. Bindschadler M & McGrath JL (2007) Sheet migration by wounded monolayers as an emergent property of single-cell dynamics. *J Cell Sci* 120(5):876-884

71. Friedl P, Hegerfeldt Y, & Tusch M (2004) Collective cell migration in morphogenesis and cancer. *Int J Dev Biol* 48:441-449

72. Montell DJ (2008) Morphogenetic Cell Movements: Diversity from Modular Mechanical Properties. *Science* 322(5907):1502-1505

Appendix II. Quantitative immunofluorescence for measuring spatial compartmentation of covalently-modified signaling proteins

Abstract

Intracellular signaling pathways control cell behaviors and multicellular morphodynamics. A quantitative understanding of these pathways will provide design principles for tuning these signals in order to engineer cell behaviors and tissue morphology. The transmission of information in signaling pathways involves both site-specific covalent modifications and spatial localization of signaling proteins. Here, we describe an algorithm for quantifying the spatial localization of covalently-modified signaling proteins from images acquired by immunofluorescence (IF) staining. As a case study, we apply the method to quantify the amount of dually phosphorylated ERK in the nucleus. The algorithm presented here provides a general schematic that can be modified and applied more broadly to quantify the spatial compartmentation of other covalently-modified signaling proteins.

Reprinted from Kim, J.-H. and A. R. Asthagiri from *Systems Analysis of Biological Networks* for the series *Methods in Bioengineering,* Artech House (2009)

Introduction

Signal transduction networks control all aspects of cell behavior, such as metabolism, proliferation, migration, and differentiation (1). Thus, engineering cell behaviors will hinge on understanding and tuning information flow in these signaling pathways. Intracellular signals transmit information in at least two major ways. First, signaling proteins undergo covalent modifications that alter their intrinsic enzymatic activity and/or their interactions with binding partners. In addition to the connectivity of the signal transduction network, signaling proteins are localized spatially. Where a signal is located can influence its accessibility to upstream and downstream factors, and therefore, can play a significant role in controlling information flux (2).

Green fluorescent protein (GFP) has provided a powerful way to track the localization of signaling proteins (3). Variants of GFP spanning a wide range of spectral properties have opened the door to monitoring co-localization of signaling proteins. A key challenge, however, is that quantifying signal propagation must involve not only tracking protein localization, but also the covalent state of that signal.

Sensor platforms that track both spatial localization and covalent state/activity are emerging. Several involve fluorescence resonance energy transfer (FRET), a phenomenon wherein the close proximity of two complementary fluorphores allows one (the donor) to excite the other (acceptor) (4). The quenching of the donor and the excitation of the acceptor serves as a FRET signal. One general strategy has been to

introduce a chimeric version of the signaling protein. Both the acceptor and donor are placed in the protein whose folding into an active confirmation changes the FRET signal. Examples include the Raichu sensors for the cdc42/Rac/Rho family of GTPases (5). In another design, the fluorophores have been placed in chimeric pseudosubstrates for tyrosine kinases (6)and caspases (7). When these signaling enzymes act on the substrate, the re-folding or the cleavage of the substrate changes the FRET signal. A final approach is to place one fluorophore on the signaling enzyme and the other fluorophore on a binding partner. When these are recruited to each other, FRET signal ensues. Examples of this third approach include the Raichu-CRIB sensors for Rho family of GTPases (8).

A major drawback of these tools, however, is that they are highly tailor-made and do not report on the remarkable diversity of covalent modifications that a single signaling protein undergoes. For example, the PDGF receptor is phosphorylated at multiple tyrosine residues, and each phosphorylation site enables its interaction with distinct downstream targets (9). Such multisite covalent modifications are prevalent across signaling proteins. New mathematical modeling frameworks are being developed to handle the huge number of states in which a single signaling protein may be found (10). Proteomic approaches are being developed to quantify site-specific covalent modifications in cell extracts on a large scale (11). While this approach allows large-scale, quantitative analysis of covalent modifications to signaling proteins, it does not gauge subcellular spatial information.

Thus, complementary methods are needed to quantify spatial information on signaling proteins that have undergone site-specific covalent modifications. Classical immunofluorescence (IF) staining provides an excellent starting point. In IF staining, antibodies are used to detect an antigen (e.g., signaling protein) in fixed cells (12). These antibodies may be tagged with fluorophores, including quantum dots that have unique advantages over GFP. Furthermore, antibodies for site-specific covalent modifications are widely available commercially. A limiting factor, however, is that images acquired by IF are primarily analyzed qualitatively. Here, we describe image analysis algorithms that may be used to quantify IF images in an automated manner. As a case study, we apply the algorithms to quantify the level of nuclear extracellular-regulated kinase (ERK) signaling.

Experimental Design

In this work, we developed and tested image analysis algorithms to quantify the spatial localization of phosphorylated signaling proteins. We focused on phosphorylated ERK, a signal that localizes to the nucleus and is required for cell proliferation (13). We performed a dose-dependence assay to gauge how the localized signal responds to different amounts of stimuli. Such dose-response studies provide a well-defined approach to test whether our measurement methodology could discern quantitative changes in signaling.

It is useful to conduct such experiments in systems that have been confirmed to trigger the signal of interest using other experimental assays. Therefore, we chose a stimulus, epidermal growth factor (EGF), that is well known to trigger ERK signaling (14-15). We used MCF-10A cells that respond to EGF by triggering ERK phosphorylation as confirmed by Western blotting (16).

Materials

Cell culture

6 well plate (Corning)

Micro cover glass, 18 mm circle (VWR)

Dulbecco's modified Eagle's medium/Ham's F-12 containing HEPES and L-glutamine (Gibco)

Epidermal growth factor (Peprotech)

Hydrocortisone (Sigma-Aldrich)

Insulin (Sigma-Aldrich)

Choleratoxin (Sigma-Aldrich)

Bovine serum albumin (Sigma-Aldrich)

Trypsin EDTA 0.05% (Gibco)

Penicillin/streptomycin (Gibco)

Buffers/Reagents

Phosphate buffered saline (PBS)

Paraformaldehyde (Sigma-Aldrich)

Tween-20 (Sigma-Aldrich)

Methanol (EMD)

Glycine (Sigma-Aldrich)

Triton X-100 (Sigma-Aldrich)

Goat serum (Gibco)

NP-40 (Sigma-Aldrich)

NaCl (Sigma-Aldrich)

Na_2HPO_4 (Sigma-Aldrich)

NaH_2PO_4 (Sigma-Aldrich)

NaN_3 (Sigma-Aldrich)

PD98059 (Calbiochem)

Na_3VO_4 (Sigma-Aldrich)

NaF (Sigma-Aldrich)

β-glycerophosphate (Sigma-Aldrich)

Immunofluorescence reagents

Primary antibodies:

Phospho-p44/42 MAPK (Thr202/Tyr204)

Polyclonal: #9101 (1:200) and Monoclonal: #4377 (1:50)

(Cell Signaling Technology)

Secondary antibody:

Alexa Flur 488 (1:200) (Molecular Probe)

4',6-diamidino-2-phenylindole (DAPI) (Sigma-Aldrich)

ProLong Gold antifade (Molecular Probe)

Methods

Cell culture and stimulation for phospho-ERK measurements

1. Culture MCF-10A cells in Dulbecco's modified Eagle's medium/Ham's F-12 containing HEPES and L-glutamine supplemented with 5% (v/v) horse serum, 20 ng/mL EGF, 0.5 μg/ml hydrocortisone, 0.1 μg/ml cholera toxin, 10 μg/ml insulin, and 1% penicillin/streptomycin.
2. Plate cells on sterilized glass cover glass placed in the 6-well tissue culture plates at 1 x 10^5 cells per well and grow cells in growth medium for 24 h to allow adhesion.
3. For G_0 synchronization, wash cells twice with PBS and culture them in serum-free medium for 24 h: DMEM/F-12 supplemented with 1% penicillin/streptomycin and 0.1% bovine serum albumin.
4. For EGF stimulation, reconstitute recombinant human EGF in sterile H_2O at 100 μg/ml and dilute it in serum-free medium to designated concentrations.
5. Make sure EGF containing medium is warmed to 37 ^oC. Then stimulate cells for

15 min by adding 2 ml of EGF containing medium to each well. Either cells incubated in the absence of EGF or treated with a pharmacological inhibitor of MEK, PD98059, can be used as a negative control while cells treated with 10 ng/ml can serve as a positive control.

Antibody labeling of ppERK

1. After 15 min of EGF stimulation, place 6-well plates on the ice and wash cells twice with ice-cold PBS.
2. Fix cells in freshly prepared 2% paraformaldehyde (pH 7.4) for 20 min at room temperature in the presence of phosphatase inhibitors at the following concentrations: 1 mM sodium orthovanadate, 10 mM sodium fluoride, and 10 mM β-glycerophosphate. Rinse with 0.1 mM solution of Glycine in PBS three times.
3. Permeabilize cells in PBS containing 0.5% NP-40 and the phosphatase inhibitors for 10 min at 4^{o}C with gentle rocking. Rinse with PBS three times.
4. Dehydrate cells in ice-cold pure methanol for 20 min at -20^{o}C. Rinse with PBS three times.
5. Block with IF Buffer: 130 mM NaCl, 7 mM Na_2HPO_4, 3.5 mM NaH_2PO_4, 7.7 mM NaN_3, 0.1% bovine serum albumin, 0.2% Triton X-100, 0.05% Tween-20 and 10% goat serum for 1 h at room temperature.
6. Incubate with anti-phospho-p44/42 MAPK antibody in IF buffer overnight at 4^{o}C. Rinse three times with IF buffer at room temperature on the rocker for 20 min each. Washing step is essential to minimize background staining.

7. Sequentially incubate with Alexa dye-labeled secondary antibodies (Invitrogen-Molecular Probe) in IF buffer for 45 min at room temperature. Rinse three times with IF buffer at room temperature on the rocker for 20 min each. Make sure to protect samples from light.
8. Counterstain nuclei with 0.5 ng/ml DAPI (Sigma-Aldrich) for 15 min at room temperature and rinse with PBS twice with gentle rocking for 5 min each.
9. Mount with ProLong Gold antifade (Invitrogen-Molecular Probe). Dry overnight in a place that can protect samples from light.

Fluorescence microscopy imaging of ppERK and automated image analysis

1. Acquire fluorescence images using filters for DAPI and FITC. Start with a sample that is expected to give the highest FITC signal (e.g., the positive control, 10 ng/ml EGF). Using this positive control, empirically choose an exposure time so that the highest pixel intensity in a given field is close to the saturation level (generally 255). Be sure that the chosen exposure time does not saturate the FITC signal in other fields of the positive control sample. These steps identify an exposure time that maximizes the dynamic range of ppERK signals that may be quantified. The exposure time determined in this way should then be fixed and used to capture images from all other samples.
2. Segment DAPI (nuclei) images using a combination of edge detection and Watershed algorithms. The algorithm to process a single image is written in MATLAB (MathWorks) as described below (steps 2a-e). This algorithm can be iterated to process multiple images in a single execution.

a. Import a DAPI image using *imread* function.

```
DAPI = Imread ( 'DAPI image.tif' )
```

b. *edge* function detects the edge of the objects using gradients in pixel intensity across the objects and returns a binary image where the edge of objects is traced. Different masks are available in *edge* function. 'sobel' and 'canny' methods were successfully used in this study.

```
[edgeDAPI, thresh] = edge ( DAPI, 'sobel')
```

Optionally, *imdilate* and *imerode* functions can be used together to enhance the results of edge detection.

c. Fill in the inside of the traced nuclei using *imfill* function.

```
edgefillDAPI = imfill (edgeDAPI, 'holes')
```

d. Edge detection method often cannot distinguish cells that are spaced too closely. Watershed algorithm can be used along with distance transform to separate merged multiple nuclei. Use of *bwdist* and *watershed* functions will generate an image having lines that would separate touching cells. Optionally, *imhmin* function can be used to prevent oversegmentation which is a known problem of watershed algorithm in some cases. Finally, change the obtained image into the binary image to match the class type.

```
distDAPI = -bwdist (~edgefillDAPI)

  distDAPI2= imhmin (dsitDAPI,1)
```

```
ridgeDAPI= watershed(distDAPI2)

ridgeDAPI2= im2bw(ridgeDAPI)
```

e. Merge two images generated by edge detection algorithm and watershed algorithm to create a single nuclear compartment image.

```
segmentedDAPI = edgefillDAPI & ridgeDAPI2
```

3. Additionally, apply size thresholds to the images to exclude non-cellular objects. The distribution of nucleus size can be approximated as a normal distribution. Thus, use three standard deviations above and below the mean area of nuclei as the upper and lower cut-off values.
4. Using FITC images, calculate the average fluorescence level of the non-cell areas on a per pixel base to account for the background level for each image.
5. Using the segmented images (nuclear mask) and FITC image together, calculate the area of individual nucleus and sum up the FITC values in this area. Finally, the phospho-protein intensity for each cell can be calculated in a following way: multiply the average background level by the area of the nucleus and subtract this value from the total FITC in the nucleus.

$$ppERK = \sum_{nucleus} FITC - \overline{Background} \times AR_{nucleus}$$

Data Acquisition, Anticipated Results, and Interpretations

We quantified the level of phosphorylated ERK (ppERK) in the nucleus of MCF-10A cells that were stimulated with 0.01 or 10 ng/ml EGF or left untreated for 15 minutes. At a qualitative level, the dose-dependent phosphorylation of ERK was evident (Figure 1).

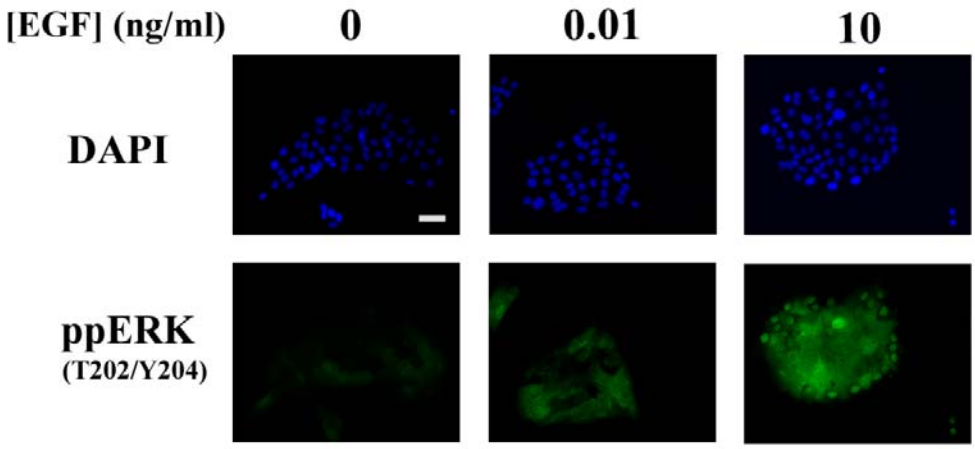

Figure 1. Serum-starved MCF-10A cells were stimulated with 0, 0.01, and 10 ng/ml EGF. Following 15 min of stimulation, cells were immunostained against ppERK (FITC) and nuclei were counterstained with DAPI. The scale bar represents 50 μm

Furthermore, the localization of ppERK to the nucleus was most evident at the highest EGF concentration. The dose-dependent activation of ERK was confirmed using our quantitative image processing algorithms (Figure 2). At the highest EGF concentration, the average amount of nuclear ppERK was approximately five-fold above the response when EGF was absent. Meanwhile, a relatively moderate amount of EGF (0.01 ng/ml) induced only a 3-fold increase in nuclear ppERK.

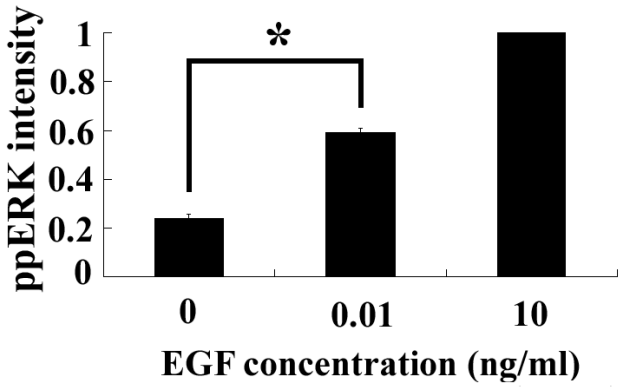

Figure 2. Average nuclear ppERK intensities in samples treated with 0, 0.01, and 10 ng/ml EGF. The *error bars* indicate S.E. (n=3) with duplicates performed in each experiment. The *asterisk* denotes $p < 0.01$ (Student's *t* test)

Since these measurements were conducted at the single-cell level, one can analyze the variation in cell responses across the population. We generated a histogram representing the distribution of nuclear ppERK levels across the population for the three different EGF concentrations (Figure 3). In the absence of EGF, most cells fall into a narrow range of low nuclear ppERK intensity. As the EGF concentration was increased, this distribution shifted gradually to the right. These results indicate that the level of

nuclear ppERK is a graded response to EGF stimulation at the single-cell level.

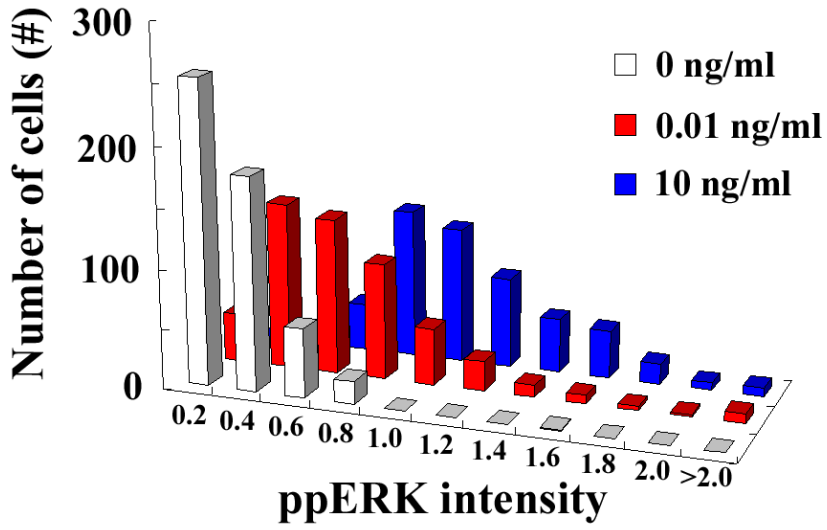

Figure 3. Histogram representation of the distribution of nuclear ppERK levels in cell populations treated with 0, 0.01, and 10 ng/ml EGF.

Statistical Guidelines

Total of three independent trials (n=3) were conducted to gather statistically meaningful data. In each trial, duplicates were prepared for each condition to minimize errors associated with sample preparation. For each sample, five images were collected at the multiple fields. All together, we analyzed at least 150 cells for each condition.

In each trial, the average amount of nuclear ppERK for each condition was expressed relative to the level in 10 ng/ml EGF sample. Thus, a statistical test was not performed between the 10 ng/ml EGF sample and other samples. One tailed-Student's *t* test was performed between 0 and 0.01 ng/ml EGF sample and indicated that these values

were different with a p-value less than 0.01. Error bars represent standard error with n = 3.

Discussion and Commentary

Intracellular signaling pathways control cell behaviors and multicellular morphodynamics. A quantitative understanding of these pathways will provide design principles for tuning these signals in order to engineer cell behaviors and tissue morphology. The transmission of information in these pathways involves both site-specific covalent modifications to signaling proteins and spatial localization of these signals. Here, we describe algorithms for quantifying signal localization from immunofluorescence (IF) staining for phosphorylated ERK. Our data reveal that in epithelial cells, ERK exhibits a graded response to EGF not only at the population level, but also at the level of individual nuclei. These results are consistent with the other studies that reported graded ERK responses to various stimuli in other mammalian cell systems (17-18). The algorithms presented here should facilitate quantitative, high throughput analysis of images acquired by IF staining.

Troubleshooting Table

Problem	**Explanation**	**Potential Solutions**
Background is too high	- Nonspecific binding of primary or secondary antibody	- Make sure to follow the required blocking and washing steps thoroughly.

	- Basal ERK activity mediated by autocrine factor.	- Perform a negative control using only the secondary antibody and skipping the primary antibody incubation to assess the level of nonspecific binding. - Prepare a sample treated with PD98059 to quench ERK activity all together.
The number of segmented nuclei is significantly less than the actual number of nuclei.	- Failure to detect the edge of some of the nuclei	- Increase the exposure time until DAPI signals at the location of nuclei become saturated. It will ensure the contrast between nuclei and the background. - Alternatively, *imadjust* or *contrast* algorithms can be used in MATLAB to enhance the contrast of a DAPI image before performing nuclear segmentation.
The number of nuclei is	- Many non-cellular objects	- Rinse and wipe the slides

significantly overcounted.	were considered as nuclei. - Oversegmentation from watershed algorithm.	with alcohol to get rid of dried salts and stain. - Avoid air bubbles when mounting the sample with antifade. - Adjust the upper and lower limits of area threshold of nuclei appropriately to exclude non-cellular objects with qualitative verification. - Use *imhmin* function to reduce oversegmentation.

Application Notes

The method described in this report would be particularly useful in quantifying the spatiotemporal signaling response at a single-cell level. The algorithm should allow automated and high throughput quantification of subcellular compartmentation of signaling events in response to multiple combinations and doses of environmental stimuli. It should also prove useful for quantitative studies of cell-to-cell variation in signaling. Such measurements would provide valuable quantitative data for systems-level analysis of signal transduction networks, the regulatory architecture that governs cellular decision-making.

Summary Points

- Before beginning image acquisition, choose an exposure time that maximizes the dynamic range of signals that may be quantified. Chosen exposure time should be fixed and used to capture images from all the samples.
- Qualitatively verify that the edge detection and watershed algorithms properly segment individual nuclei.
- Size thresholds are often necessary to exclude non-cellular objects.
- Account for background fluorescence level to measure exclusively fluorescence signals from signaling proteins.
- Choose a proper sample size (e.g., the number of cells analyzed in each trial), depending on the degree of cell-to-cell variance of the target proteins.
- Add phosphatase inhibitors at fixation and permeabilization steps if target signal molecules are phospho-proteins.
- Rigorous washing after incubation with antibodies is essential to minimize background staining.

Acknowledgements

The authors thank the members of the Asthagiri lab for helpful discussions. Funding for this work was provided by the Jacobs Institute for Molecular Engineering for Medicine.

References

1. Asthagiri AR & Lauffenburger DA (2000) Bioengineering models of cell signaling. *Annu Rev Biomed Eng* 2:31-53
2. Haugh JM (2002) Localization of receptor-mediated signal transduction pathways: the inside story. *Mol Interv* 2(5):292-307
3. Misteli T & Spector DL (1997) Applications of the green fluorescent protein in cell biology and biotechnology. *Nat Biotechnol* 15(10):961-964
4. Pollok BA & Heim R (1999) Using GFP in FRET-based applications. *Trends Cell Biol* 9(2):57-60
5. Mochizuki N, *et al.* (2001) Spatio-temporal images of growth-factor-induced activation of Ras and Rap1. *Nature* 411(6841):1065-1068
6. Ting AY, Kain KH, Klemke RL, & Tsien RY (2001) Genetically encoded fluorescent reporters of protein tyrosine kinase activities in living cells. *Proc Natl Acad Sci USA* 98(26):15003-15008
7. Tyas L, Brophy VA, Pope A, Rivett AJ, & Tavare JM (2000) Rapid caspase-3 activation during apoptosis revealed using fluorescence-resonance energy transfer. *EMBO Rep* 1(3):266-270
8. Graham DL, Lowe PN, & Chalk PA (2001) A method to measure the interaction of Rac/Cdc42 with their binding partners using fluorescence resonance energy transfer between mutants of green fluorescent protein. *Anal Biochem* 296(2):208-217

9. Claesson-Welsh L (1994) Platelet-derived growth factor receptor signals. *J Biol Chem* 269(51):32023-32026

10. Hlavacek WS, *et al.* (2006) Rules for modeling signal-transduction systems. *Sci STKE* 2006(344):re6

11. Wolf-Yadlin A, Hautaniemi S, Lauffenburger DA, & White FM (2007) Multiple reaction monitoring for robust quantitative proteomic analysis of cellular signaling networks. *Proc Natl Acad Sci USA* 104(14):5860-5865

12. Giepmans BN, Adams SR, Ellisman MH, & Tsien RY (2006) The fluorescent toolbox for assessing protein location and function. *Science* 312(5771):217-224

13. Wetzker R & Bohmer FD (2003) Transactivation joins multiple tracks to the ERK/MAPK cascade. *Nat Rev Mol Cell Biol* 4(8):651-657

14. Gutkind JS (2000) Regulation of mitogen-activated protein kinase signaling networks by G protein-coupled receptors. *Sci STKE* 2000(40):RE1

15. Yarden Y & Sliwkowski MX (2001) Untangling the ErbB signalling network. *Nat Rev Mol Cell Biol* 2(2):127-137

16. Graham NA & Asthagiri AR (2004) Epidermal growth factor-mediated T-cell factor/lymphoid enhancer factor transcriptional activity is essential but not sufficient for cell cycle progression in nontransformed mammary epithelial cells. *J Biol Chem* 279(22):23517-23524

17. Mackeigan JP, Murphy LO, Dimitri CA, & Blenis J (2005) Graded mitogen-activated protein kinase activity precedes switch-like c-Fos induction in mammalian cells. *Mol Cell Biol* 25(11):4676-4682

18. Whitehurst A, Cobb MH, & White MA (2004) Stimulus-coupled spatial restriction of extracellular signal-regulated kinase 1/2 activity contributes to the specificity of signal-response pathways. *Mol Cell Biol* 24(23):10145-10150